2012

Small Molecules as Negative Allosteric Modulators of Alpha7 nAChRs

Osama Alwassil
Virginia Commonwealth University

SMALL MOLECULES AS NEGATIVE ALLOSTERIC MODULATORS OF α7 nAChRs

A thesis submitted in partial fulfillment of the requirements for the degree of Master of Science at Virginia Commonwealth University.

By

OSAMA IBRAHIM ALWASSIL

Bachelor of Pharmaceutical Sciences, Riyadh, Saudi Arabia 2005

Director: MAŁGORZATA DUKAT

Associate Professor, Department of Medicinal Chemistry

Virginia Commonwealth University

Richmond, Virginia

August 2012

Acknowledgment

I would like to express my deep appreciation to Dr. Dukat for her support and guidance through the time I spent in her lab. The quality as well as the quantity of professionalism and skills that I have been exposed to during these years makes the words unable to describe how much I am thankful for her. I would like to extend my heartfelt thanks to Dr. Richard Glennon for his help and encouragement. It was a great honor to learn from him how to tackle many challenging scientific tasks. I would also like to thank Dr. Philip Mosier for teaching me the basic as well as the advanced tools in molecular modeling. I would also like to thank Dr. Renata Kolanos, Dr. Rossana Ferrara, and Atul Jain for their guidance with synthetic problems and most of all for their friendship. I would like to thank my committee members Dr. Richard Glennon, Dr. Scott Gronert, and Dr. Galya Abdrakhmanova. I would also like to thank King Faisal University in Saudi Arabia for their financial support. The studies were partially supported by Award No. 12-2 from the Commonwealth of Virginia's Alzheimer's and Related Diseases Research Award Fund, administered by the Virginia Center on Aging, Virginia Commonwealth University.

And last but not least I would also like to thank my mother and my wife for their support. Also, I would like to thank the rest of my family for their encouragement and care.

Table of Contents

List of Tables

List of Figures

List of Schemes

List of Abbreviations

3D	Three-dimensional
5-HT	5-Hydroxytryptamine/Serotonin
α_{2B}-AR	α_{2B}-Adrenoceptors
α-BTx	α-Bungarotoxin
σ_m	Hammett electronic constant of *meta*-substituent of aromatic compound
π	Lipophilicity constant
$A\beta_{1-42}$	β-Amyloid peptide 1-42
ac	Anticlinial
ACh	Acetylcholine
AD	Alzheimer's disease
AChBP	Acetylcholine binding protein
AChR	Acetylcholine receptor
APL	Allosterically-potentiating ligand
APP	Amyloid precursor protein
Bcl2	B-cell lymphoma 2
cAMP	3',5'-Cyclic adenosine monophosphate

cDNA	Complementary deoxyribonucleic acid
CICR	Calcium-induced calcium release
CNS	Central nervous system
CoMFA	Comparative Molecular Field Analysis
CREB	cAMP response element-binding protein
DHβE	Dihydro-β-erythroidine
EC_{50}	Activation concentration (half-maximal effect)
ECD	Extracellular domain
EPI	(±)-Epibatidine
ER	Endoplasmic reticulum
ERK	Extracellular-signal regulated kinase
EtOAc	Ethyl acetate
Et_2O	Diethyl ether
EtOH	Ethanol
FDA	Food and Drug Administration
FRET	Fluorescence resonance energy transfer
GABA	γ-Aminobutyric acid
Gal	Galantamine
GC-MS	Gas chromatography–mass spectrometry
GluR	Ionotropic glutamate receptors
GOLD	Genetic optimization of ligand docking
GPCR	G-protein coupled receptor
GSK-3β	Glycogen synthase kinase-3β

HDMP	1,2,3,3a,4,8b-Hexahydro-2-benzyl-6-*N*,*N*-dimethylamino-1-methylindeno[1,2,-b]pyrrole
HEK-293	Human embryonic kidney 293
HINT	Hydrophobic interaction
IC_{50}	Inhibition concentration (half-maximal effect)
ICD	Intracellular domain
ImI	α-Conotoxin
IP_3R	Inositol (1,4,5)-triphosphate receptor
i-PrOH	Isopropanol
KO	Knock-out
LGIC	Ligand-gated ion channel
LOB	(-)-Lobeline
M (M1-M4)	Transmembrane-spanning helix
M (M1-M5)	Muscarinic acetylcholine receptor subtypes
mAChRs	Muscarinic acetylcholine receptors
MAPK	Mitogen-activated protein kinase
mCPBG	*meta*-Phenylbiguanide
mCPG	*meta*-Chlorophenylguanidine (MD-354)
mCPBG	*meta*-Chlorophenylbiguanide
MD-354	*meta*-Chlorophenylguanidine
MeCN	Acetonitrile
MLA	Methyllycaconitine
mRNA	Messenger ribonucleic acid

MWC	Monod-Wyman-Changeux
nAChRs	Nicotinic acetylcholine receptors
NAM	Negative allosteric modulator
NC-IUPHAR	International Union of Pharmacology Committee on Receptor Nomenclature and Drug Classification
NH_2CN	Cyanamide
NMDA	*N*-methyl-D-aspartate
P2X	ATP-gated purine receptors
PAM	Positive allosteric modulator
PBG	Phenylbiguanide
PDB	Protein data bank
PG	Phenylguanidine
PI3K	Phosphatidylinositol 3-kinase
PKC	Protein kinase C
PLC	Phospholipase C
PNS	Peripheral nervous system
QSAR	Quantitative structure-activity relationships
RMSD	Root-mean-square deviation
SAR	Structure-activity relationships
sc	Synclinial
SH-EP1	Human epithelial cell line
SEM	Standard error of the mean
THF	Tetrahydrofuran

TLC	Thin layer chromatography
TM	Transmembrane
TMS	Tetramethylsilane
UniProtKB	Protein Knowledgebase
VDCC	Voltage-dependent calcium channel

Abstract

SMALL MOLECULES AS NEGATIVE ALLOSTERIC MODULATORS OF α7 nAChRs

By Osama Ibrahim Alwassil, M.S.

A thesis submitted in partial fulfillment of the requirements for the degree of Master of Science at Virginia Commonwealth University.

Virginia Commonwealth University, 2012

Major Director: Małgorzata Dukat, Associate Professor, Department of Medicinal Chemistry

α7 Neuronal nicotinic acetylcholine receptors (nAChRs) are involved in essential physiological functions and play a role in disorders such as Alzheimer's disease. MD-354 (3-chlorophenylguanidine; **21**), the first small–molecule negative allosteric modulator (NAM) at α7 nAChRs, served as a lead in developing structure–activity relationships for NAMs at α7 nAChRs. MD-354 (**21**) also binds at 5-HT_3 receptors. Analogs of MD-354 with structural features detrimental to 5-HT_3 receptor affinity were evaluated in patch-clamp recordings and an aniline N-methyl analog resulted in a more potent and selective NAM than MD-354. A new N-methyl series of compounds was synthesized in which the 3-position was replaced with different substituents considering their electronic, lipophilic, and steric nature. Comparative studies were initiated to investigate whether or not the MD-354 series and the N-methyl series bind in the

same manner; 3D models of the extracellular domain of human α7 nAChRs were developed, allosteric sites identified, and docking studies conducted.

I. Introduction

Acetylcholine (ACh) is a widely distributed neurotransmitter in the nervous system. Prior to its recognition as a neurotransmitter, ACh was chemically synthesized in 1867 and was later isolated as a naturally occurring choline ester.[1,2] The theory of chemical neurotransmission in 1936 was the point at which ACh first became known as a neurotransmitter.[2,3] Acetylcholine receptors (AChRs) were later identified and classified as nicotinic acetylcholine receptors (nAChRs) and muscarinic acetylcholine receptors (mAChRs). nAChRs belong to the ligand-gated ion-channel (LGIC) receptor superfamily, whereas mAChRs are members of the G-protein coupled receptor (GPCR) superfamily.[2] α7 nAChRs are one of the major subtypes of neuronal nAChRs, and are found predominantly in the central nervous system and are a recognized target for cognitive enhancement.[4]

The LGIC superfamily of receptors is characterized by a very rapid cellular response upon exposure to agonists. Within this process of activation, the receptor undergoes a conformational change that provides the optimum condition for a specific ion to pass through the receptor's pore. The passage of a particular number of ions causes the surrounding membrane to become depolarized. Neuronal α7 nAChRs are usually localized in nerve ending regions as are

other neurotransmitter receptors such as dopamine, glutamate, and γ-aminobutyric acid (GABA) receptors.[4] The nerve ending regions can stimulate the release of ACh as well as co-existing neurotransmitters as a consequence of the change in their polarity under the activation of α7 nAChRs. The release of more than one neurotransmitter upon α7 nAChR stimulation indicates one side of the functional complexity of these receptors.[4]

α7 nAChRs have some unique features that distinguish the receptor subtype from other nAChR subtypes. α7 nAChRs are characterized by a high Ca^{2+}/Na^{+} permeability ratio and rapid desensitization.[5] In contrast to the α4β2 nAChR subtype that has a low affinity for the competitive antagonist α-bungarotoxin (α-BTx) and a high affinity for the agonist (-)-nicotine, α7 nAChRs have a high affinity for α-BTx, and low affinity for (-)-nicotine. Furthermore, α7 nAChRs can be fully activated by choline whereas choline does not activate α4β2 nAChRs.[6]

The distribution of α7 nAChRs in the central nervous system (CNS) as well as in the peripheral nervous system (PNS) suggests their involvement in the etiology of several diseases such as Alzheimer's disease (AD), schizophrenia, Parkinson's disease, depression, nicotine dependence, pain, inflammation, and lung cancer.[6] Many α7 nAChR agonists and antagonists are recognized as possible candidates for the treatment of cognitive dysfunction.[7,8] Positive allosteric modulators (PAM) of α7 nAChRs, a class of compounds that enhance the activity of the endogenous agonist acetylcholine (ACh) without direct activation of the receptors, have been proposed as a potential treatment for cognitive diseases in both the clinical and the preclinical phase.[7] Yet, another unexplored approach might involve negative allosteric modulators (NAMs). However, until very recently, such agents were not known.

m-Chlorophenylguanidine (mCPG; MD-354) was identified in our laboratory as the first small–molecule negative allosteric modulator of α7 nAChRs (IC_{50} = 7.98 μM).[9] In addition to its inhibitory activity at α7 nAChRs, MD-354 possesses high affinity at 5-HT_3 receptors (K_i = 35 nM). Because of the selectivity problem, it was crucial to investigate if removal/addition of an MD-354 structural component required for 5-HT_3 receptor binding could result in a compound that retains inhibitory activity at α7 nAChRs and, at the same time, reduce 5-HT_3 receptor affinity.

As an important tool in medicinal chemistry, molecular modeling studies were initiated to examine interaction site(s) and mechanisms by which the α7 nAChR NAMs work. Three-dimensional (3D) models of the extracellular domain (ECD) of human α7 nAChRs were constructed based on the ECD of a mouse α1 nAChR subunit crystal structure. The results of cavity-search studies and docking solutions should allow for further insight at α7 nAChR allosteric sites and provide an impact on a way to develop novel small–molecule NAMs.

II. Background

A. Acetylcholine History

Acetylcholine (ACh; **1**) (Figure 1) is an endogenous substance classified as an ester of an acid and quaternary ammonium alcohol, acetic acid and choline, respectively. It was initially prepared by a German chemist, Adolf von Baeyer, who chemically synthesized it in 1867.[1,2] The natural occurrence of this compound was not recognized until 1914 from plant material contaminated by ergot fungus.[10] The compound became known for its action in mediating parasympathetic transmission in the frog heart and, then, was the first neurotransmitter to be identified when the concept of chemical neurotransmission gained popularity between 1921 to 1925.[2,3]

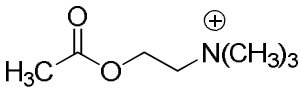

1

Figure 1. The structure of acetylcholine (ACh; **1**).

Many attempts were made, in the years thereafter, to obtain evidence for the existence of acetylcholine in the central nervous system (CNS) of animals. In the mid 1960's, a new technology, gas chromatography–mass spectrometry (GC-MS), was first introduced and using this technology on rat tissue, Holmstedt and co-workers were successful in reporting the first isolation of acetylcholine from fresh mammalian brain.[11]

The action of acetylcholine in the body varies depending mainly on the release location and the acetylcholine receptor type.[12] This change in acetylcholine behavior resulted in narrowing its therapeutic indication to limited ophthalmic practices.[13]

B. Cholinergic Receptors

The acetylcholine receptors are divided into two major classes, nicotinic acetylcholine receptors (nAChRs) and muscarinic acetylcholine receptors (mAChRs), based on their selective response to two alkaloids: nicotine (**2**) and muscarine (**3**) (Figure 2). The two classes of cholinergic receptors are structurally, as well as functionally, different with other unique properties characterizing each of them. Intensive studies throughout the years have been made on both of the two classes aiming to achieve a better understanding of their role in neuronal terminals and possible therapeutic advantages that could be gained.[12] Cholinergic receptors are

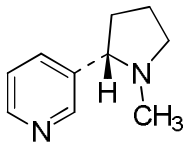

2

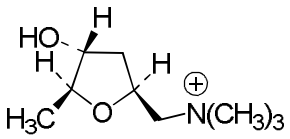

3

Figure 2. The structures of nicotine (**2**) and muscarine (**3**).

widely distributed in the CNS and are considered as important targets in the treatment of a number of diseases including schizophrenia and Alzheimer's disease (AD).[7,14]

1. Muscarinic Acetylcholine Receptors (mAChRs)

The mAChRs are homologs of rhodopsin, the visual pigment, and are members of the superfamily of G-protein coupled receptors (GPCRs) that are structurally described as a heptahelical integral membrane protein subunit that is essential in conducting signals across cell membranes.[12] The wide distribution of these receptors, especially in the CNS, attracts attention to the significance of mAChRs that is supported by their impact in regulating dopaminergic systems.[14] There are five identified subtypes of these receptors assigned as M1–M5 based on the order of their discovery.[15] Functionally, the subtypes M1, M3, and M5 couple preferentially to $G_{\alpha q}$ proteins for the activation of second messenger phospholipase C (PLC) and the release of inositol (1,4,5)-triphosphate (IP_3) that increases the level of intracellular calcium.[15] On the other hand, the subtypes M2 and M4 primarily couple to $G_{\alpha i/o}$ proteins that leads to a negative downstream signaling on adenylate cyclase which decreases the formation of the second messenger 3',5'-cyclic adenosine monophosphate (cAMP) and, eventually, decreases the level of intracellular calcium.[14,15]

2. Nicotinic Acetylcholine Receptors (nAChRs)

The nAChRs are members of the ligand-gated ion channel (LGIC) superfamily of receptors that mediate fast synaptic transmissions of neurotransmitters. Although the amount of

expression of the mAChRs subunits in the CNS is significantly higher than that of the nAChRs, nAChRs play a vital role in many physiological and pathophysiological processes.[16]

a. History and Classification

nAChRs are the classical and the most studied members of the LGIC superfamily of receptors. The large number of studies are probably related to the accessibility of the receptor, particularly from the electric organ of the *Electrophorus* fish and the *Torpedo* marine ray.[17] The first nAChR to be isolated and characterized was in 1970 by Changeux et al.[18] using a detergent extraction technique. Purification and reconstitution techniques were developed later, 1972-1980, with a more detailed characterization of the primary structure of nAChR subunit composition.[18] In 1981, Sumikawa et al.[19] were successful in expressing *Torpedo* electric organ messenger ribonucleic acid (mRNA) in *Xenopus* oocytes. The latter achievement boosted efforts toward the molecular cloning of functional nAChRs and, later, between 1982–1983, this resulted in the separation of a number of complementary deoxyribonucleic acids (cDNAs) encoding the four subunits of the *Torpedo* electric organ nAChR (i.e., α, β, γ and δ subunits).[17] Subsequently, many investigators were able to clone nAChR subunit cDNAs of numerous other species.[17] The human α7 nAChR subtype, for example, was first stably expressed for functional and pharmacological evaluation in human embryonic kidney 293 (HEK-293) cell lines by Gopalakrishnan et al. in 1995.[20]

Among the seventeen nAChR subunits of vertebrate species that have been identified, α1-α10, β1-β4, γ, δ and ε, a diverse family of nAChR subtypes can be generated by several different subunit combinations. With the exception of α8, which exists only in avian species, all of these identified subunits are present in humans as well as in other mammalian species. The assignment of the Greek letters (i.e., α, β, γ, δ and ε) basically arises from the first characterization of nAChR subunits in the electric organ of the *Electrophorus* fish and the *Torpedo* marine ray and were assigned based on the order of the molecular weight of each subunit.[21]

b. Nomenclature

Although the Greek-letter assignments were primarily based on the order of the molecular weight of each subunit at the specific conditions at which the subunits were initially purified, several criteria were later used to recognize these subunit types. The criteria for the α subunit includes the presence of two adjacent cysteine residues (Cys192 and Cys193), and the ability to be labeled by quaternary ammonium affinity-labeling reagents (i.e., an agonist binding subunit).[21] The β2-β4 subunits are described as the non-α subunit that is expressed exclusively in the vertebrate nervous system, whereas β1, γ, δ and ε subunits are defined as any non-α subunit expressed at the neuromuscular junction of vertebrates (Figure 3).[16] However, some limitations have been reported in this process of nomenclature such as the lack of agonist binding ability at α5 and α10 subunits, and the inability to describe the exact stoichiometry of some receptor-like α4β2 proteins.[21]

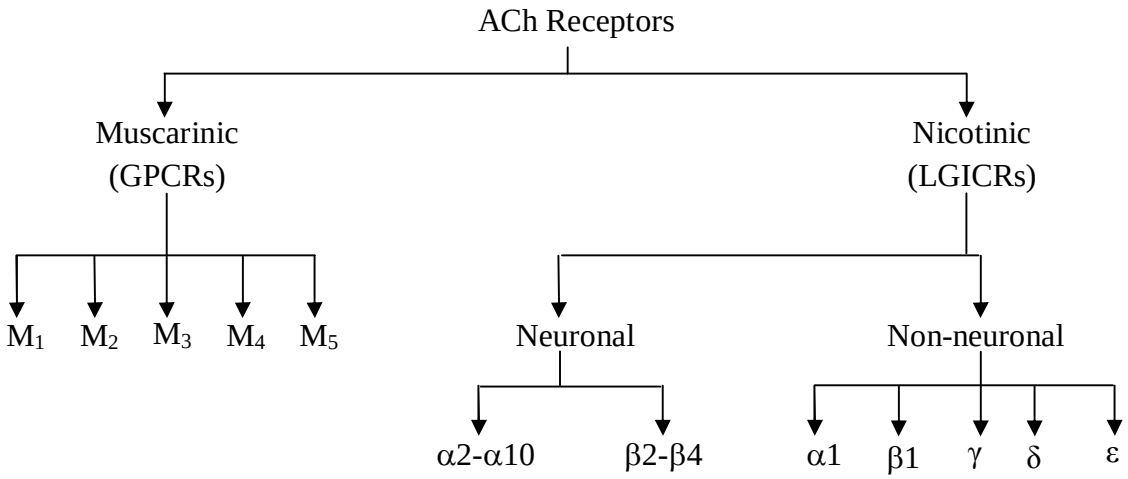

Figure 3. The classification of the two receptor classes of AChRs.[16]

The high number of identified nAChR subunits increases the probability of many different combinations of subunits to form pentamers with *in vivo* expression.[21,22] However, the ability of many subunits to form different pentamers is not enough to be considered as receptors. The subunit combinations should accompany the functional ability of the formed pentamer. Moreover, the differences of the subunits' combination order affect the pharmacological properties of the receptor (e.g., agonist and antagonist sensitivity).[21] This added another challenge to the nomenclature to find a method to describe the different composition and stoichiometry of nAChRs.[16,23] Lukas et al.,[24] in a working International Union of the Pharmacology Committee on Receptor Nomenclature and Drug Classification (NC-IUPHAR), recommended the use of an asterisk as a "wild card" at the end of receptor name (e.g., α4β2*) to indicate possible additional subunits that might be present in a neuronal nAChR complex. The exact composition and stoichiometry, if known, could also be described using a subscript number (e.g., $(\alpha1)_2\beta1\gamma\,\delta$ receptor).[21,24]

The α7, α4β2, and α3β4 receptors are the most common neuronal nAChR subtypes.[21] The α7 receptor subtype is a pentamer that is considered as the most abundant homomeric nAChR in the central nervous system.[21] α4β2 Receptors are heteromeric receptors that are the major nAChRs in mammalian brain.[21] On the other hand, a common heteromeric nAChR (i.e., α3β4) represents the most abundant nAChRs in the autonomic ganglia, adrenal medulla, and in regions of the dorsal medulla, pineal gland, medial habenula, nucleus interpeduncularis, and retina.[21]

Despite that most of the nAChRs exist presynaptically, to enhance neurotransmitter release, postsynaptic nAChRs play an important role in fast excitatory transmission.[16,25] The activation of these receptors causes membrane depolarization through direct calcium influx or an indirect process which is mediated by voltage-dependent calcium channel (VDCC) activation.[25] Downstream induction of calcium from the endoplasmic reticulum (ER) in a process called calcium-induced calcium release (CICR), mediated by ryanodine receptors and inositol (1,4,5)-triphosphate receptor (IP_3R) second-messenger systems, might also be involved.[25] The previous three routes control the cytoplasmic calcium level that contributes in many downstream cascade events on calcium-dependent kinases (e.g., protein kinase C (PKC), and extracellular-signal regulated kinase/mitogen-activated protein kinase (ERK/MAPK), and the transcription factor CREB (cAMP response element-binding protein). These signaling molecules, eventually, participate in many significant processes that include neurotransmitter release, recovery of nAChR desensitization, and gene expression.[16,25]

c. Ligand-Gated Ion-Channel (LGIC) Receptors

The LGIC group of receptors is a superfamily of receptors that includes Cys-loop receptors, ionotropic glutamate receptors (GluR), and ATP-gated purine receptors (P2X).[26] The extensive characterization of nAChRs was the major basis to rank the LGIC group as the best known of receptor families.[26,27] nAChRs are considered as cationic-selective channels that belong to the Cys-loop receptor group which also includes serotonin 5-HT_3 receptors, and both of these receptor are responsible for conducting excitatory signals. On the other hand, the anionic selective channels of the Cys-loop receptor group include $GABA_A$, $GABA_C$ and glycine receptors and these receptors are responsible for conducting inhibitory synaptic activity. Both cationic and anionic receptors belong to the Cys-loop group due to their shared feature of a 15-residue-spacing of two cysteine amino acids that are connected by a disulfide bridge.[27] All of the above classifications of LGIC receptors are based on ion selectivity, amino acid sequence homology, and agonist selectivity.[28]

Recent crystallization techniques, and other structural determination methods of ACh-binding protein (AChBP), have had a great impact in defining the molecular detail of nAChRs. Structurally, the nAChR is constructed of five subunits (i.e., a pentameric receptor), assembled symmetrically around a central channel.[22] Each nAChR consists of three major domains: an extracellular domain (ECD), a transmembrane domain (TM), and an intracellular domain (ICD) (Figure 4). The ECD of the nAChR subunit is about 200 residues long and, based on the similarity and differences of the subunits, the receptor could be a homomeric receptor (e.g., α7 nAChR), or a heteromeric receptor (e.g., α4β2 nAChR), respectively.[29,30] The TM protein of

each subunit is formed of four transmembrane-spanning helices (M1-M4), whereas the ICD is made up primarily from the intracellular loops of TMs, mainly from the short intracellular loop connecting M1 to M2 and, to a larger extent, the long intracellular loop connecting M3 to M4 (Figure 5).[29,31] From each of the five subunits that form the receptor, there are hydrophilic amino acids lining the M2 ends that shape an intracellular and/or an extracellular ring that determines, to some extent, the ion selectivity of the receptor channel.[5] The ECD has attracted the most attention since it contains the putative binding site (i.e., the orthosteric site) for many ligands, including ACh.[5] Numerous studies demonstrated that the orthosteric binding site is mainly formed by the interface between the α-subunit with the contribution of residues from loops A, B, and C (i.e., the principal or (+) site of the binding pocket), and the neighboring subunit residues with the contribution of loops D, E, and F (i.e., the complementary or (-) site of the binding pocket) (Figure 4).[32]

The exact three-dimensional description of nAChRs is a useful tool for the design of novel drugs that aim to treat diseases such as AD. Several studies on *Torpedo* nAChR electron microscopy data and the crystal structure of the AChBP were able to determine nAChR dimensions.[30,33,34] Each nAChR subunit is about 62 Å high, 47 Å wide, and 34 Å thick.[30] The diameter of the pentamer is 80 Å, whereas the diameter of the central pore is around 18 Å.[30,33] Fluorescence resonance energy transfer (FRET) was used to determine the position of the orthosteric cavity which is located above the membrane surface by about 30 Å.[35]

Upon functioning, nAChRs undergo certain structural changes that reflect the level of activation that the receptor adopts. The allosteric nature and the dynamics of nAChRs were explained by the Monod-Wyman-Changeux (MWC) model.[36,37] According to the MWC

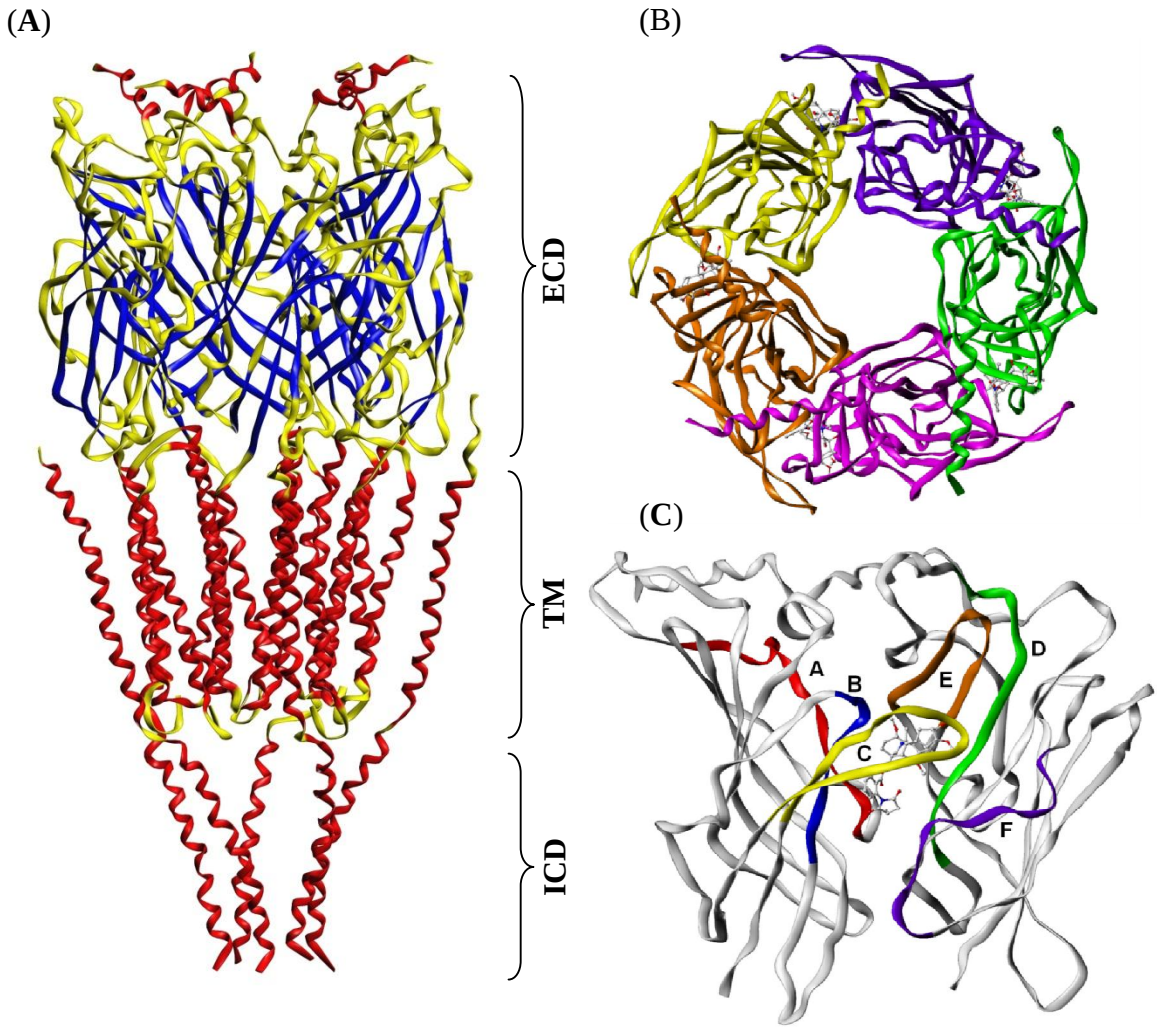

Figure 4. Structural description of nAChRs based on molecular modeling. (A) A whole receptor representation adopted from PDB (PDB ID: 2BG9B) including the three main domains; the ECD, the TM domain, and the ICD. (B) A top view of five different colored subunits forming the receptor. (C) The orthosteric binding site formed by loops located at the interface between the two subunits; the principal subunit ribbon colors: Red, loop **A**; blue, loop **B**; yellow, loop **C**; the complementary subunit ribbon colors: green, loop **D**; orange, loop **E**; purple, loop **F**.

model, there are three main states in which nAChRs exist: the resting state (R), the active state (A), and the desensitized state (fast-onset (I) and slow-onset (D)) (Figure 6).[16] The transition of nAChRs between one state and another is regulated by the free energy differences which are

affected by the existence of interacting ligand in the receptor's vicinity.[16] nAChR agonists and antagonists stabilize the active and the resting state, respectively. However, the active state of

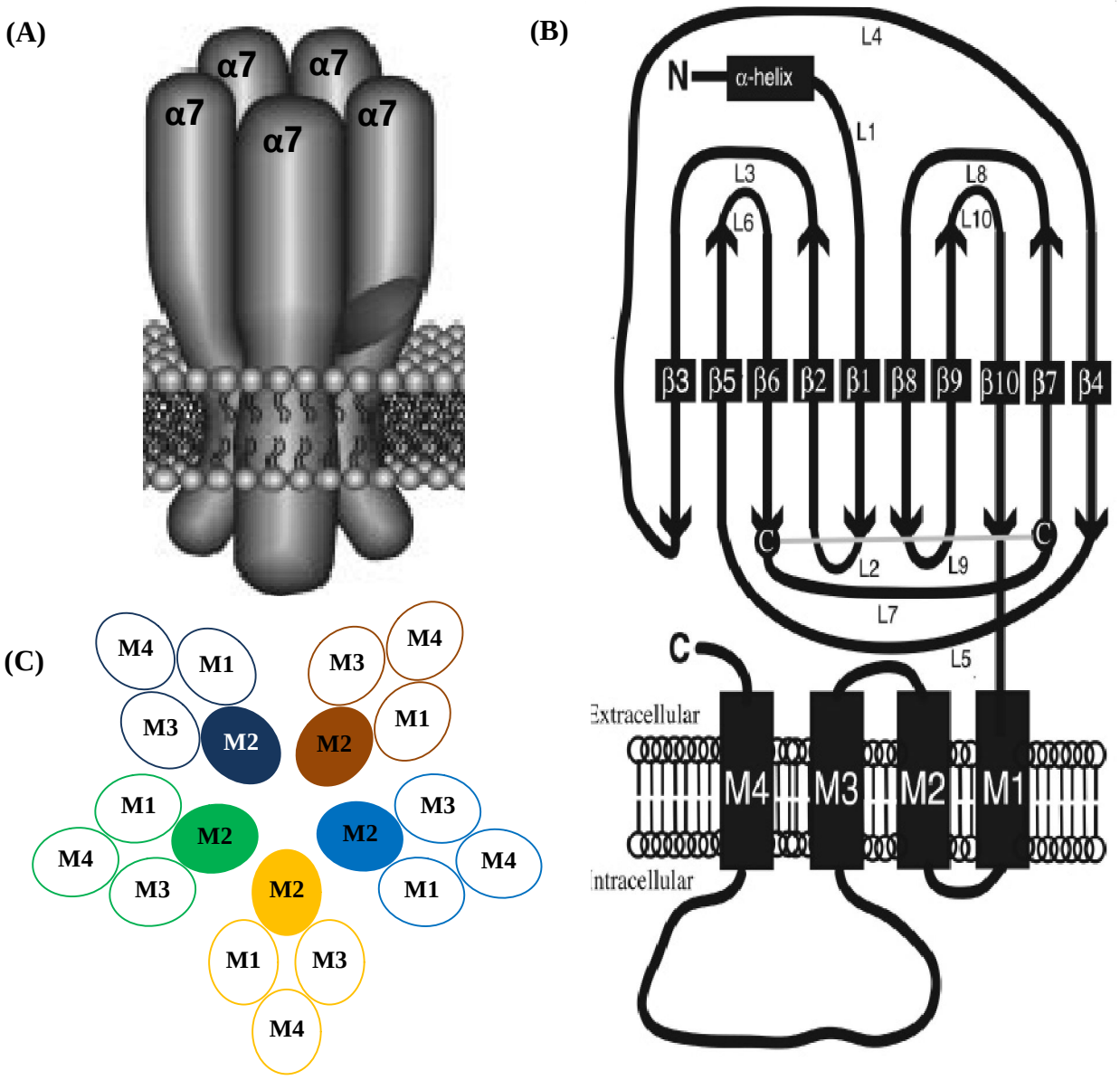

Figure 5. Structural details of the nAChR. (A) A side view representation of the pentameric arrangement of the subunits around the pore. (B) Schematic depiction of the secondary structures of the nAChR subunit including the exact order of α helices, β sheets, and loops connecting them in three main domains (i.e., ECD, TM, ICD). (C) Top view representation of the TM domains of the pentameric receptor showing M2 of each subunit lining the receptor pore.[16,26]

nAChRs can occur without the existence of interacting agonists (i.e., constitutive activity).[16] The conformational changes in nAChRs caused by different ligands have been the target of many comparative analyses and molecular dynamics studies.[38,39] The closure and the extension of loop C upon activation and inhibition of the receptor, respectively, was clearly detected as the most marked conformational change after the interaction of ligand with the binding pocket.

Most of the structural data were originally obtained or confirmed by crystal structures that were published in recent years.[31] The crystallographic techniques were originally based on data coming from low- to medium-resolution electron microscopy studies on *Torpedo* receptors and provided only general information on the structure and size of the receptor, the ligand interaction site, and the arrangement of the secondary structure around the receptor pore. In 2001, Brejc et al.[30] were able to provide the crystal structure of molluscan AChBP. Also, Unwin had a great impact on this field when he published the first molecular model of the *Torpedo* AChR at 4 Å resolution using cryo-electron microscopy in 2005.[40] A recent, important crystal structure determination was reported by Dellisanti et al.[32] on the ECD of the mouse α1 nAChR in the closed state at 1.94 Å resolution. The crystallized protein is a good template for the molecular modeling of the ECD of human α7 nAChR since it shares a 38% sequence identity.[32]

The expression and distribution of nAChR subunits show a high level of α7 receptors in the brain, the second most common nAChR in brain after α4β2 nAChRs, which accounts for 90% of neuronal nAChRs. The cortex, hippocampus, and subcortical limbic area is the primary localization of the α7 subunit, while low levels of the subunit are reported in the thalamic area

and basal ganglia.[16,41,42] The assembly and expression of another participant subunit in the formation of α7 nAChRs might affect either the ion selectivity and desensitization properties of

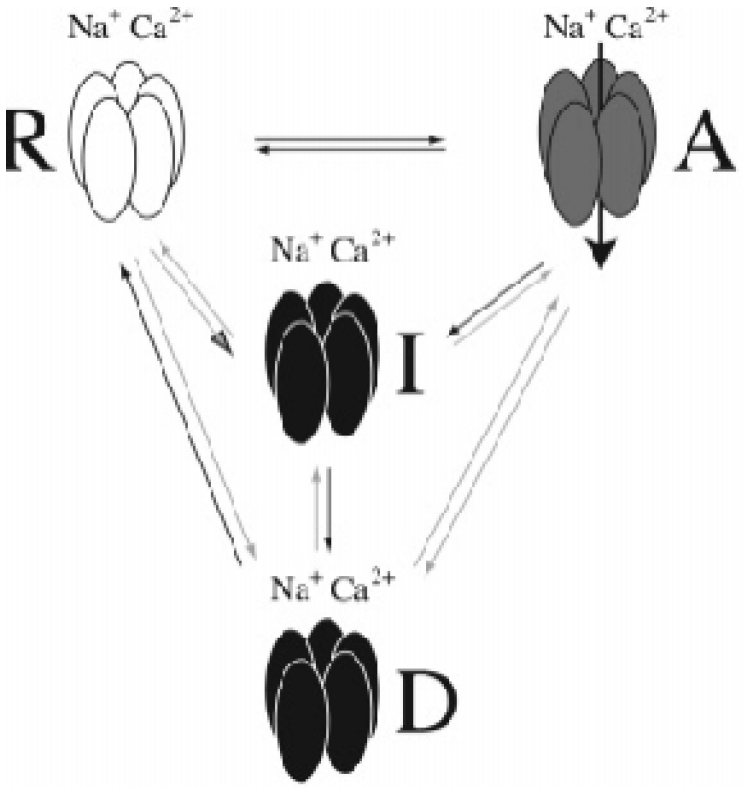

Figure 6. Representation of the different states of the MWC model that explain the allosteric nature of nAChRs; the resting state (R), the active state (A), the fast-onset desensitized state (I), and the slow-onset desensitized state (D).[16]

the newly formed heteromeric receptor.[5] Although the human α7 nAChR subtype was first expressed in 1995, α4β2 and $(\alpha)_2\beta\gamma\delta$ subunits were first successfully expressed in mouse fibroblasts (i.e., M8 and AM4 cell lines) three years before.[20,43,44] The existence of these different expressed subunits in distinct areas in the CNS and/or in the periphery with dissimilar conditions can vary significantly the precise function that these receptors play in normal physiological states as well as in the development of many diseases.[5]

The distribution of α7 nAChRs in brain regions involved in cognitive function and emotional behavior indicates a strong relationship between some CNS diseases and the pathophysiological state of these receptors.[20] Alzheimer disease (AD) is one of the diseases assumed to be a consequence of abnormalities in α7 nAChR signaling which appears in patients as general cognitive impairments accompanied by an episodic decline in memory.[45] Several studies suggest that the progression of AD is associated with an increase of β-amyloid peptide 1-42 ($A\beta_{1-42}$) interactions with α7 nAChRs leading to downstream signaling that causes tau protein hyperphosphorylation, the structural protein stabilizing the microtubules, and neuronal degeneration.[46] This harmful interaction and signaling have been the target of many studies that tested a number of novel α7 nAChR ligand effects. α7 nAChR agonists and positive allosteric modulators (PAMs) were proposed as possible therapeutic agents for AD patients through their ability to prevent toxic α7 nAChR–$A\beta_{1-42}$ interactions and their activation to the neuroprotective pathway in α7 nAChR downstream signaling. Despite that most of the reported results were focused on the successful desired effect of α7 receptor agonists and PAMs targeting AD therapy, low doses of α7 receptor antagonists have been reported to produce a similar desired effect.[45-47] Methyllycaconitine (MLA), an example of an α7 nAChR antagonist, shows a neuroprotective role which suggests that the neuroprotective pathways were originally due to a desensitization/inactivation mechanism on α7 nAChRs.[48] The hippocampus and cortex are the key brain regions at which the AD experiments are taking place since they represent the major memory processing regions and the primary expression sites for α7 nAChRs.[47]

d. α7 nACh Receptor Agonists

A number of naturally-occurring alkaloids represent the earlier, nonselective, and high affinity agonists for nAChRs: (-)-nicotine (**2**) (Figure 2), (-)-lobeline (LOB; **4**) and (±)-epibatidine (EPI; **5**) (Figure 7) are some examples of these alkaloids that have been extensively studied to understand their molecular role in activating nAChRs.[16,49,50] From such studies, agonist selectivity for α4β2 and α7 nAChRs was found to be highly dependent on local binding and long-range electrostatic interactions between the receptors and the protonated portion or the cationic part of the agonist structures.[51] Detailed information of the atomic interactions guided the synthesis of novel, highly selective agonists targeting nAChR subtypes. [50]

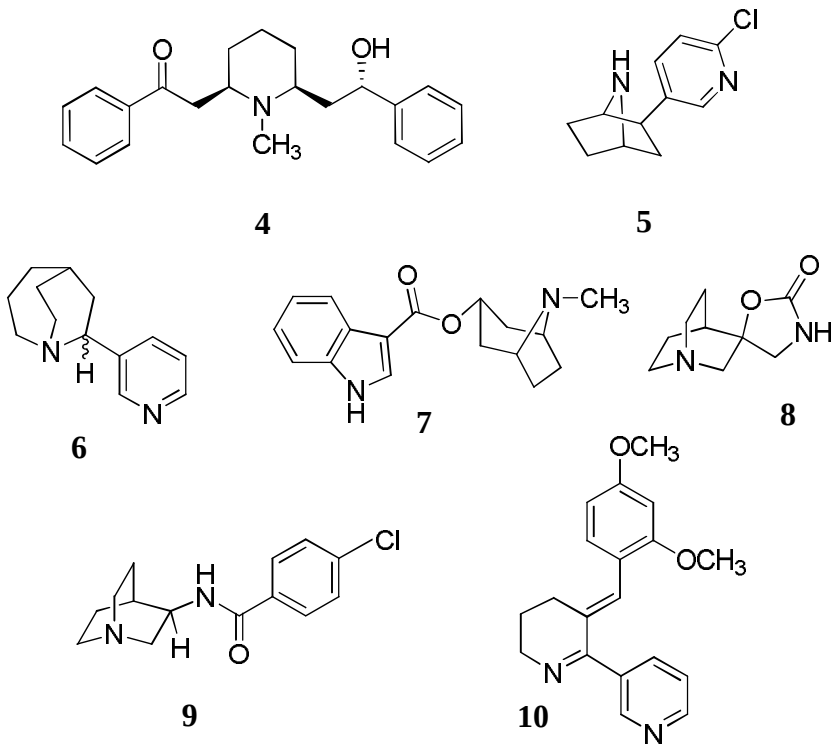

Figure 7. The chemical structures of selective and nonselective α7 nAChR agonists: (-)-lobeline (LOB; **4**), (±)-epibatidine (EPI; **5**), TC-1698 (**6**), tropisetron (**7**), AR-R17779 (**8**), PNU-282987 (**9**), and GTS-21 (**10**).

The primary work of many medicinal chemistry practices in the field of nAChRs took place on a series of novel compounds based on the nicotine (**2**) and epibatidine (**5**) skeletons. The replacement of the pyrrolidine group of nicotine with an azabicyclo[3.2.2]nonane ring (i.e., TC-1698; **6**) (Figure 7), for example, yielded a full agonist at α7 nAChRs (EC_{50} = 0.44 μM).[16] Among several challenges that faced the syntheses of novel α7 nAChR ligands, selectivity remains the biggest issue due to cross-activity with 5-HT_3 receptors arising from the high homology in the orthosteric site between the two receptor types.[16] The 5-HT_3 receptor antagonist tropisetron (**7**) (Figure 7), for example, is a partial agonist at α7 nAChRs (EC_{50} = 0.38 μM).[16] A derivative of quinuclidine structures, spirooxazolidinone AR-R17779 (**8**) (Figure 7), is a selective and a full agonist at α7 nAChRs (EC_{50} = 10 μM). The new generation of these series includes the *p*-chlorbenzamide analog PNU-282987 (**9**), which is highly selective and a potent (EC_{50} = ~3 μM) α7 nAChR agonist.[16] The anabaseine analog GTS-21 (**10**) is considered a prototypical selective partial agonist of the α7 nAChRs (EC_{50} = 6 μM).[16] Unlike ACh, the ACh precursor and metabolic product, choline, exerts selective-full agonist activity at α7 nAChRs (EC_{50} = ~1 mM).[16,50]

e. α7 nACh Receptor Antagonists

The majority of the typical α7 nAChR antagonists are found as naturally occurring substances. Two examples of these are the highly selective competitive antagonists: the peptide toxin α-bungarotoxin (α-BTx) (IC_{50} = 0.005 μM), from the Taiwan banded krait (*Bungarus multicinctus*), and the alkaloid methyllycaconitine (MLA; **11**) (Figure 8) (IC_{50} = 0.0017 μM), isolated from *Delphinum* and *Consolida* species.[16] The selectivity among nAChR subtypes

diminished with other antagonists such as dihydro-β-erythroidine (DHβE; **12**), d-tubocurarine (**13**), and the peptide toxin α-conotoxin (ImI). A 4-oxystilbene derivative, MG624 **(14)**, was reported as a highly potent α7 nAChR antagonist over α4β2 and α1β1γδ nAChRs (IC_{50} = 0.11 μM).[16]

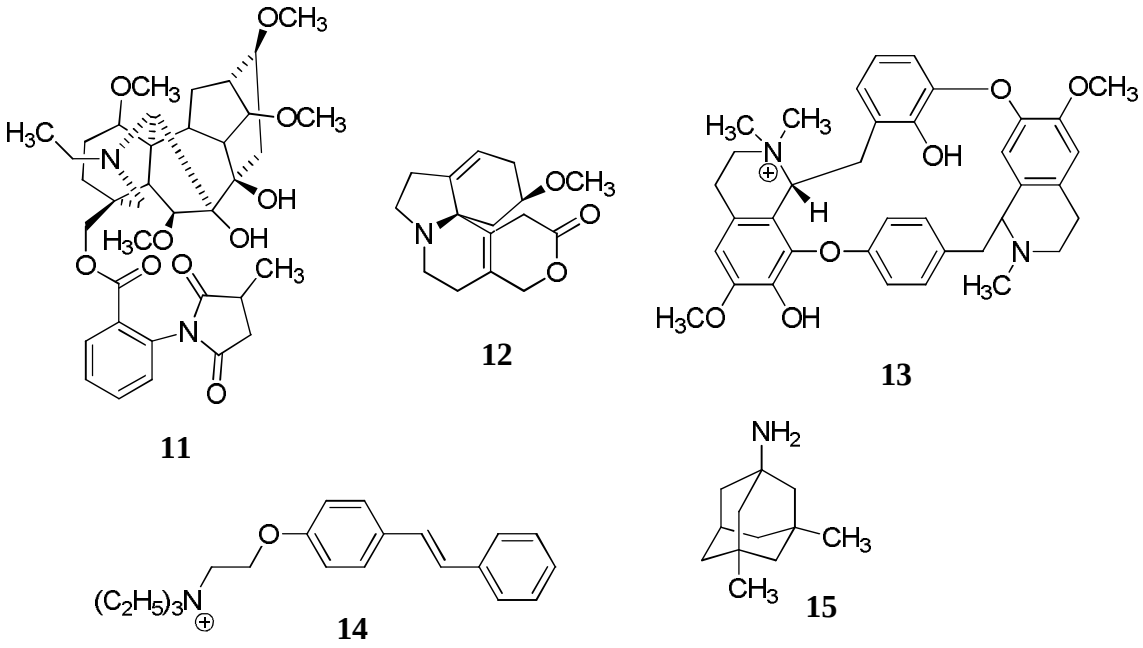

Figure 8. The chemical structures of selective and nonselective α7 nAChR antagonists: methyllycaconitine (MLA; **11**), dihydro-β-erythroidine (DHβE; **12**), d-tubocurarine (**13**), MG624 (**14**), and memantine (**15**).

Martin et al.[48] reported that MLA (**11**), a selective α7 nAChR antagonist, is able to play a neuroprotective role in AD. The explanation of this action involves the inhibition/desensitization action by the α7 nAChR antagonist that is actually a neuroprotective pathway against $A\beta_{1-42}$-induced neurotoxicity.[48] Another low molecular-weight, selective α7 nAChR antagonist is memantine (**15**) (Figure 8) which is an approved drug for AD.[52] Although the approval of memantine was based on its ability to antagonize GluR *N*-methyl-D-aspartate (NMDA)

receptors, Banerjee et al.[53] considered the inhibitory activity of memantine on α7 nAChRs (IC_{50} = 0.34 μM) as the action advantageous to AD therapy.[52,54]

f. α7 nACh Receptor Allosteric Modulators

Allosteric modulators are receptor ligands that interact with different sites (i.e., allosteric sites) than the orthosteric site and mediate either or both the binding and the signaling of the orthosteric ligand. An allosteric modulation mechanism is widely appreciated and clinically founded by the action of benzodiazepines on $GABA_A$ receptors.[55] Several possible allosteric binding sites on nAChRs have been experimentally identified in the ECD and TM domain through photoaffinity labeling, epitope mapping, crystallography, and mutagenesis studies.[56-59] This type of receptor ligand is a promising approach for medicinal compounds that presents several advantages over classical orthosteric agents (i.e., agonists and antagonists).[60,61] The saturability of the allosteric site provides better control over an administered agent.[60] This advantage eliminates any competitive undesired effects (e.g. toxic effect) that might interfere with the desired effect. Another advantage is that an allosteric modulator is expected to work only at a time when endogenous agonist exists at the orthosteric site.[60] By this feature, the allosteric modulator effect would vary depending on the nerve tone and the tissue state which, apparently, differs from that of the orthosteric ligand that works in a continuous fashion irrespective to nerve activity. A third advantage is the receptor subtype selectivity of allosteric ligands over classical orthosteric ligands and this is because the orthosteric sites of nAChRs are the most conserved region among the receptors subtype.[60,61]

Allosteric modulators are divided, based on their activity on the receptors, into two main classes, positive allosteric modulators (PAMs) and negative allosteric modulators (NAMs). Generally, PAMs are allosteric ligands responsible for improving the action of endogenous agonists, whereas NAMs are involved in reducing the endogenous agonist's effect.[6,62]

1. Positive Allosteric Modulators (PAMs)

From a thermodynamic point of view, PAMs enhance the agonist effect by lowering the energy barrier between the receptor's active and resting states (Figure 6).[63] PAMs are believed to work either by improving the affinity of an orthosteric ligand due to the conformational changes that PAMs generate in the receptors, or by enhancing the coupling between the orthosteric site and the area of the receptor responsible for gating.[59] In addition, α7 nAChR PAMs are classified into two types depending on the desensitization profile of each PAM. For instance, galantamine (Gal; **16**) (Figure 9) is considered a Type I PAM since it does not affect the desensitization time of α7 nAChRs, whereas PNU-120596 (**17**) prolongs the desensitization time and is classified as a Type II PAM.[16,64]

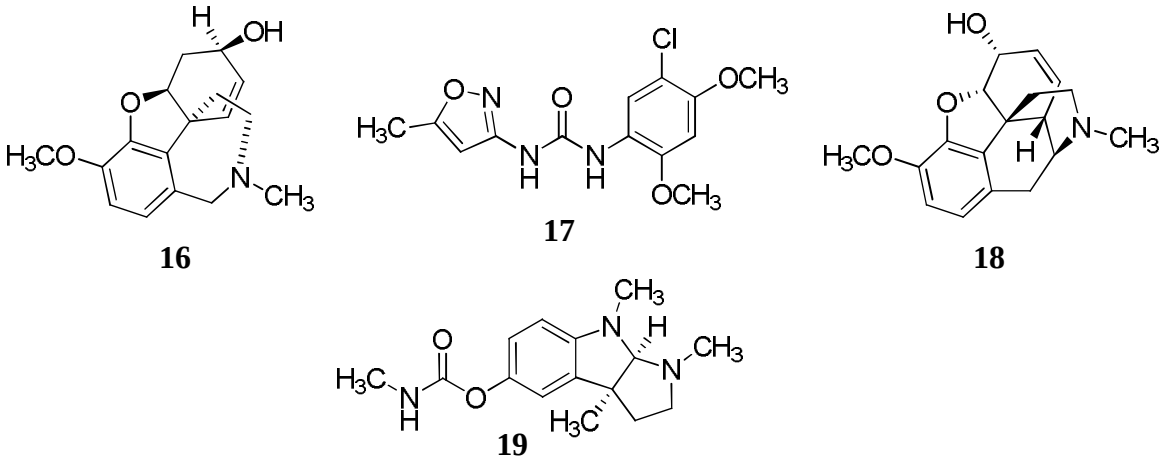

Figure 9. The chemical structures of α7 nAChR PAMs: galantamine (Gal; **16**), PNU-120596 (**17**), codeine (**18**), and physostigmine (**19**).

Some studies have classified compounds like Gal (**16**), codeine (**18**), and physostigmine (**19**) (Figure 9) as allosterically-potentiating ligands (APLs) instead of being PAMs.[59] Although these two classes represent positive modulation in a general sense, some differences related to their mechanism and the location at which PAMs and APLs modulate their agonist effects have been reported.[59]

2. Negative Allosteric Modulators (NAMs)

NAMs are allosteric ligands that elevate the energy barrier between the receptor's active and resting states.[63] Among efforts for identifying $GABA_A$ allosteric modulators, Yoshimura et al.[55] screened a library of modulators for nAChRs and identified UCI-30002 (**20**) (Figure 10) as one of the first reported highly correlated NAMs of neuronal nAChRs; however, the compound was non-selective, and evidence of its action as a NAM at α7 nAChRs was not provided. Our

laboratory[9,65] reported *meta*-chlorophenylguanidine (MD-354; **21**) as the first subtype-selective small molecule to function as a NAM at α7 nAChRs. Abdrakhmanova et al.[66] later reported a potent selective α7 nAChR NAM, 1,2,3,3a,4,8b-hexahydro-2-benzyl-6-N,N-dimethylamino-1-methylindeno[1,2,-b]pyrrole (HDMP; **22**) (IC_{50} = 0.07 μM) which is selective for α7 over α4β2 and α3β4 nACh receptors.

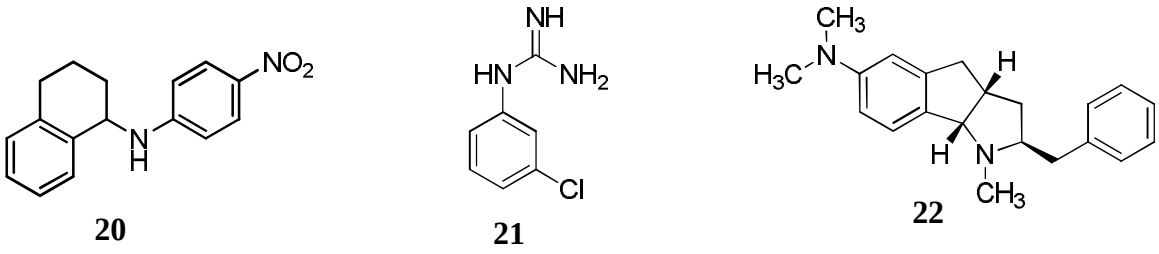

20 **21** **22**

Figure 10. The chemical structures of non-selective (i.e., UCI-30002 (**20**)) and selective (i.e., *meta*-chlorophenylguanidine (MD-354; **21**) and HDMP (**22**)) NAMs of α7 nAChRs.

Earlier in our laboratory, the compound MD-354 (**21**) (Figure 10) was synthesized among several arylguanidine derivatives for an SAR study at 5-HT_3 receptors.[65] MD-354 possessed high affinity at 5-HT_3 receptors (K_i = 35 nM) and showed affinity for α_{2B}-adrenoceptors (α_{2B}-ARs) nearly equal to that for 5-HT_3 receptors.[67,68] Although MD-354 does not produce antinociceptive effects by itself, it remarkably potentiated an inactive dose of clonidine to produce an antinociceptive effect without potentiating clonidine's sedative effect in the mouse tail-flick assay.[68,69] In contrast, MD-354 was found to block the antinociceptive effects of (-)-nicotine in the mouse tail-flick assay which lead to the conclusion that MD-354 could not be a general analgesia-enhancing agent and raised the possibility of involvement of another mechanism in such effects.[9] Further studies showed that MD-354 lacked affinity for the

most abundant neuronal nAChRs (i.e., the α4β2 subtype) and was able to antagonize the antinociceptive activity of (-)-nicotine on the second most abundant neuronal nAChRs (i.e., the α7 subtype) in the tail-flick assay.[9] Binding studies that showed that MD-354 lacked affinity for α7 nAChRs, and the functional data which confirms the inhibition by MD-354 (IC_{50} = 7.98 μM) of α7 nAChRs led to the conclusion that MD-354 allosterically antagonizes α7 nAChRs. MD-354 was the first small molecule to function as a NAM at α7 nAChRs.[9]

g. The Role of α7 nAChR in Alzheimer's Disease (AD)

Despite that the molecular details of AD-related memory loss and that the exact role of $Aβ_{1-42}$ and tau protein in cognitive alterations is still not fully understood, a number of studies were dedicated to investigate the biological relevance of these to the disease.[45] Dziewczapolski et al.[70] reported a transgenic mouse model of AD that overexpressed the mutated human amyloid precursor protein (APP) and was missing the gene responsible for α7 nAChR expression (APP α7KO). The APP α7KO mice were able to significantly solve the Morris water maze test in a better performance time compared with APP mice and APP α7KO mice significantly maintained the protection of brain from the reduction of the level of synaptophysin, the presynaptic marker that correlates better with the AD progression than Aβ plaques and cell death, in comparison with APP mice.[70] Zheng et al.[71] were able to detect parallel events represented by the activation of multiple kinases (e.g., MAPK, glycogen synthase kinase-3β (GSK-3β)) which clarified the mechanism that links α7 nAChR–$Aβ_{1-42}$ interactions and tau protein hyperphosphorylation (Figure 11). Moreover, Hu et al.[8] successfully reported both the phosphorylation of GSK-3β in

concordance with the tau protein hyperphosphorylation that resulted from the α7 nAChR–$A\beta_{1-42}$ interactions and the attenuation of this undesired effect by α7 nAChR-selective agonists and antagonists.

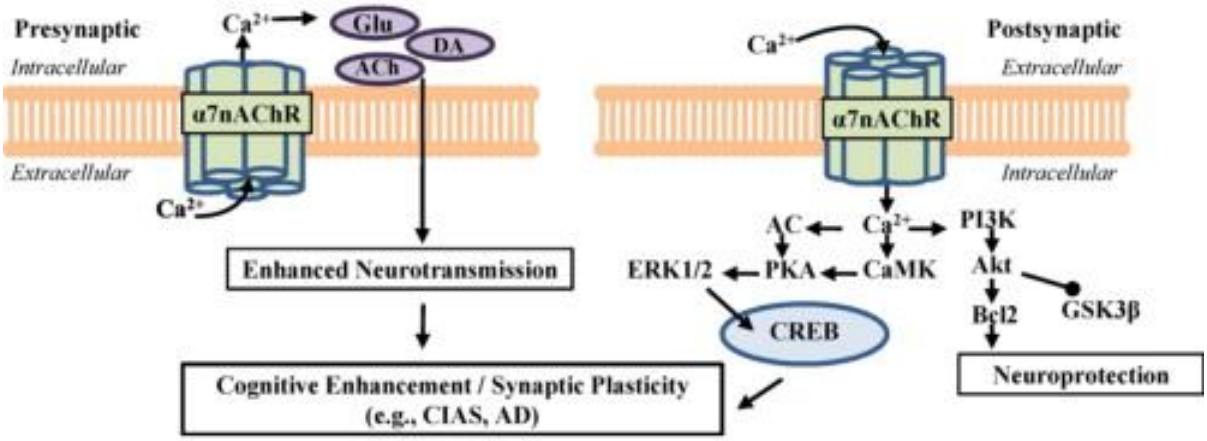

Figure 11. The downstream signaling pathways of α7 nAChRs.[47]

It is also worth mentioning that there is more than one reported mechanism by which α7 nAChR activation benefits AD patients. Acute administration of α7 nAChR selective agonists has been shown to increase ERK 1/2 and CREB phosphorylation that work as a significant signaling pathway in enhancing synaptic plasticity and cognitive function (Figure 11).[47] In addition, a neuroprotective pathway against the neurotoxicity that resulted from α7 nAChR–Aβ interactions, represented by phosphatidylinositol 3-kinase (PI3K), protein kinase Akt, and B-cell lymphoma 2 (Bcl2) signaling, has been reported as the consequence of the administration of α7 nAChR agonists that provide protection(Figure 11).[47]

III. Specific Aims

The arylguanidine MD-354 (**21**) was identified by Dukat and co-workers[9,65] as the first example of a small-molecule negative allosteric modulator (NAM) of α7 nACh receptors. Unfortunately, MD-354 also binds at 5-HT_3 serotonin receptors with high affinity. The overall purpose of the current project is to decrease or eliminate the affinity of MD-354 at 5-HT_3 receptors while retaining its actions as a NAM of α7 nACh receptors.

5-HT_3 receptor antagonists are used clinically for the treatment of nausea and vomiting induced by chemotherapy and radiation.[72] Agonists have not been nearly as well investigated. A prior goal of our laboratory was to develop the SAR of 5-HT_3 receptor agonists in order to determine what structural features contribute to their action. PBG (**23**; 5-HT_3 K_i ca 1,200 nM) and later mCPBG (**26**; 5-HT_3 K_i ca 18 nM) (Table 1) were examples of the first known 5-HT_3 receptor agonists.[65] An initial investigation showed that the entire biguanide moiety of PBG (**23**) and mCPBG (**26**) is not essential for binding at 5-HT_3 receptors and a novel series of compounds (i.e., arylguanidines) was introduced.[65,73,74] The functional activity of the new series, represented by MD-354 (**21**), at 5-HT_3 receptors was investigated using the shrew emesis assay and suggested a partial agonist effect.[67] The reasonably high affinity of MD-354 (**21**) at 5-HT_3 receptors (K_i = 35 nM) led to a structure-affinity investigation and a quantitative structure-

activity relationship (QSAR) study that covered aryl substitution and the guanidine moiety.[65,73,74] After examining K_i data obtained from the two series (Table 1), it was proposed that arylbiguanides and arylguanidines might bind at 5-HT_3 receptors in a similar manner.[74] This study involved application of a widely accepted concept proposed by Portoghese[75] in his study on analgesics, which stated that "If identically substituted compounds in two different series are interacting with receptors in a similar manner, then the quantitative contribution of various substituents to the analgesic effect should produce, under steady-state conditions, proportionate variations of activity in both series".

Table 1. The binding affinities of a number of the same-substituent pairs of arylbiguanides and arylguanidines at 5-HT_3 receptors.[73]

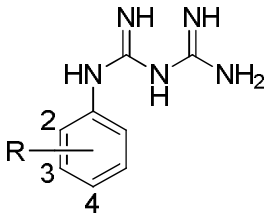

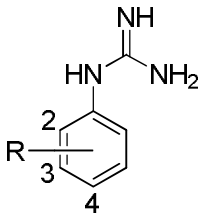

R		K_i (nM)		K_i (nM)
–H	**23**	1,200.0	**31**	2,340.0
4-Me	**24**	890.0	**32**	442.0
2-Cl	**25**	62.0	**33**	190.0
3-Cl	**26**	18.0	**21**	35.0
4-Cl	**27**	210.0	**34**	326.0
3,4-di-Cl	**28**	12.0	**35**	3.1
3,5-di-Cl	**29**	1.8	**36**	5.0
3,4,5-tri-Cl	**30**	2.7	**37**	0.7

In the arylguanidine series, the introduction of a chloro group at the aryl 3-position (i.e., MD-354; **21**) showed high binding affinity at 5-HT_3 receptors.[73] Affinity decreased by the replacement of the 3-Cl group of MD-354 with a more electron-withdrawing group such as 3-CF_3 (K_i = 2,440 nM).[73] The introduction of a lipophilic methyl group at the 3-position also resulted in decreased affinity (K_i = 6,520 nM).[73] Follow-up studies on the 3-position using Hansch analysis were conducted and identified a correlation between 5-HT_3 receptor affinity (pK_i) and σ_m.[74] On the other hand, the presence of a lipophilic substituent at the 4-position is favorable, whereas an electron-withdrawing group at the 4-position (e.g., 4-Cl (Table 1; **27**), 4-CF_3) resulted in about a 10-fold increase in affinity.[73,74] Using Hansch analysis, there is a better correlation between 5-HT_3 receptor affinity (pK_i) and the π value of 4-position substituents.[74] The 4-position can tolerate lipophilic groups of limited size and this result was also supported by a Comparative Molecular Field Analysis (CoMFA).[73,74]

With respect to the guanidine moiety of the arylguanidines, replacement of the aniline NH by a methylene group, or replacement of a terminal NH by a carbonyl oxygen atom resulted in decreased affinity at 5-HT_3 receptors (i.e., **38**, **39**; Figure 12).[65,73] Moreover, the replacement of a hydrogen atom at any of the three guanidine nitrogen atoms by a methyl group resulted in a major decrease, or in a lack, of affinity (i.e., **40**, **41**, **42**; Figure 12).[73] Conformationally restricted structures also resulted in a decrease or loss of affinity that might be due to a disadvantageous binding conformation or lack of bulk tolerance (i.e., **43**, **44**; Figure 12).[73]

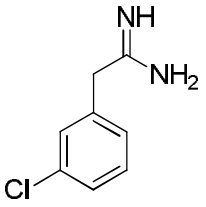

38

[K_i = 1,200 nM]

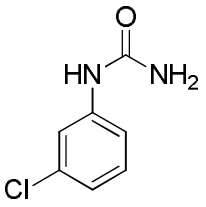

39

[K_i > 10,000 nM]

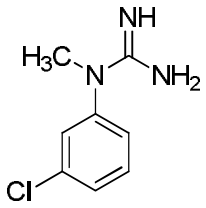

40

[K_i = 6,200 nM]

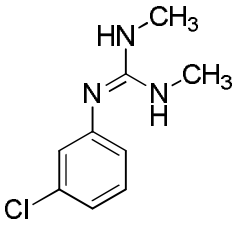

41

[K_i > 10,000 nM]

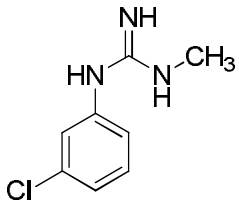

42

[K_i > 10,000 nM]

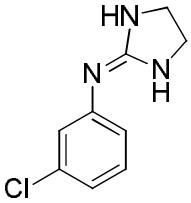

43

[K_i > 10,000 nM]

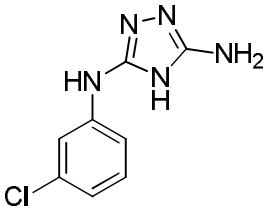

44

[K_i > 10,000 nM]

Figure 12. Chemical structures representing different modifications in the guanidine moiety of MD-354 (**21**) and *m*CPBG (**26**). 5-HT_3 receptor affinity is provided [in brackets] as K_i values.[65,73]

The data obtained from the extensive structure-affinity studies allowed Dukat to develop/propose a pharmacophore for arylguanidine interactions with 5-HT_3 receptors (Figure 13).[76]

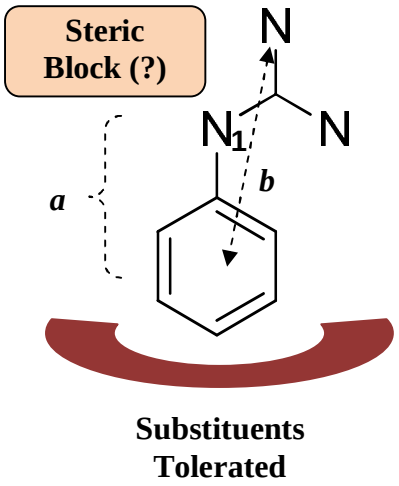

Figure 13. Schematic representation of Dukat's pharmacophore model for the binding of arylguanidines at 5-HT_3 receptors. Aromatic ring, adjacent nitrogen atom (N_1), and terminal amine group form the three major components of the model. Although substituents at the *meta* and *para* positions of the aromatic ring can increase affinity, steric bulk is less likely to be tolerated at N_1. (a) Represents the distance between N_1 and the adjacent aromatic ring centroid which is 2.7 Å. (b) Represents the distance between the terminal amine group and the aromatic ring centroid which is 4.5 – 4.9 Å.[76]

The cross-reactivity of many α7 nAChR and 5-HT_3 receptor ligands probably arises from the high homology (~ 30%) between the two receptor types, which is considered as the highest similarity within the LGIC superfamily.[77] As a consequence, MD-354 (**21)** has been found to act as a partial agonist at 5-HT_3 receptors (in an *in vivo* model) and as a NAM at α7 nAChRs (IC_{50} = 7.98 μM).[9] Moreover, arylguanidine SAR for 5-HT_3 receptor binding affinity showed that introduction of certain aryl substituents reduces 5-HT_3 receptor affinity (i.e., **31**, **45**, **46;** K_i =

2,340, 2,440, 1600 nM; respectively) and that N-methylation of the aniline nitrogen atom (i.e., **40**) results in a significant reduction in affinity (K_i = 6,200 nM) as well.[65,73] The effect of these structural changes on the actions of MD-354 (**21**) at α7 nACh receptors is unknown. Also, there is no reason to expect that the guanidine 5-HT_3 receptor pharmacophore will be identical with its α7 nACh receptor pharmacophore. Thus, compounds **31**, **40**, **45**, and **46** will be examined to determine the influence of various substituents on NAM action at α7 nACh receptors. Should any of these structural alterations be tolerated, this could result in arylguanidines with enhanced selectivity as α7 nAChR NAMs. That is, an attempt will be made to take advantages of those structural features of arylguanidines already known to be detrimental to 5-HT_3 receptor binding; incorporation of these substituents into novel arylguanidines might lead to compounds with enhanced selectivity as NAMs of nACh receptors.

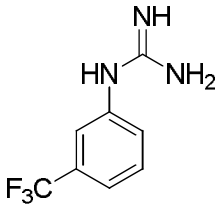

45

[K_i = 5,700 nM]

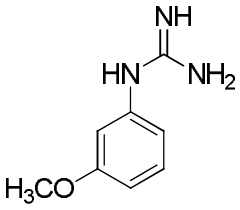

46

[K_i = 1,600 nM]

Figure 14. Arylguanidines derivatives with different electronic substitution at the 3-position. 5-HT_3 receptor affinity is provided [in brackets] as K_i values.[65]

A new series of compounds based on the introduction of different aryl substitution of **40** will be synthesized and investigated. The chloro group at the 3-position will be replaced with different substituents considering the electronic, the lipophilic, and the steric nature of the new substituent. The introduction of the other halogens (i.e., -F, -Br, and –I) instead of the chloro

group will allow for testing mainly the effect of substituent size variation over a relatively fixed electron-withdrawing nature. Furthermore, the replacement of the chloro group with $-OCH_3$ or $-CH_3$ groups as electron donating groups, as well as being lipophilic substituents, will explore the effect of such modification on activity.

Another primary goal is to construct and validate a homology model of the ECD of the α7 nAChR. The significance of such a computational tool in drug design, as an important element in medicinal chemistry, is widely appreciated. The constructed model will be used to identify the putative allosteric binding site(s) and to determine the interaction mode(s) of **21** and **40** with α7 nAChRs. Since the α7 nAChR is a homomeric structure, the molecular modeling of only two attached subunits (i.e., a dimer) is justified, and should be sufficient, to mimic the essential ligand binding domain. The construction will undergo a number of steps and different software will be employed. Aligning the amino acid sequence of the targeted portion of the protein and the matching portion of the selected template amino-acid sequence will be performed using ClustalX 2.0.[78] The generation of multiple models lacking validation will be constructed using Modeller 9.7. Different docking programs (e.g., GOLD Suite 5.0 and AutoDock 4.1), as well as accurate residue orientation processes, should allow for model validation by comparing the results with previously published biochemical or crystallographic data. Therefore, the blind docking feature of AutoDock 4.1 using Gal (**16**) as well as the Connolly surface feature of SYBYL 8.1 and the hydrophobic interaction (HINT) program will be used to explore the possible interaction site(s) at the ECD of α7 nAChRs. GOLD Suite 5.0 will be used for model validation through the docking of α7 nAChR agonists (i.e., acetylcholine (**1**), nicotine (**2**), EPI (**5**)) and the antagonist MLA (**11**) and comparing the results with reported crystal structures (PDB ID: 2XZ5 , 1UW6, 2BYQ, and 2BYR, respectively).[38,79,80] Prior to docking of the studied

molecules (i.e., **21**, **40**), the two compounds will be subject to a systematic search to investigate favorable low-energy conformations. The validated ECD models of α7 nAChRs will then be used for the new docking studies after specifying the targeted allosteric cavity. The resulting complexes of **21** and **40** with the candidate ECD models of α7 nAChRs will provide beneficial information that will help in the prediction of required structural modifications to the current series.

General Hypothesis: The structural modifications of MD-354 (**21**) known to be detrimental for 5-HT_3 receptor binding might provide a possible avenue to enhance α7 nAChR selectivity. In fact, there is no a priori reason to believe that what is detrimental for one effect (e.g., 5-HT_3 receptor binding) should be detrimental for a second effect (e.g., α7 nAChR NAM action).

IV. Results and Discussion

A. Synthesis of Initial Arylguanidines

N-(3-Chlorophenyl)-*N*-methylguanidine hydrochloride (**40**) was previously prepared in our laboratory and the re-synthesis of this compound required three steps described in Scheme 1.[73] The 3-chloroformanilide intermediate **48** was obtained by heating 3-chloroaniline (**47**) at reflux in an aqueous formic acid solution (95-97%). The formamide group was then reduced using borane in tetrahydrofuran and the HCl salt **49** was prepared. An ethanolic solution of **49** was heated at reflux with cyanamide to give **40.** The structure of the known compound was confirmed by IR, ^{1}H NMR, and melting point.

Scheme 1.[a]

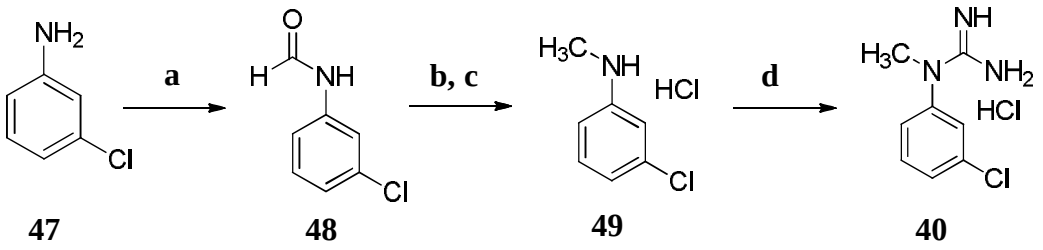

47 **48** **49** **40**

[a]Reagents and conditions: a. Formic acid, reflux; b. BH_3•THF, THF, reflux; c. HCl/Et_2O; d. NH_2CN, absolute EtOH, reflux.

The nitrate salt of *m*-chlorophenylguanidine (MD-354; **21**), hydrochloride salt of phenylguanidine (PG; **31**); nitrate salt of 3-trifluorophenylguanidine (**45**) and hydrochloride salt of 3-methoxyphenylguanidine (**46**) were available from previous studies.

B. Biological Data

The whole-cell configuration of the patch-clamp technique was employed to obtain functional data at nAChRs. Rat α7 nAChRs were expressed in stably transfected human embryonic kidney (HEK) 293 cells. In addition, the expression of rat α3β4 nAChRs were obtained in HEK 293 cells, whereas a human epithelial cell line (SH-EP1) was used in expressing human α4β2 nAChRs. The latter two receptor types are important to study the selectivity of our compounds among nACh receptor subtypes since activation of these receptors resulted in serious side effects. For example, activation of α4β2 nAChRs can be accompanied by nausea and vomiting adverse effects in humans.[81] On the other hand, activation of α3β4 nAChRs at autonomic ganglia and the CNS is associated with constipation, heart problems and weight loss, respectively.[82]

The project was initiated by the finding that MD-354 (**21**) does not bind at the orthosteric site of α4β2 (K_i > 10,000 nM) or α7 nACh receptors (K_i > 10,000 nM) but blocks the antinociceptive effect of the agonist nicotine in the mouse tail-flick assay.[9] Electrophysiological studies showed that MD-354 (**21**) is a noncompetitive α7 nACh receptor antagonist (IC_{50} = 7.98 μM).[9] Is MD-354 the first small-molecule NAM or is it a channel blocker? The NAM activity of MD-354 (**21**) was confirmed through the elimination of possible competitive antagonism activity

since competitive antagonists do not produce inhibition at currents evoked by an ACh-saturated concentration (Figure 15A). Also, the elimination of possible channel blocking activity was achieved by showing that MD-354 (**21**) produces a voltage-independent effect at various holding potentials whereas channel blockers are voltage-dependent (Figure 15B).

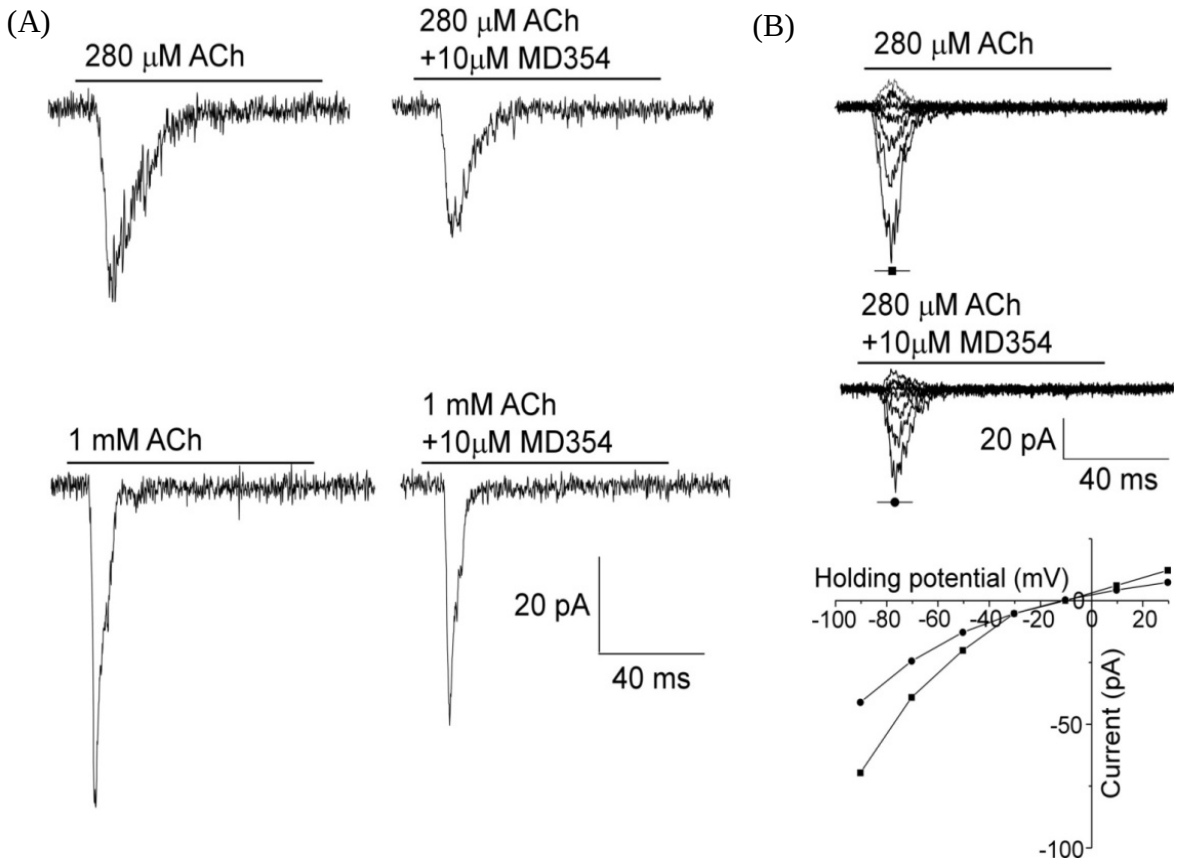

Figure 15. The inhibitory effects of MD-354 (**21**) at 10 μM at α7 nAChRs. (A) The inhibitory effects of MD-354 on α7 nAChRs at an EC_{50} concentration of ACh (i.e., 280 μM) and at a saturated concentration of ACh (i.e., 1 mM). (B) The inhibitory effects at various holding potentials in the range from -100 to +30 mV. The upper part represents superimposed traces of ACh-induced currents in the absence and presence of **21**. In the lower part, squares represent the maximal amplitude in the absence of **21** plotted versus the corresponding holding potential, whereas circles represent the maximal amplitude in the presence of MD-354 (**21**) at a concentration around its IC_{50} value plotted versus the corresponding holding potential.

The examination of NAM action of a fixed concentration (i.e., 10 μM) of compounds **21**, **31**, **40**, **45**, and **46** at α7 nACh receptors resulted in a different extent of inhibition compared to the normalized current evoked by ACh at its EC_{50} (Figure 16). These results emphasize that the structural alterations on MD-354 (**21**), focusing on analogs with substituents that are detrimental to 5-HT_3 receptor binding, appear to be tolerated and that the inhibitory activity (i.e., NAM) at α7 nACh receptors was maintained.

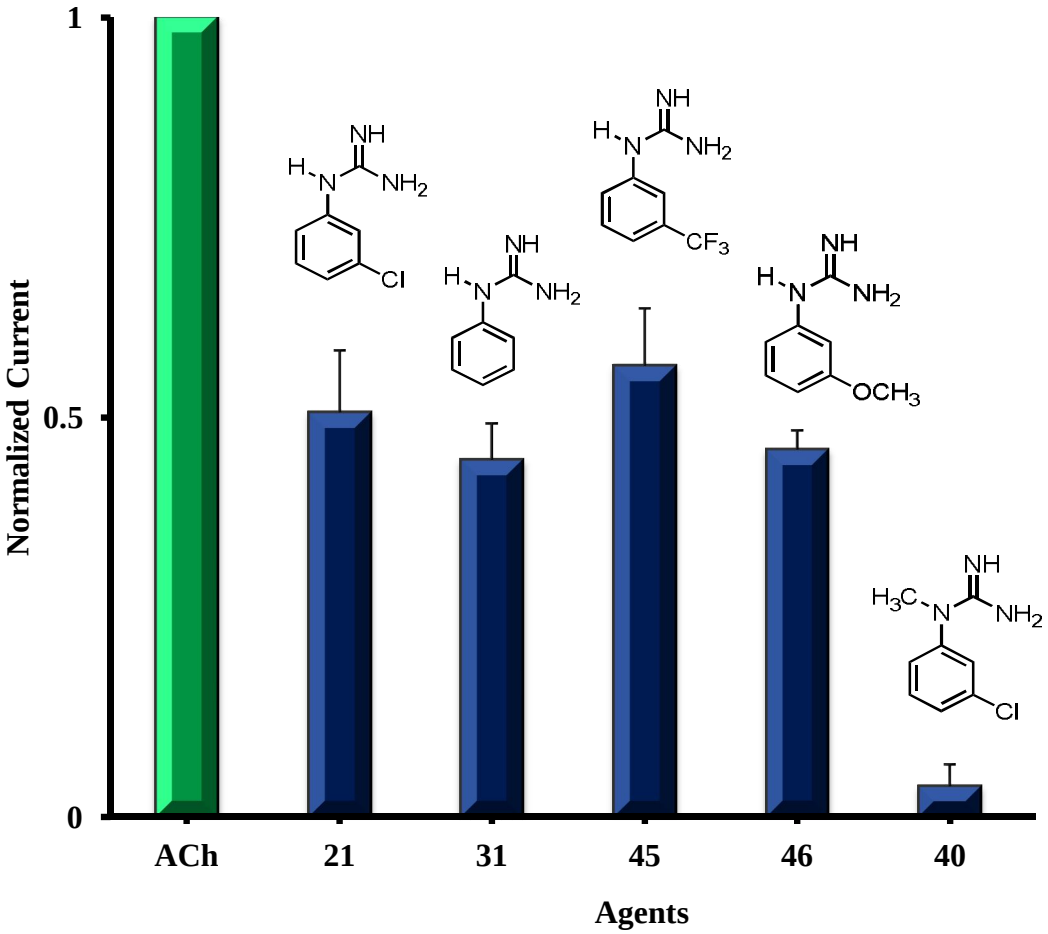

Figure 16. Mean effect of **21**, **31**, **40**, **45**, and **46** at 10 μM concentration on acetylcholine (ACh; EC_{50} = 280 μM) function at α7 nAChRs relative to ACh (normalized current = 1).

Based on the inhibitory activity at α7 nACh receptors of compounds **21**, **31**, **40**, **45**, and **46**, IC_{50} values were obtained (Table 2). The resulting IC_{50} values showed that when the chloro group of MD-354 (**21**) is removed, potency is decreased (i.e., **31**, IC_{50} = 34.84 μM). In the same manner, inhibitory potency is reduced when the chloro group of **21** is replaced with the more electron withdrawing group $–CF_3$ (i.e., **45;** IC_{50} = 18.46 μM). Compound **46** (IC_{50} = 7.54 μM), where $–OCH_3$ is an electron donating group at the 3-position of the phenyl ring, shows a potency comparable to that of MD-354 (**21**) at α7 nACh receptors, however, its low affinity at 5-HT_3 receptors makes **46** a more selective α7 nACh receptor inhibitor than **21**. A major increase in potency at α7 nACh receptors is shown by the N-methyl analog of MD-354 (i.e., **40**; IC_{50} = 1.26 μM) (Figure 17). Compound **40** exhibits more than 1,000-fold shift in selectivity (5-HT_3 receptor K_i = 6,200 nM) and higher potency at α7 nACh receptors compared to **21** (5-HT_3 receptor K_i = 35 nM).

Table 2. The IC_{50} values of MD-354 analogs for attenuation of an ACh-induced response at α7 nACh receptors, and their affinity for 5-HT_3 serotonin receptors.

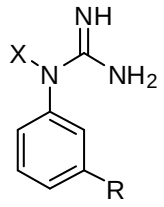

Compound	X	R	α7 nAChR IC_{50} ± SEM (μM)	5-HT_3 R K_i (nM)**
21	H	Cl	7.98*	35
31	H	H	34.84 ± 6.85	2,340
45	H	CF_3	18.46 ± 0.42	2,440
46	H	OCH_3	7.54 ± 0.74	1,600
40	CH_3	Cl	1.26 ± 0.26	6,200

* α7 nAChR IC_{50} value of **21** reported by Dukat et al.[9]

** 5-HT_3 receptor K_i values reported by Dukat et al.[65,73]

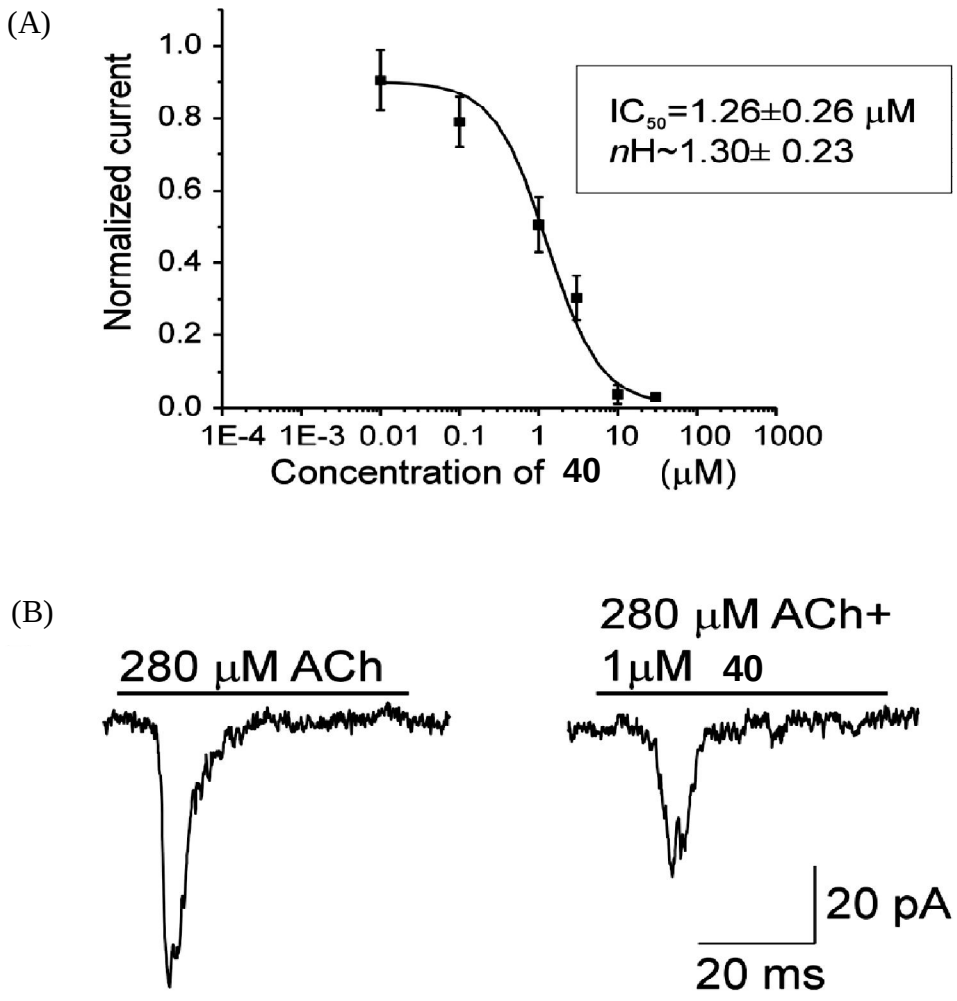

Figure 17. Functional description of the N-methyl analog of MD-354 (i.e., **40**) activity at α7 neuronal nAChRs. (A) Dose-dependent inhibition of **40** at α7 nAChRs. The Hill equation was applied to the curve, and the data were fit. Symbols and bars represent the mean ± SEM. (B) The inhibitory effect of **40** at a concentration of 1 μM. Holding potential in (A), and (B) was −80 mV.

The NAM activity of **40** was confirmed through the elimination of possible competitive antagonism activity (Figure 18A) and the elimination of possible channel blocking activity (Figure 18B).

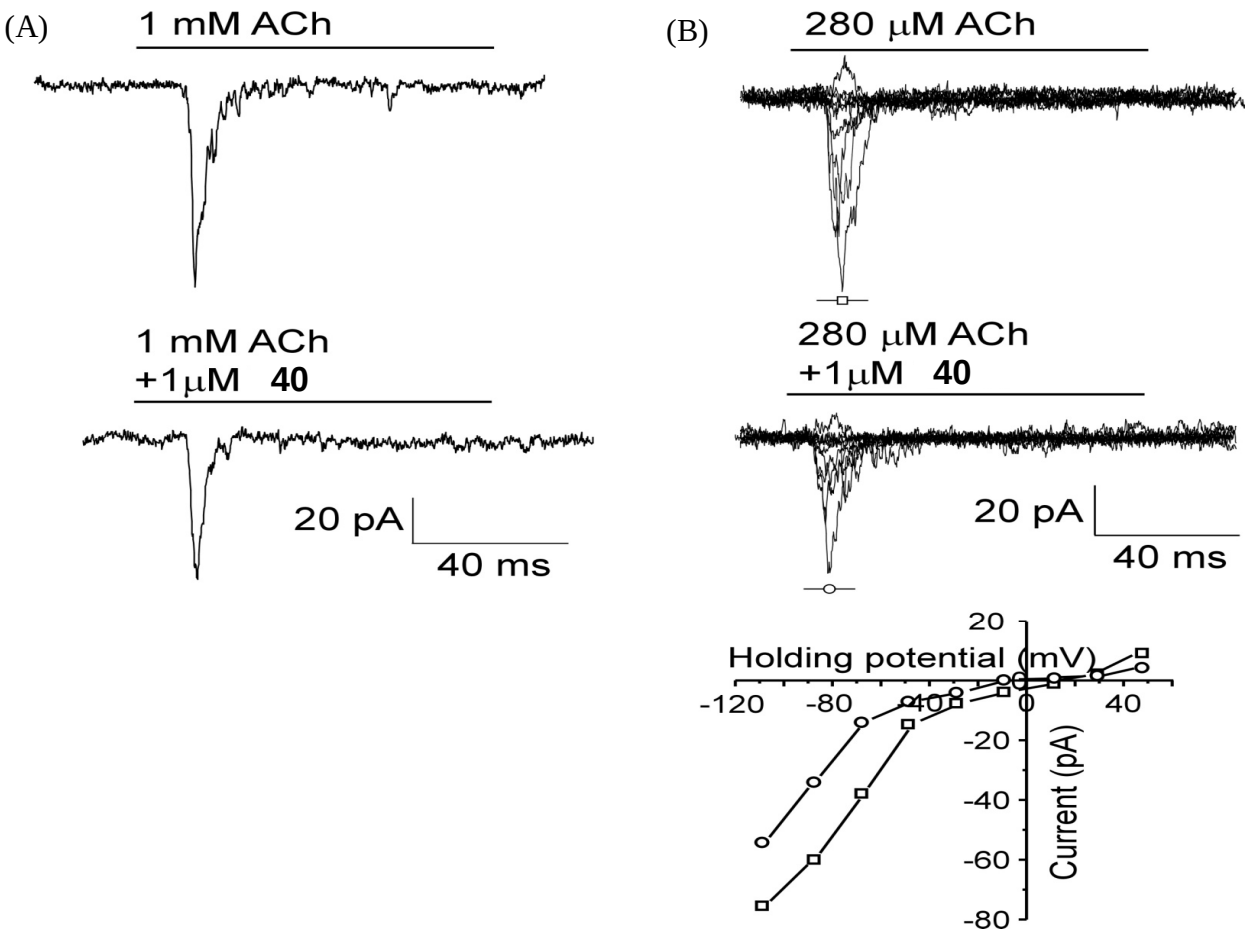

Figure 18. The inhibitory effects of **40** at 1 μM at α7 nAChRs. (A) The inhibitory effects of **40** on α7 nAChRs at an EC_{50} concentration of ACh (i.e., 280 μM) and at a saturated concentration of ACh (i.e., 1 mM). (B) The inhibitory effects at various holding potentials in the range from -100 to +60 mV. The upper part represents superimposed traces of the ACh-induced currents in the absence and presence of **40**. In the lower part, squares represent the maximal amplitude in the absence of **40** plotted versus the corresponding holding potential, whereas circles represent the maximal amplitude in the presence of **40** at a concentration around its IC_{50} value plotted versus the corresponding holding potential.

The activity of **21**, **31**, **40**, **45**, and **46** at a fixed concentration of 10 μM at α3β4 nACh receptors was investigated to test the selectivity of these compounds among nAChR subtypes (Figure 19). MD-354 (**21**) showed the lack of activity at 10 μM concentration on ACh-induced

currents at α3β4 nAChRs relative to ACh EC_{50} = 100 μM (Figure 20), whereas **31** and **40** slightly attenuated the ACh (EC_{50} = 100 μM)-evoked currents. Compounds **45** and **46** reduced the current of ACh to a different extent.

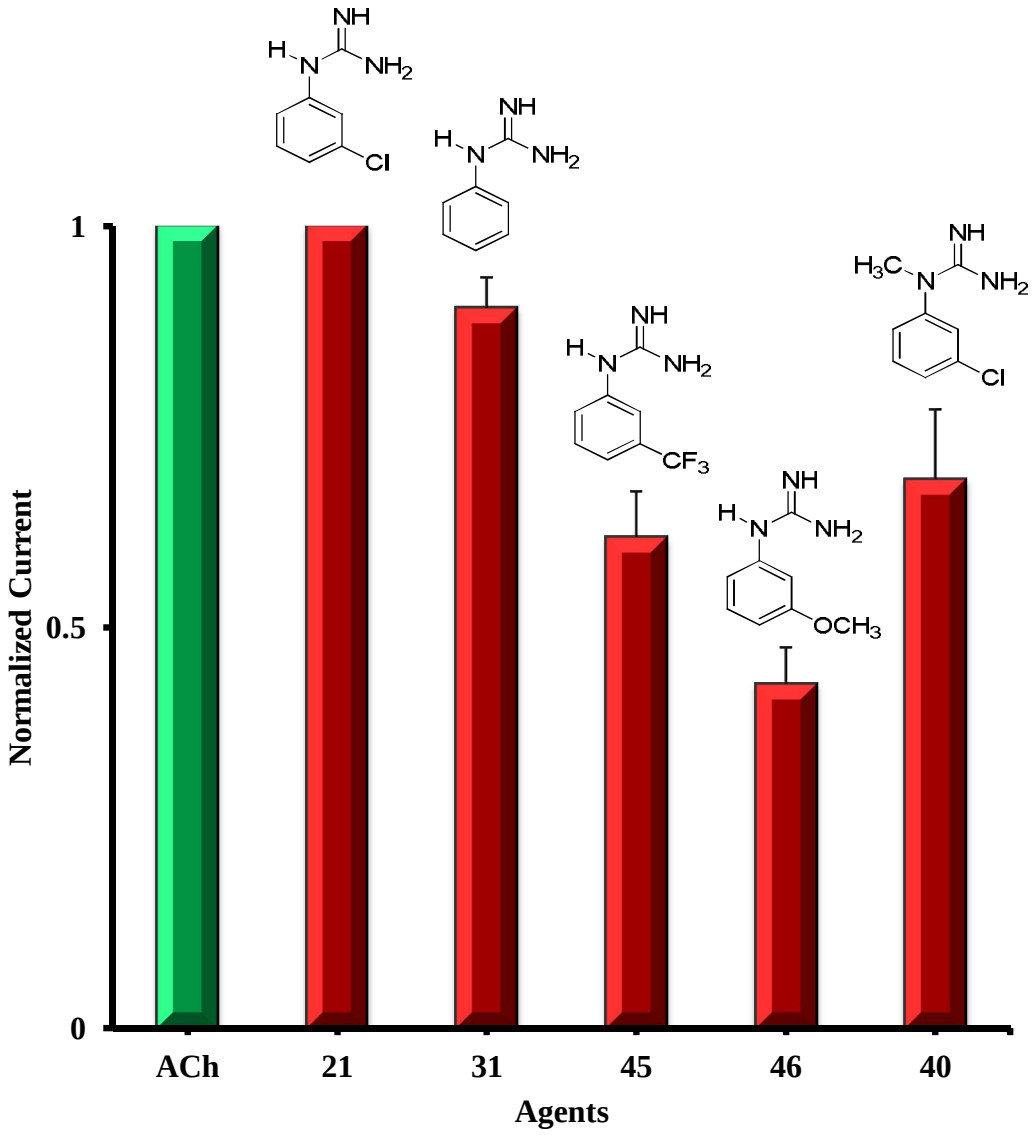

Figure 19. Mean effect of **21**, **31**, **40**, **45** and **46** at 10 μM concentration on acetylcholine (ACh) function at α3β4 nAChRs relative to ACh EC_{50} = 100 μM (normalized current = 1).

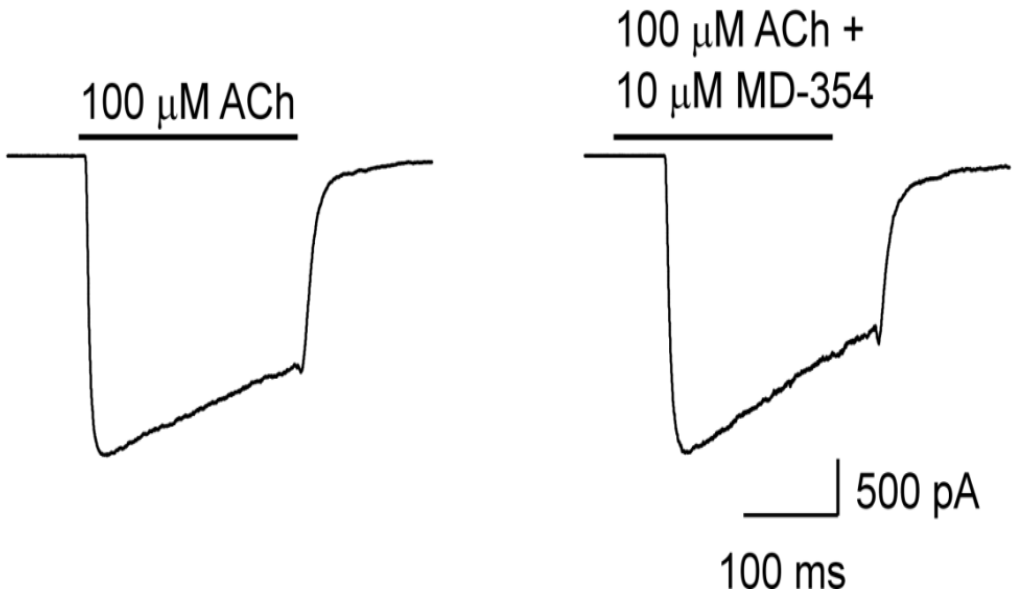

Figure 20. The inhibitory effect of MD-354 (**21**) at 10 μM concentration in representative cell expressing α3β4 nAChRs. Holding potential for these recordings was - 80 mV.

MD-354 (**21**) neither displayed affinity (K_i > 10,000 nM) nor possessed functional activity at α4β2 nAChRs. The activity of **21** as well as **40** at α4β2 was investigated as part of the selectivity test of these compounds among nAChR subtypes (Figure 21). Both compounds at concentrations comparable to the IC_{50} for α7 neuronal nACh receptors showed no activity on ACh induced-current (EC_{50} = 20 μM) at α4β2 nACh receptors. In addition, both compounds were examined for their agonist activity at α4β2 nACh receptors at their IC_{50} concentration and failed to mimic ACh actions.

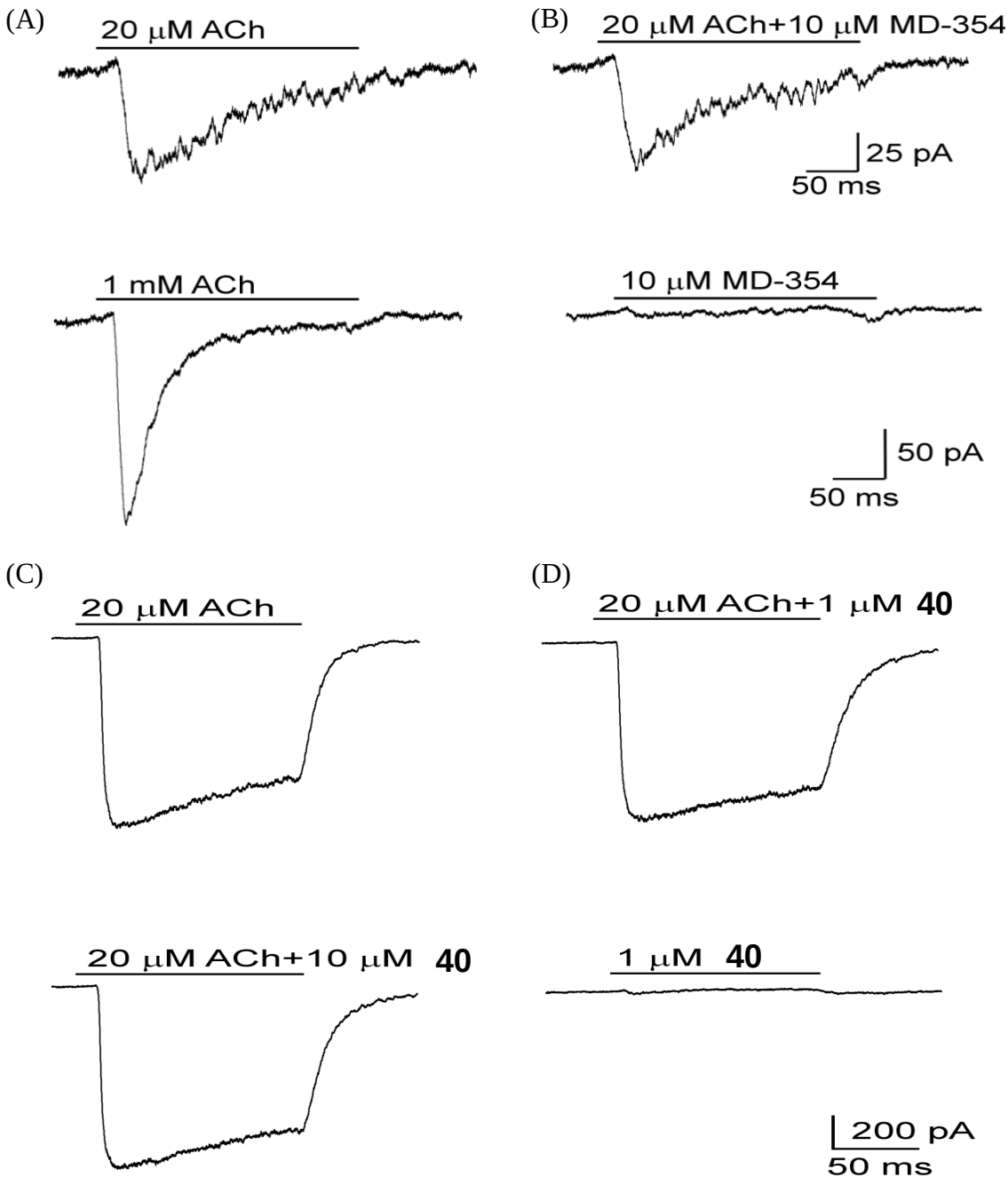

Figure 21. Effect of MD-354 (**21**) and **40** on α4β2 nAChRs. (A) Effect of ACh at EC_{50} = 20 μM and saturated concentration = 1 mM. (B) Effect of MD-354 (**21**) on ACh (EC_{50} = 20 μM) evoked-current and by itself at α4β2 nAChRs. (C) Effect of ACh (EC_{50} = 20 μM) alone and effect of ACh at EC_{50} = 20 μM accompanied by 10 μM of **40**. (D) Effect of **40** at 1 μM on ACh (EC_{50} = 20 μM) evoked-current and by itself at α4β2 nAChRs. Holding potential for these recordings was - 80 mV.

The biological data obtained above provide essential information on some of the compounds of interest. It also formed the bases for the need of further investigations to determine and optimize the required structural features of the small-molecule NAMs at α7 neuronal nAChRs.

C. Compound Optimization

Considering the functional data from MD-354 (**21**) and its N-methyl analog **40**, a new series of compounds was synthesized. The chloro group at the 3-position of *N*-(3-chlorophenyl)-*N*-methylguanidine (**40**) was replaced with a number of substituents considering the electronic, the lipophilic, and the steric nature of the new substituent (Table 3). In addition, the activity of any new modification at α7 nACh receptors will be compared to that determined for the same modification in the MD-354 series to test if parallel structural modification would result in parallel change in activity which might suggest whether or not the two series bind at the same manner (Table 3). The introduction of other halogen atoms (i.e., -F, -Br, and –I) at the 3-position will allow for testing mainly the effect of substituent size variation over a relatively fixed range of electron-withdrawing effects. A recent study on a number of structurally related α7 nACh receptor modulators described the diverse impact of different halogen atoms at the same ring position on the compound pharmacological properties.[83] That is, the replacement of a bromine atom in the *para* position of an aromatic ring of an allosteric agonist with an iodine atom or a chlorine atom resulted in PAM activity with different levels of desensitization, activation rates, and inactivation rates, whereas a fluorine atom at the same position antagonized the allosteric agonist effect of the *para*-bromo compound. Furthermore, replacement of the chloro group with -

CH_3 or -OCH_3 groups as electron donating groups, as well as being lipophilic substituents, will explore the effect of such modification on activity.

Table 3. Structural representation and substituent constants of the new N-methyl series and the MD-354 series of arylguanidines.

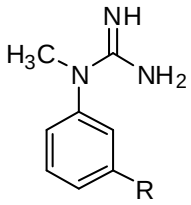

N-methyl Series

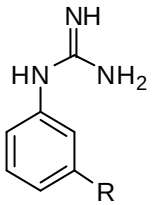

MD-354 Series

Compound	R	π^a	σ_m [a]	Compound
40	Cl	0.71	0.37	**21**
50	H	0.00	0.00	**31**
51	Br	0.86	0.39	**56**
52	F	0.14	0.34	**57**
53	I	1.12	0.35	**58**
54	CH_3	0.56	-0.07	**59**
55	OCH_3	-0.02	0.12	**46**

[a] π and σ_m aromatic R substituent constants reported by Hansch et al.[84]

The *N*-methyl-*N*-phenylguanidines (with the exception of **53**) were synthesized as described in Scheme 2. The targeted compounds were unknown except for *N*-methyl-*N*-phenylguanidine hydrochloride (**50**).[85] The process of synthesis consisted of a one-step reaction for compounds *N*-methyl-*N*-phenylguanidine hydrochloride (**50**), *N*-(3-bromophenyl)-*N*-methylguanidine hydrochloride (**51**), *N*-(3-fluorophenyl)-*N*-methylguanidine hydrochloride (**52**),

and *N*-(3-methoxyphenyl)-*N*-methylguanidine hydrochloride (**55**) where the appropriate anilines (i.e., **60** – **64**; Scheme 2) were heated at reflux with cyanamide in absolute ethanol. The hydrochloride salt of *N*-(3-methylphenyl)-*N*-methylguanidine (**54**) was converted to the nitrate salt with ammonium nitrate. The structure of *N*-methyl-*N*-phenylguanidine hydrochloride (**50**) was confirmed by IR, ^{1}H NMR, and melting point, whereas the structures of the remaining compounds were confirmed by IR spectrometry, ^{1}H NMR spectrometry, and elemental analysis for C, H, N.

Scheme 2.[a]

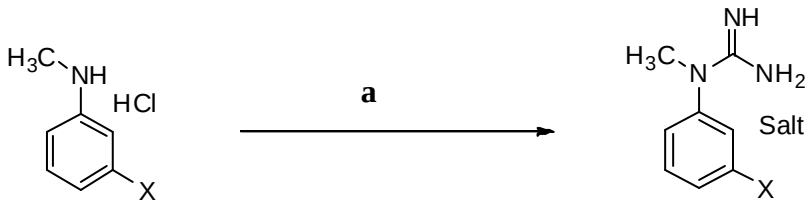

X	Compound
–H	**60**
-Br	**61**
-F	**62**
$-CH_3$	**63**
$-OCH_3$	**64**

X	Salt	Compound
–H	HCl	**50**
-Br	HCl	**51**
-F	HCl	**52**
$-CH_3$	HNO_3	**54**
$-OCH_3$	HCl	**55**

[a]Reagents and conditions: a. i) NH_2CN, EtOH, reflux; ii) (only to **54**) NH_4NO_3, H_2O.

N-(3-Iodophenyl)-*N*-methylguanidine hydrochloride (**53**) was prepared as described in Scheme 3. This was an unknown compound at the time of synthesis, but was prepared according to a literature procedure for a similar compound.[85,86] The first step of this reaction is a one-pot procedure in which a mixture of 3-iodoaniline (**65**) and trimethyl orthoformate (**66**) was heated at 120 °C in the presence of sulfuric acid. In a rearrangement step, the mixture was then heated at 170 °C that resulted in an *N*-methylformanilide intermediate. 3-Iodo-*N*-methylaniline (**67**) was obtained by heating the *N*-methylformanilide intermediate at reflux with an aqueous solution of HCl. The final step was performed by heating the ethanolic solution of **67** at reflux with cyanamide to give **53.** The desired compound was confirmed by IR spectrometry, ^{1}H NMR spectrometry, and elemental analysis for C, H, N.

Scheme 3.[a]

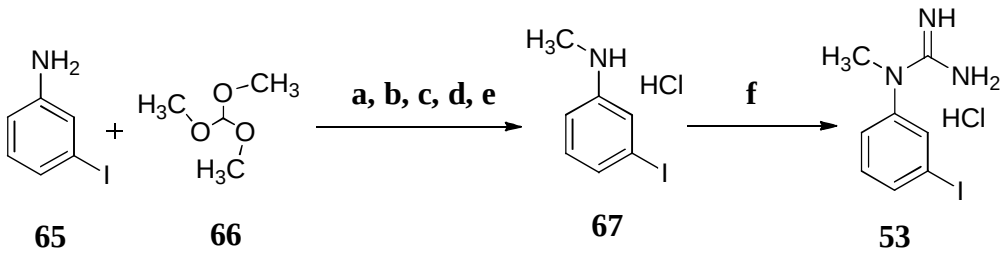

65 **66** **67** **53**

[a]Reagents and conditions: a. Sulfuric acid (concentrated solution), heat (120 °C); b. Heat (170 °C); c. HCl, H_2O, reflux; d. NaOH, H_2O; e. HCl/absolute EtOH; f. NH_2CN, absolute EtOH, reflux.

The necessity of introducing the N-methyl series was also to test whether or not the two series interact with α7 nACh receptors in a similar manner depending in the fold difference in biological data obtained. For this reason, the inhibitory activity of **50** at α7 nACh receptors was

tested and together with the inhibitory activity of compound **40** from the new N-methyl series were selected to be compared with that of **21** and **31** of the MD-354 series (Figure 22) (Table 4).

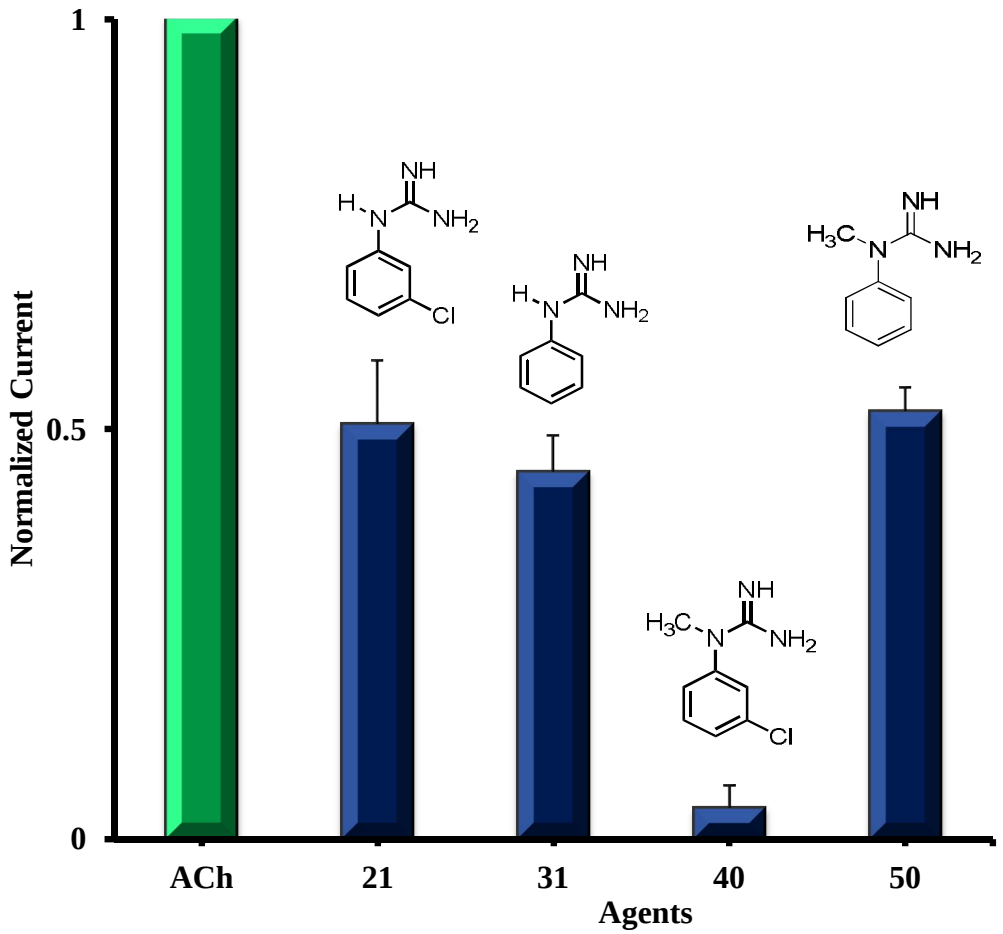

Figure 22. Mean effect of **21**, **31**, **40**, and **50** at 10 μM concentration on acetylcholine (ACh; EC_{50} = 280 μM) function at α7 nAChRs relative to ACh (normalized current = 1).

Table 4. The IC_{50} values of **21**, **31**, **40**, and **50** for α7 nACh receptors.

Compound	IC_{50} ± SEM (μM)	Compound	IC_{50} ± SEM (μM)
21	7.98*	**40**	1.26 ± 0.26
31	34.84 ± 6.85	**50**	30.81 ± 2.13

* α7 nAChR IC_{50} value of **21** reported by Dukat et al.[9]

The functional data on two compounds of each series (i.e., **21** and **31** of MD-354 series, and **40** and **50** of the new N-methyl series) revealed the inhibitory activity of these compounds at α7 nACh receptors. The number of compounds tested here might not be sufficient to decide that the N-methyl series binds in the same manner with α7 nAChRs as MD-354 series. The possibility that the N-methyl series might bind to a different allosteric site than that of the MD-354 series, or the N-methyl series could bind to the same allosteric site as that of the MD-354 series remains to be considered.

Data for compounds **51**, **52**, **54**, and **55** were not available at the time this thesis was being written. Studies are currently underway.

D. Molecular Modeling

All the previous functional data were used in the molecular modeling studies to speculate the possible location of the binding site as well as the mode of interaction by which small-molecule NAMs exerts their effect at α7 nACh receptors.

1. Alignment of Sequences and Model Construction

The sequences adopted in this project were obtained from the Protein Knowledgebase (UniProtKB). Alignment of the ECD portion of three nAChR species (i.e., human α7 nAChR, rat α7 nAChR, and mouse α1 nAChR) was performed using the ClustalX program as an initial step toward the construction of the human α7 nAChR ECD model (Figure 23). An alignment was established to identify and match conserved residues between the human α7 nAChR the template mouse α1 nAChR ECDs.

Important regions in the aligned sequences were identified including the loops A, B, C, D, E, and F that primarily formed the orthosteric binding sites in these receptors. Other important amino acids including Trp171, Tyr115, Tyr217, the two cysteine residues (i.e., Cys150 and Cys164) forming the disulfide bond characterizing the Cys-loop, and the adjacent two cysteine residues (Cys212 and Cys213) forming the disulfide bond at the C loop were also matched.

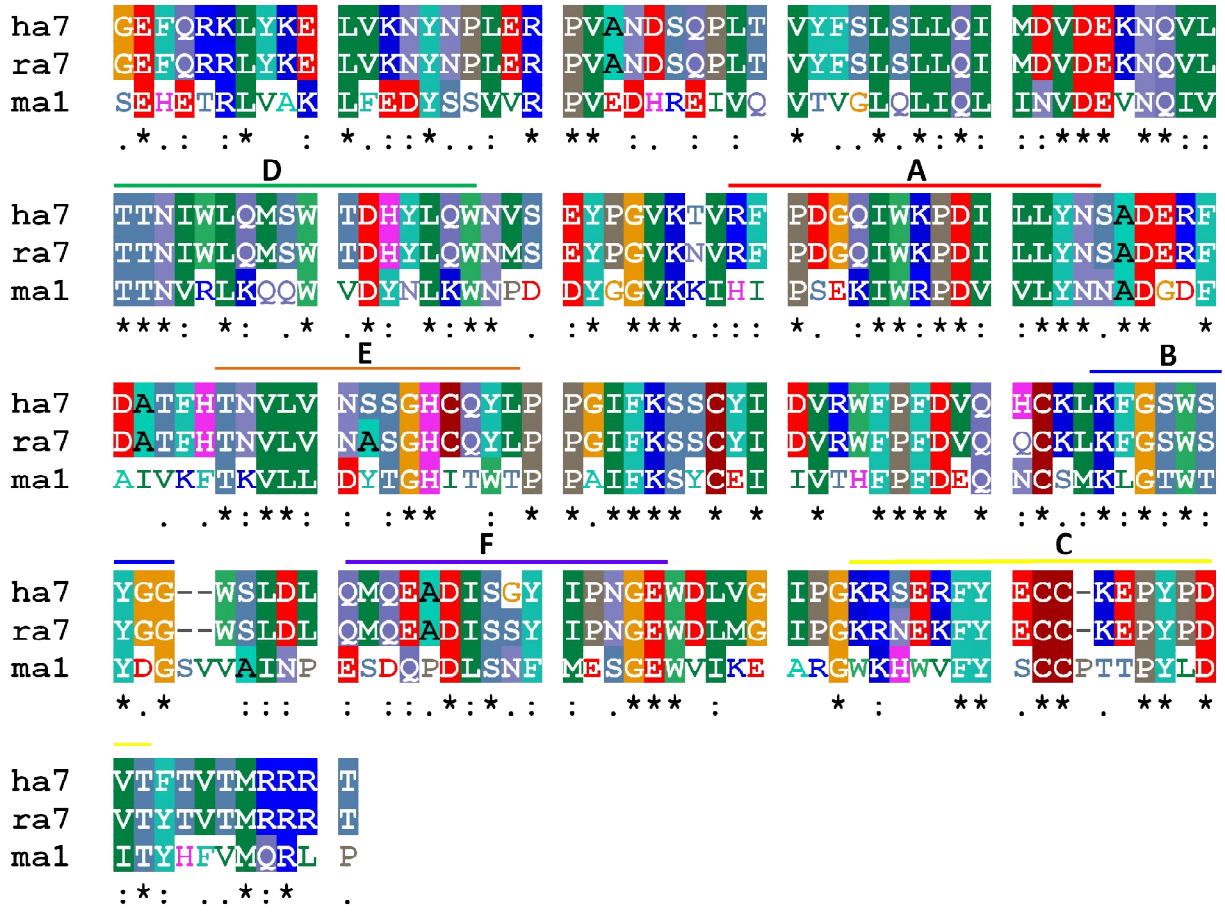

Figure 23. Sequence alignment of the ECD portion of three nAChR species. The asterisks (*) indicate conserved amino acids, whereas the colons (:) and periods (.) indicate strongly and weakly conserved amino acids, respectively. The main loops in the ECD are represented by the colored lines.

The construction of the homology model of the human α7 nAChR ECD was based on the crystal structure of the ECD of the mouse α1 nAChR subunit bound to α-bungarotoxin at 1.94 Å resolution (PDB ID 2QC1).[32] The template shares a high degree of homology with the human α7 nACh receptor subunit (38%) compared with the AChBP of *Lymnaea stagnalis* (24%).[87] However, a recent study revealed the crystal structure of the ECD of a receptor chimera

constructed from the human α7 nAChR and the AChBP of *Lymnaea stagnalis*.[88] The new crystal structure shares 64% sequence identity with the native α7 nACh receptor ECD.

The three-dimensional structures of 100 models of human α7 nAChR ECDs were built by homology modeling in the form of one monomer using Modeller 9.7. Script was used to rejoin disulfide bonds and to form dimers by copying each model and merging each copy to the original monomer based on dimers available from the AChBP crystal structure. Since α7 nACh receptors are homomeric and the orthosteric binding site is located between each two subunits, dimer formation provided the essential part of the ECD for the molecular modeling study.

2. Structural Validation

As part of the model validation procedure, known α7 nACh receptor agonists (ACh (**1**), nicotine (**2**), and epibatidine (**5**)) were docked in a directed docking experiment (i.e., 10 Å from the C_α of Trp171) and it was verified that the ligands bind properly to the orthosteric binding site. GOLD docking was able to place ACh (**1**), nicotine (**2**), and epibatidine (**5**) in similar locants as reported in crystal structures.[38,79,80] A common model amongst 100 with all three ligands docked was selected as the candidate model for orthosteric agonists. The resultant docking solutions were subjected to an energy minimization step that was constructed using the Tripos Force Field (Gasteiger–Hückel charges, distance-dependent dielectric constant = 4.0). The stereochemistry of the candidate α7 ECD model was examined by PROCHECK analysis and a Ramachandran plot of the model was generated (Figure 24). In the Ramachandran plot, amino acids falling in the red region are most favored, in the yellow region are additionally

allowed, in lighter yellow regions are generously allowed, and in the white region are disallowed. The Ramachandran plot showed that 93.6% of the residues were in the most favored regions, 5.8% of residues were in additionally allowed regions, 0.3% of residues were in the generously allowed regions, and only 0.3% of the residues were in disallowed regions. Glu120 appeared in the disallowed region and is located in the lining face of the receptor channel in an area away from the orthosteric binding site. The amino acid residues' bond angles, bond lengths, and torsion angles were analyzed by the ProTable module in SYBYL. The docking solutions were analyzed based on crystal structures of those agonists in complex with AChBPs (PDB ID: 2XZ5 , 1UW6, and 2BYQ).[38,79,80] Selected residues from the orthosteric binding site of the α7 nAChR ECD model and the AChBP crystal structure were used for alignment and the root-mean-square deviation (RMSD) was examined to test the validation of the candidate model for each agonist. Amino acids at the C loop were not included since the constructed models were based on the crystal structure of the mouse α1 nAChR ECD subunit bound to the antagonist α-bungarotoxin (i.e., closed state) where extension of the loop C causes difficulty in mimicking the loop orientation in the generated models.

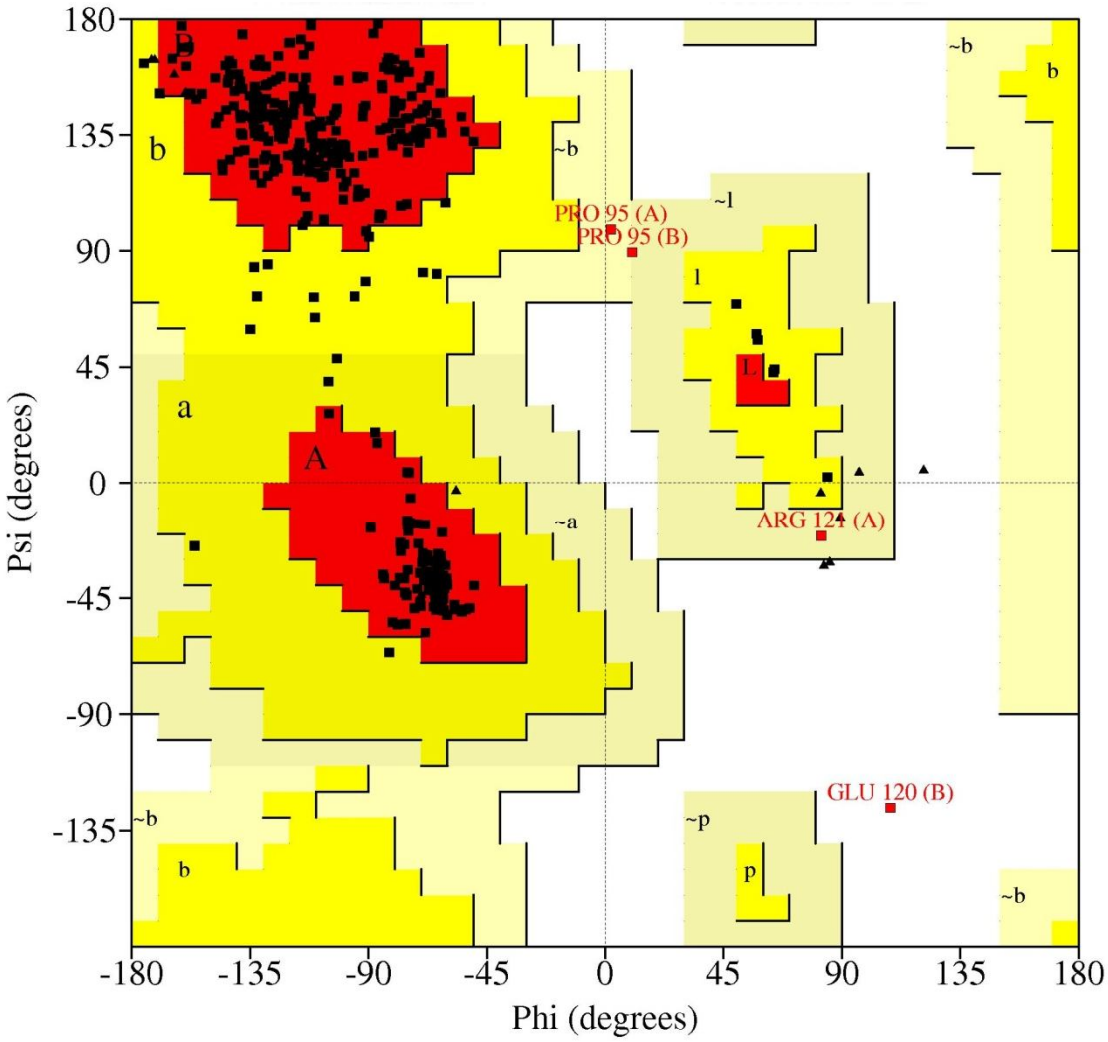

Figure 24. A Ramachandran plot of the candidate α7 nAChR ECD model for agonists. Phi and psi represent the backbone conformation angles of the amino acids.

ACh (**1**)-docked poses were visually inspected taking into consideration the GoldScore fitness function to select the final solution. The backbone residues involved in the binding pocket were aligned to that of the corresponding residues in the crystal structure of the AChBP (PDB ID: 2XZ5) and the calculated RMSD was 0.6 Å (Table 5). Similar interactions of ACh in both the candidate model and the AChBP crystal structure were observed which includes a cation-π

interaction between the quaternary amine group in ACh and the conserved Trp171 residue from the B loop (Figure 25).

Table 5. Amino acids from the ACh α7 nAChR ECD model and the AChBP crystal structure that are involved in the orthosteric binding site that were used in alignment and RMSD calculations.

α7 nAChR ECD model		**AChBP***	
Principal or (+) face	**Complementary or (-) face**	**Principal or (+) Face**	**Complementary or (-) face**
Tyr115	Gln139	Tyr91	Met114
Trp171	Leu141	Trp145	Ile116
Ser172		Val146	
Tyr210	Excluded C loop residues in RMSD calculation	Tyr186	Excluded C loop residues in RMSD calculation
Cys212		Cys188	
Cys213		Cys189	
Tyr217		Tyr193	

* AChBP crystal structure reported by Brams et al.[79]

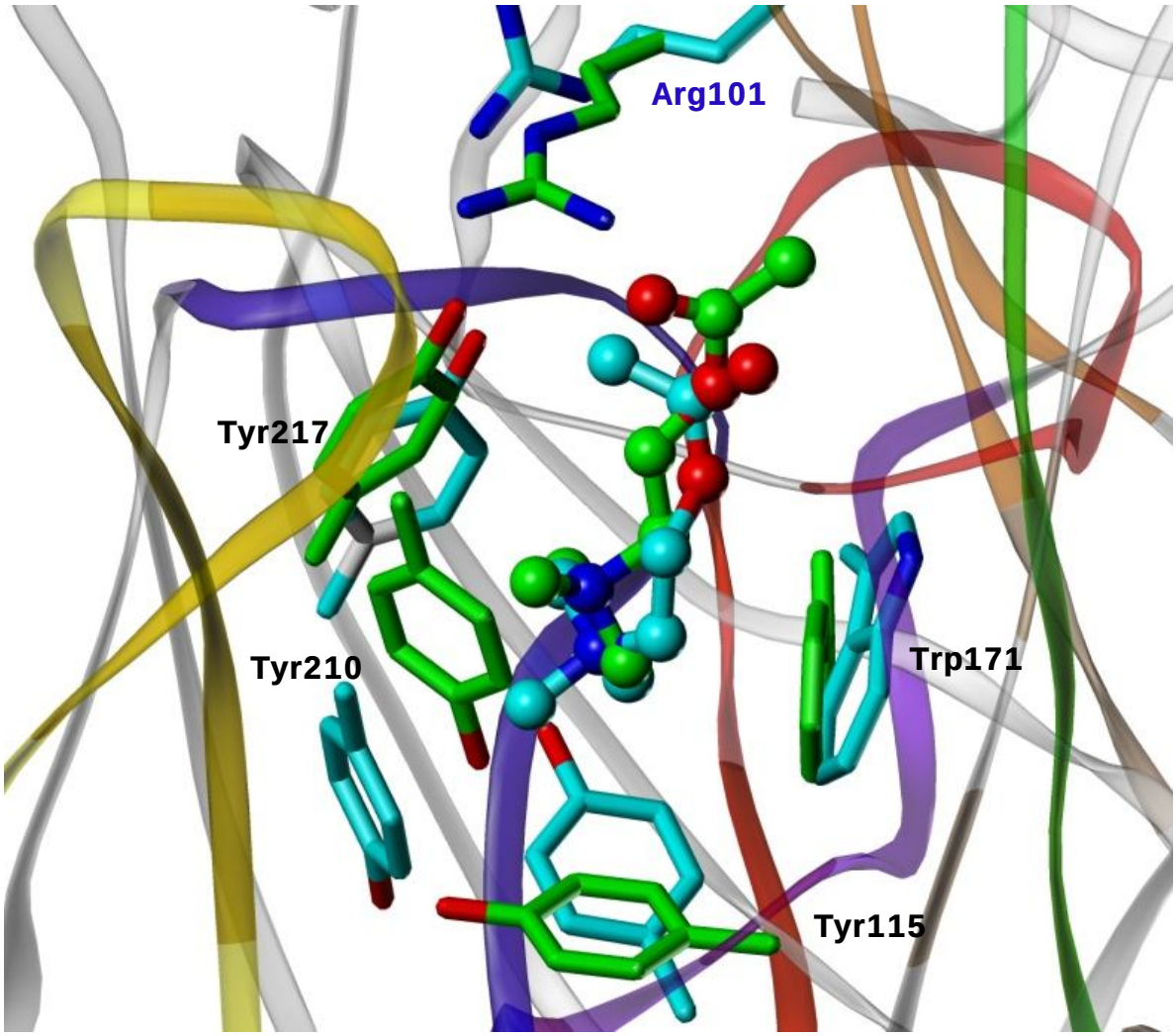

Figure 25. The binding mode of docked ACh in the α7 nAChR ECD model (rendered as green ball-and-stick model) aligned to the AChBP crystal structure in complex with ACh (rendered as cyan ball-and-stick model). Residues labeled in black represent the principal face, whereas residues labeled in blue represent the complementary face.

Nicotine (**2**)-docked poses were visually inspected taking into consideration the GoldScore fitness function to select the final solution. The backbone of residues involved in the binding pocket were aligned with that of the corresponding residues in the crystal structure of the

AChBP (PDB ID: 1UW6) and the calculated RMSD was 0.5 Å (Table 6). Similar interactions of nicotine in both the candidate model and the AChBP crystal structure were observed; however, a cation-π interaction between the cationic amine group in the pyrrolidine ring of nicotine and the conserved Trp171 from the B loop in the crystal structure was not observed in the docked model (Figure 26).

Table 6. Amino acids from the nicotine α7 nAChR ECD model and the AChBP crystal structure that are involved in the orthosteric binding site used in alignment and RMSD calculations.

α7 nAChR ECD model		**AChBP***	
Principal or (+) face	**Complementary or (-) face**	**Principal or (+) face**	**Complementary or (-) face**
Tyr115	Trp77	Tyr98	Trp53
Trp171	Leu141	Trp143	Met114
Tyr210	Excluded C loop residues in RMSD calculation	Tyr185	Excluded C loop residues in RMSD calculation
Cys212		Cys187	
Cys213		Cys188	
Tyr217		Tyr192	

* AChBP crystal structure reported by Celie et al.[80]

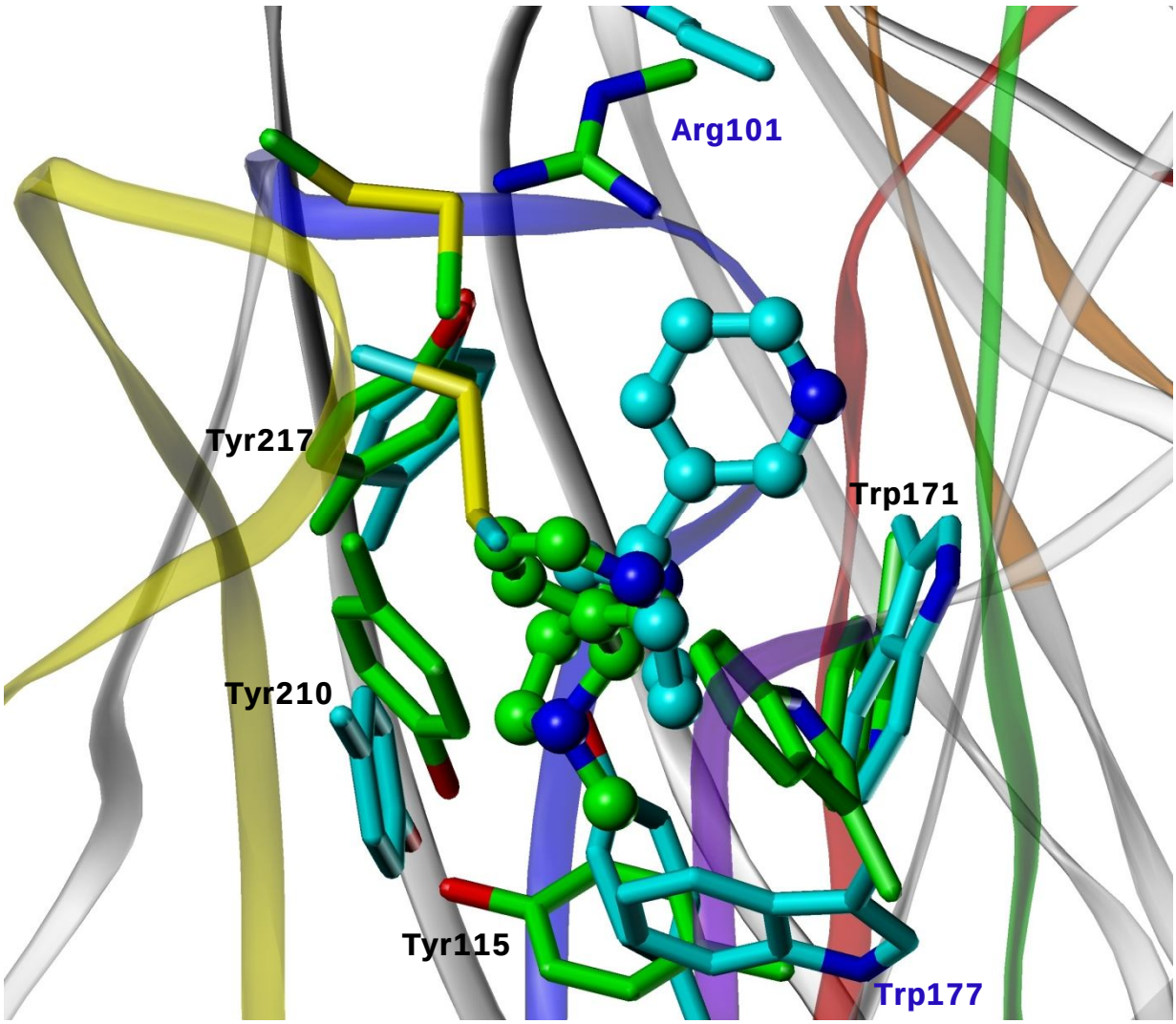

Figure 26. The binding mode of docked nicotine in the α7 nAChR ECD model (rendered as green ball-and-stick model) aligned to the AChBP crystal structure in complex with nicotine (rendered as cyan ball-and-stick model). Residues labeled in black represent the principal face, whereas residues labeled in blue represent the complementary face.

The docked poses of epibatidine (**5**) in the candidate model were subjected to the process of inspection and evaluation to select the final solution. The backbone residues involved in the binding pocket were aligned to that of the corresponding residues in the crystal structure of

AChBP and the calculated RMSD was 0.8 Å (Table 7). Similar interactions of epibatidine in both the candidate model and the AChBP crystal structure were observed which included a cation-π interaction between the cationic amine group in the azabicyclo[2.2.1]heptane system of epibatidine and the conserved Trp171 from the loop B (Figure 27).

Table 7. Amino acids from the epibatidine α7 nAChR ECD model and the AChBP crystal structure that are involved in the orthosteric binding site used in alignment and RMSD calculations.

α7 nAChR ECD model		**AChBP***	
Principal or (+) face	**Complementary or (-) face**	**Principal or (+) face**	**Complementary or (-) face**
Tyr115	Gln139	Tyr91	Met114
Trp171	Leu141	Trp145	Ile116
Ser172		Val146	
Tyr210	Excluded C loop residues in RMSD calculation	Tyr186	Excluded C loop residues in RMSD calculation
Cys212		Cys188	
Cys213		Cys189	
Tyr217		Tyr193	

* AChBP crystal structure reported by Hansen et al.[38]

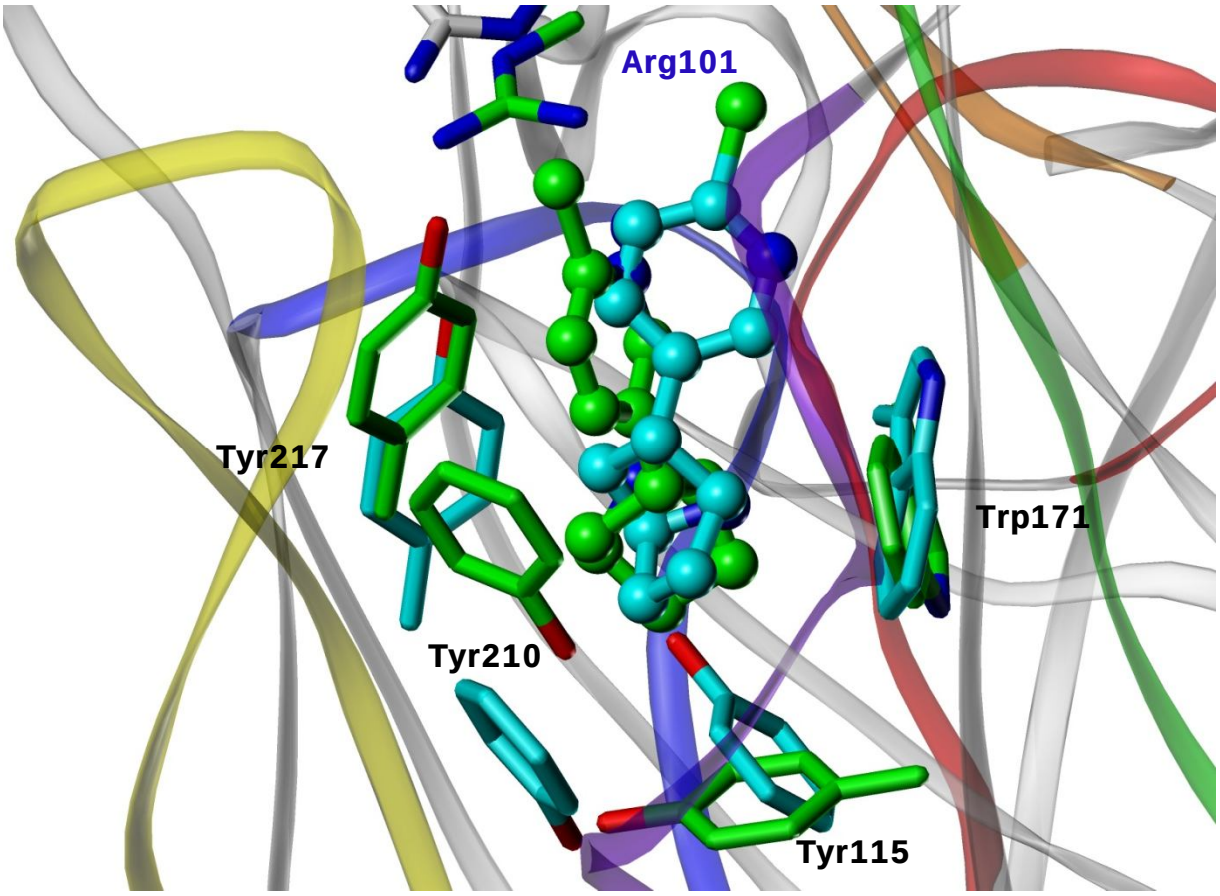

Figure 27. The binding mode of docked epibatidine in the α7 nAChR ECD model (rendered as green ball-and-stick model) aligned to the AChBP crystal structure in complex with epibatidine (rendered as cyan ball-and-stick model). Residues labeled in black represent the principal face, whereas residue labeled in blue represent the complementary face.

Based on the docking poses of the agonists (ACh (**1**), nicotine (**2**), and epibatidine (**5**)), models generated showed docking results that are sufficiently close to the crystal structural findings. Then validation targeting the closed state of the receptor using the α7 nAChR antagonist was constructed. The α7 nAChR antagonist MLA (**11**) was docked to the original 100 models and the docked poses were visually inspected taking into consideration the GoldScore fitness function to select the final model and docking solution to be compared to the crystal

structure of MLA in complex with the AChBP.[38] The MLA structure in the candidate model was aligned to that of the crystal structure of the AChBP (PDB ID: 2BYR) and the calculated RMSD was 1.0 Å (Figure 28).

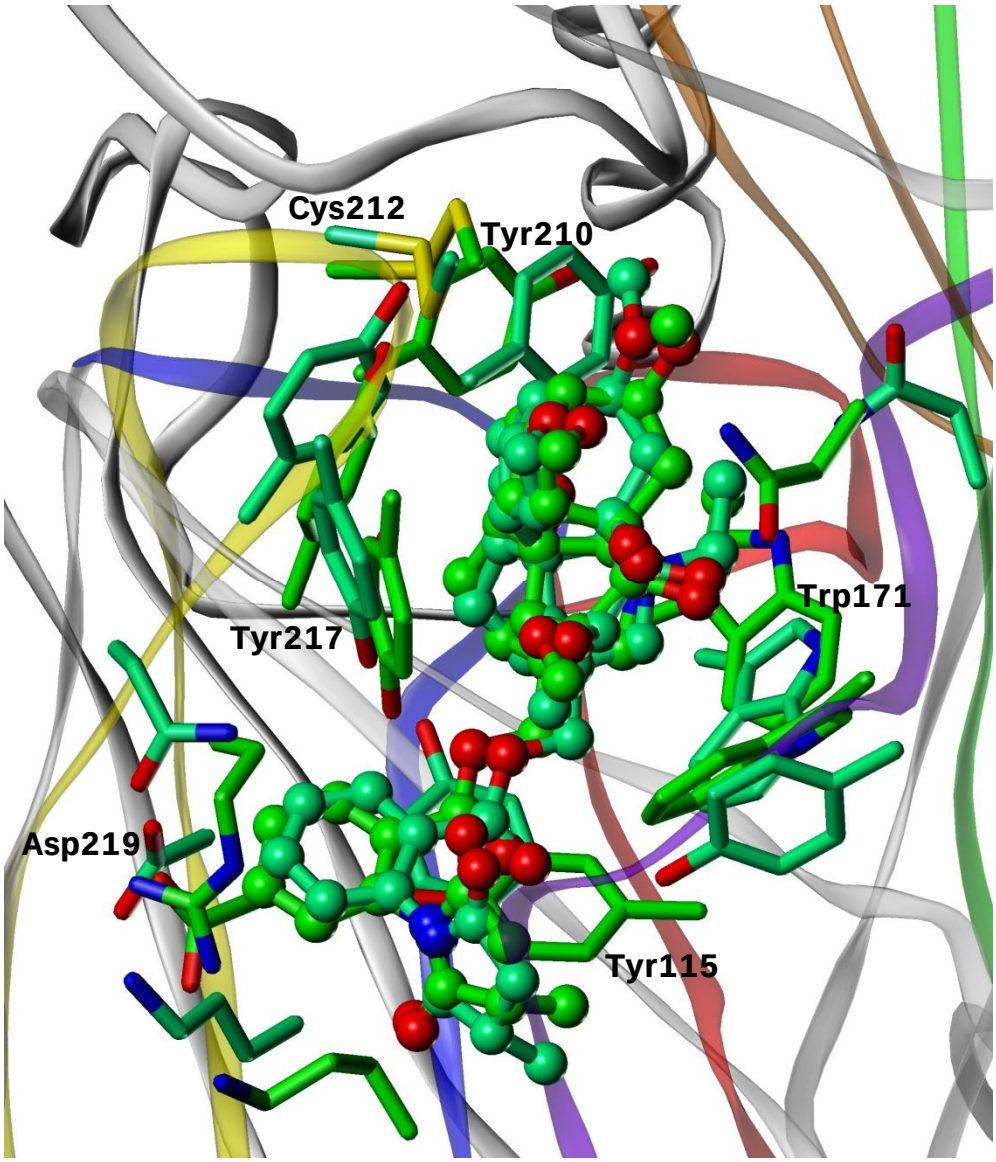

Figure 28. The binding mode of docked MLA in the α7 nAChR ECD model (rendered as green ball-and-stick model) aligned to the AChBP crystal structure in complex with MLA (rendered as cyan ball-and-stick model). The high degree of alignment between the two MLA molecules can be seen. Interacting residues are primarily formed by the principal face.

The high degree of alignment between MLA in the candidate α7 nAChR ECD model and the MLA in AChBP crystal structure was expected since the template ECD of the mouse α1 nAChR subunit was crystallized with the antagonist α-bungarotoxin (i.e., closed state). A Ramachandran plot was generated and the plot showed that 79.4% of the residues were in most favored regions, 23.1% of residues were in the additionally allowed regions, 0.5% of residues were in the generously allowed regions, and none of the residues were in disallowed regions (Figure 29).

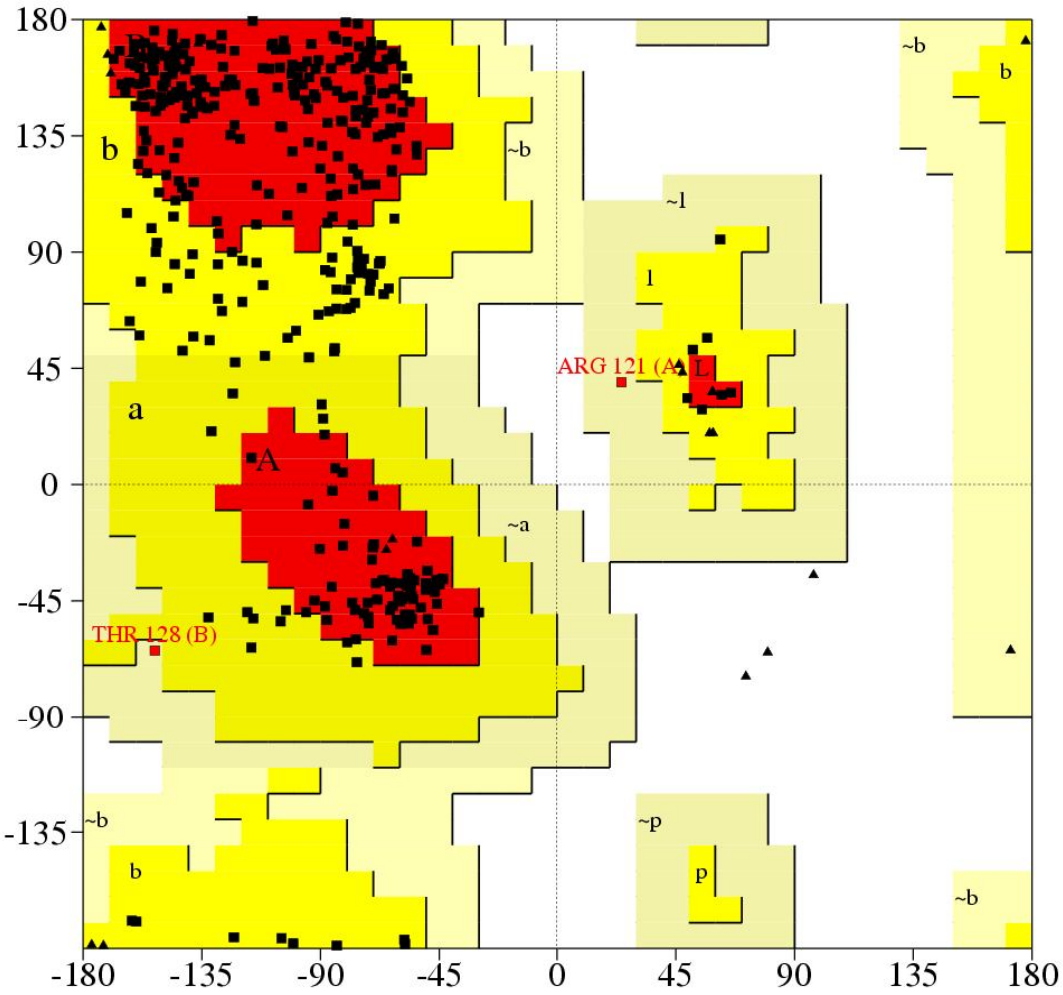

Figure 29. A Ramachandran plot of the candidate α7 ECD nAChR model for antagonists. Phi and psi angles represent the backbone conformation of the amino acids.

After validation of the α7 ECD nACh receptor models in the open and closed state, the process of exploring and targeting the allosteric sites were initiated in an effort to explain the activity of MD-354 (**21**) as well as **40** as NAMs at α7 nACh receptors. The procedure started with allosteric site identification step to speculate the putative binding site.

3. Identification of Allosteric Binding Sites

The identification of five initial cavities was obtained through the blind docking feature of AutoDock 4.1 using Gal (**16**) as well as the Connolly surface feature of SYBYL 8.1 and a systematic cavity search using the hydrophobic interaction (HINT) program. Two out of the five explored cavities showed a possibility of accommodating small-molecule NAMs as interaction site(s) at the ECD of α7 nAChRs and these were supported by empirical data.[56,59] The first cavity (Figure 30) is characterized by a Thr197 (chimeric chicken α7/mouse 5-HT_3 receptor-channel complex) mutagenesis study and the residue is located right below the orthosteric binding site.[59] The second cavity (Figure 31) is characterized by Lys125 (*Torpedo* nAChR) in a photoaffinity labeling study as the target of allosteric potentiating ligands (APLs).[56] Amino acid residues lining both sites were identified (Table 8), and were in agreement with the previous reported residues lining these two putative allosteric sites by Luttmann et al.[89]

Table 8. List of amino acid residues lining allosteric sites 1 and 2.

	Allosteric Site 1	**Allosteric Site 2**
Principal or (+) face	Tyr115, Asn116, Ser117, Ser148, Ser149, Cys150, Cys164, Lys165, Leu166, Lys167, Tyr218, Thr221[a].	Met63, Asp64, Asp66, Asn69, Val71, Thr73, Asn75, Asp119, Glu120, Asp123, Ile145, Lys171[b].
Complementary or (-) face	Leu60, Gln61, Asn75, Gly189, Tyr190, Ile191.	Met63, Asp64.

[a] Thr221 corresponds to the reported Thr197 in the mutagenesis study.[59]
[b] Lys171 corresponds to the reported Lys125 in the photoaffinity labeling study.[56]

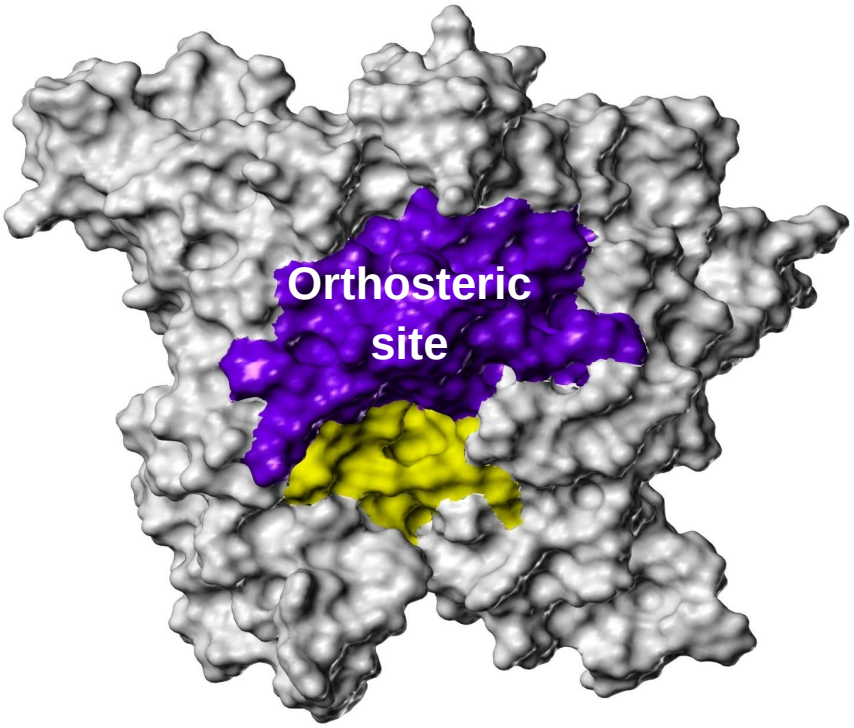

Figure 30. The location of the first identified allosteric cavity (yellow) below the orthosteric site (blue) in the ECD model of the α7 nAChR.

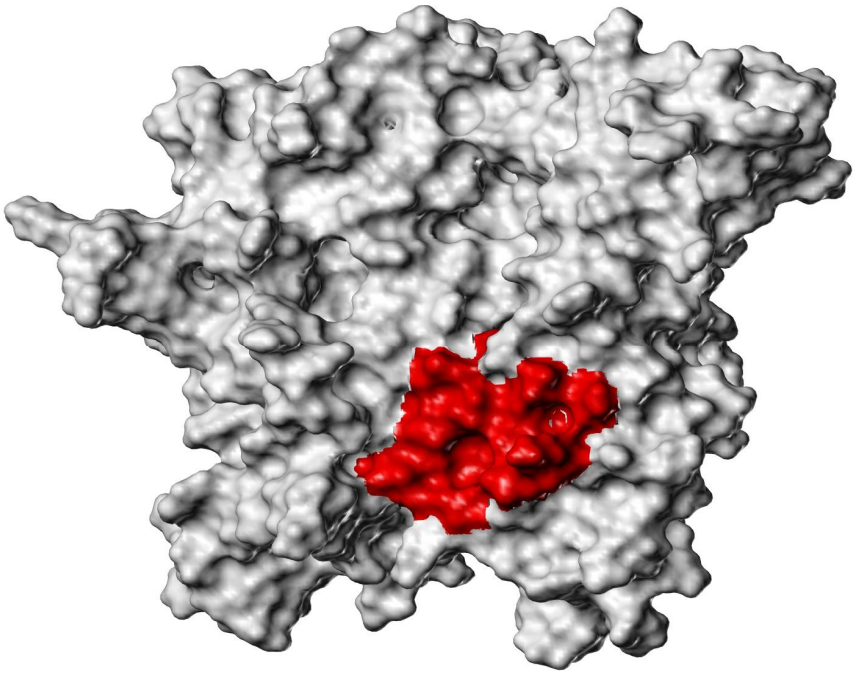

Figure 31. The location of the second identified allosteric cavity (red) on the internal side of the receptor channel in the ECD model of the α7 nAChR.

The functional data differences between MD-354 (**21**) and **40** could arise either from the differences in the binding site or in the mode of action of the molecule. To investigate that, structural preparation was necessary to determine the favorable low-energy conformation of both compounds.

4. Structural Preparation for Docking

Earlier in our laboratory, a computational structural investigation on MD-354 (**21)** resulted in four rotameric conformations.[90] The same systematic search algorithm was applied (semi-empirical molecular orbital AM1 calculations) to identify possible low-energy rotamers of **40** (Figure 32). Four low-energy rotamers of **40** were identified and computationally prepared

for docking; (+/-) synclinial (sc), (+/-) anticlinial (ac) (Figure 32). Each rotamer of MD-354 (**21**) and **40** was docked in allosteric site 1 and 2 to cover the possible conformations that might interact with α7 nACh receptors.

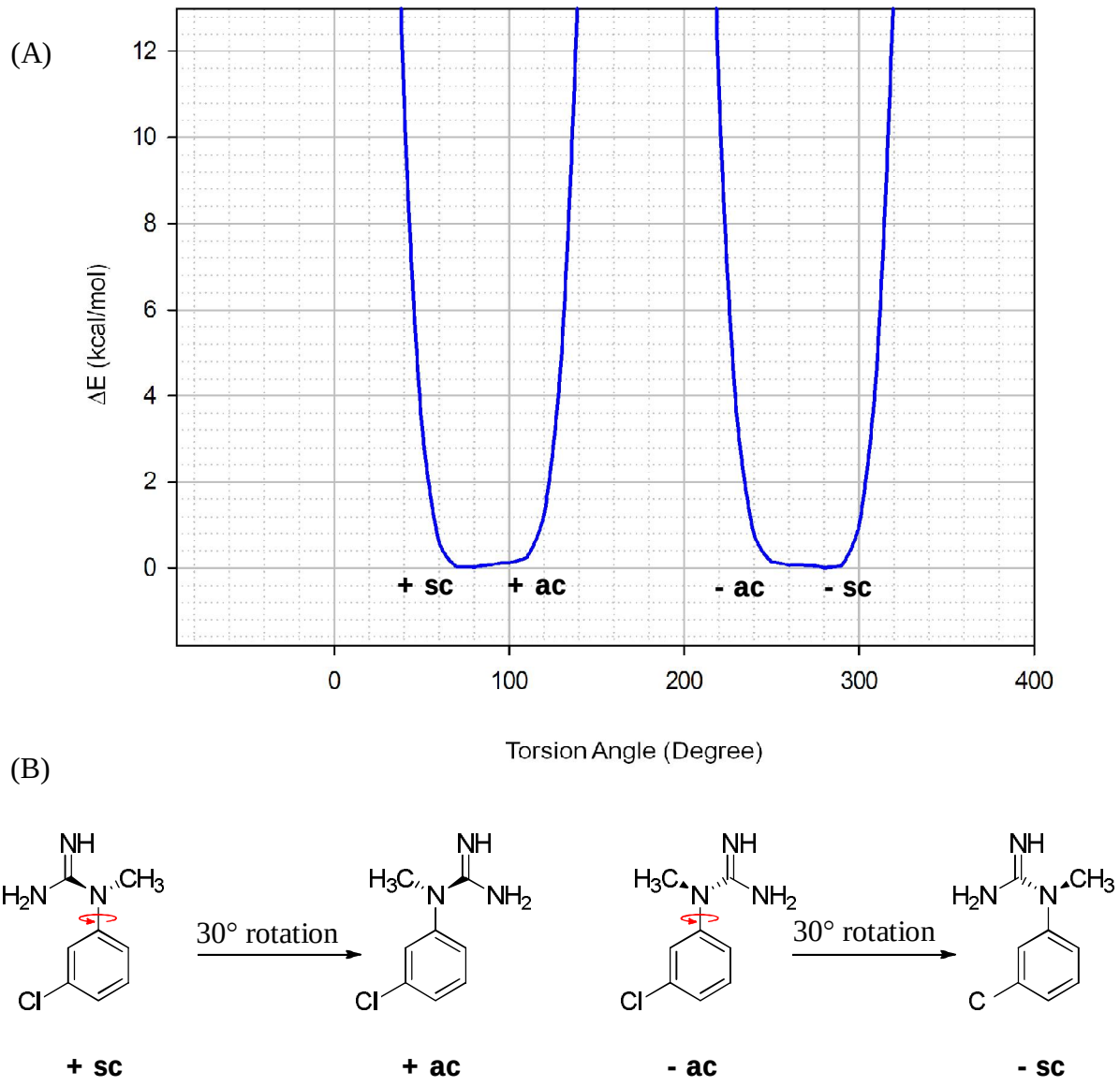

Figure 32. Low-energy rotamer identification of **40**. A. Calculated energy associated with different torsion angels of the rotatable bond. B. Structural representation of the four identified rotamers, (+/-) synclinial (sc), (+/-) anticlinial (ac).

Before docking **21** and **40** at the constructed α7 ECD nACh receptor models, an argument about two possible ways for the docking of rotamers was analyzed. The first way is to use either the validated agonist model or the validated antagonist model for docking since the two models have a high probability to mimic the exact loop orientation of the receptor ECD at the open and closed state, respectively. The second way is to utilize the original 100 models for docking to predict the candidate model of each allosteric site using the same standard of high GoldScore fitness function value as well as visual evaluation that was applied in the previous validation step. The latter was selected since the previous validation for the agonist and antagonist models is, in fact, a validation for the orthosteric binding site region and not for the other model regions.

5. Docking Solutions

Docking solutions, performed by GOLD Suite 5.0, were analyzed by SYBYL 8.1. Docking of both **21** and **40** showed different possible poses that were visually inspected taking into consideration the GoldScore fitness function to select the final solution. Energy minimization was carried out using the Tripos Force Field (Gasteiger-Hückel charges, distance-dependent dielectric constant = 4.0).

Plausible binding modes for **21** and **40** in allosteric site 1 (characterized by a Thr221) revealed two main clusters (Figure 33). The rotamers of **21** appear to utilize the same binding mode (N1 and N2 form ionic hydrogen bonds with Asp219; hydrophobic interactions exist

between the phenyl ring and Thr221) with alternate locations of the chloro group (possible hydrophobic interaction with the aliphatic chain of Lys204). In contrast, N2 and N3 of **40** form ionic hydrogen bonds with Asp219 as the major difference detected at this allosteric site. N3 shows further a hydrogen bond interaction with Thr221. In addition to a pose similar to **21**, **40** utilizes a binding mode with the phenyl ring oriented in a different direction; that is, the chloro group of **40** displays Van der Waals interactions with Arg208. The introduction of the N1-methyl group to MD-354 (i.e., **40**) appears as the key difference in activity since the methyl group on N1 precludes ionic hydrogen bonding with Asp219. Furthermore, differences in interacting residues might provide another explanation of the functional activity differences (Table 9).

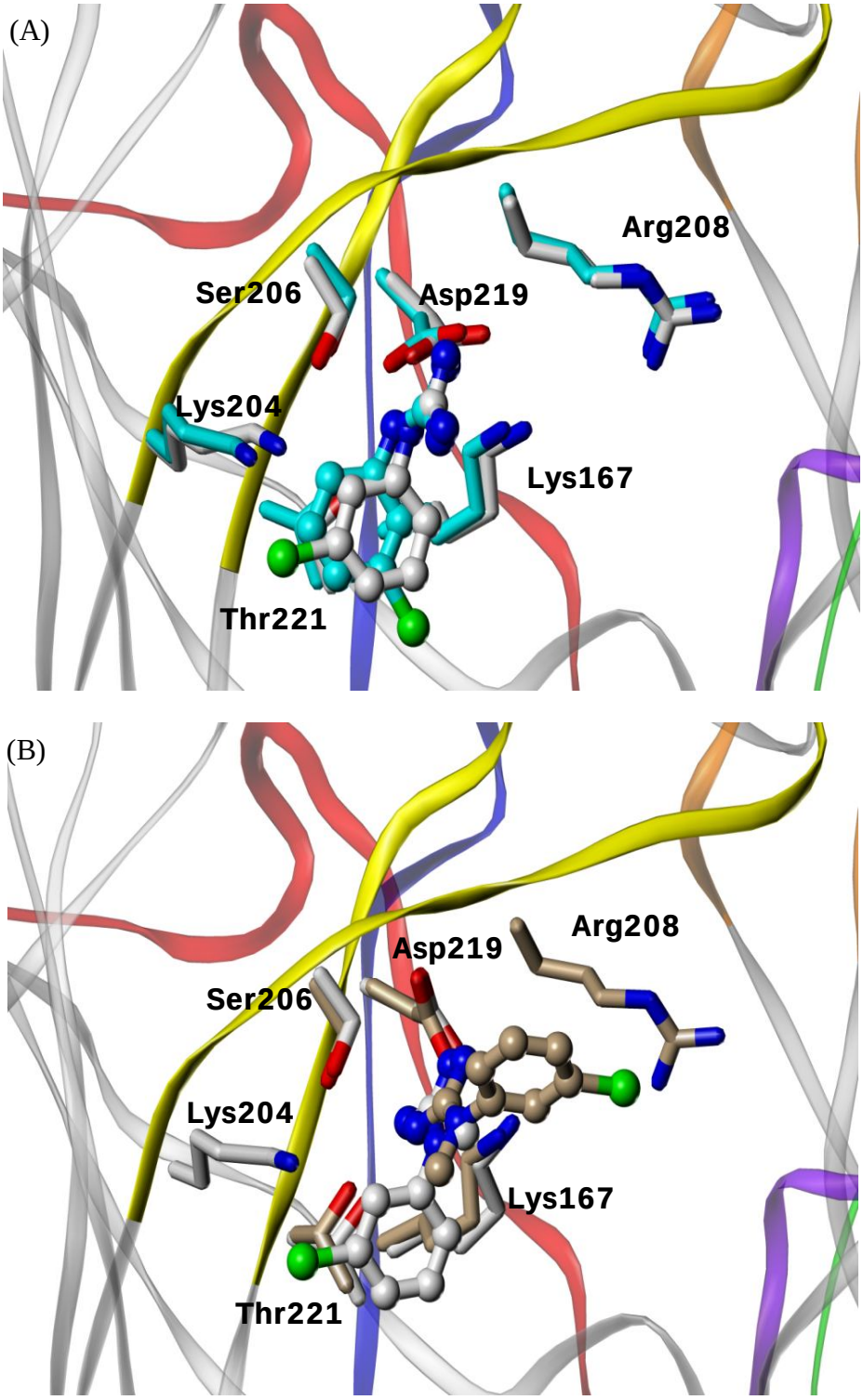

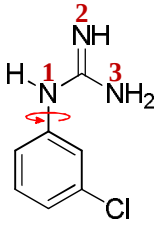

21

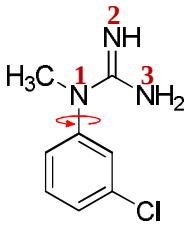

40

Figure 33. Binding modes of **21** (A) and **40** (B) at allosteric site 1. Residues labeled in black represent the principal face.

The stereochemistry of the candidate α7 ECD model for allosteric site 1 was examined by PROCHECK analysis. A Ramachandran plot was generated and the plot showed that 74.7% of the residues were in the most favored regions, 24.4% of residues were in the additionally allowed regions, 0.3% of residues were in the generously allowed regions, and 0.6% of residues were in the disallowed regions (Figure 34). Arg121 from the principal subunit and Glu120 from the complementary subunit shown in the disallowed region are located in the lining face of the receptor channel in an area distant from the binding site.

Table 9. List of amino acid residues at allosteric site 1 interacting with **21** and **40**.

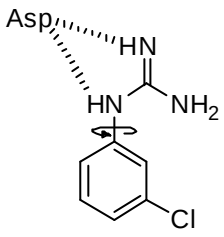

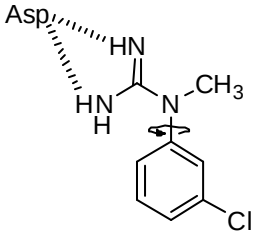

	MD-354 (21)	40
N1	Asp219	–
N2	Asp219	Asp219, D119
N3	–	Asp219, Thr221
Phenyl	Thr221, Lys204	Thr221, Lys204
-Cl	Lys204	Lys204, Arg208

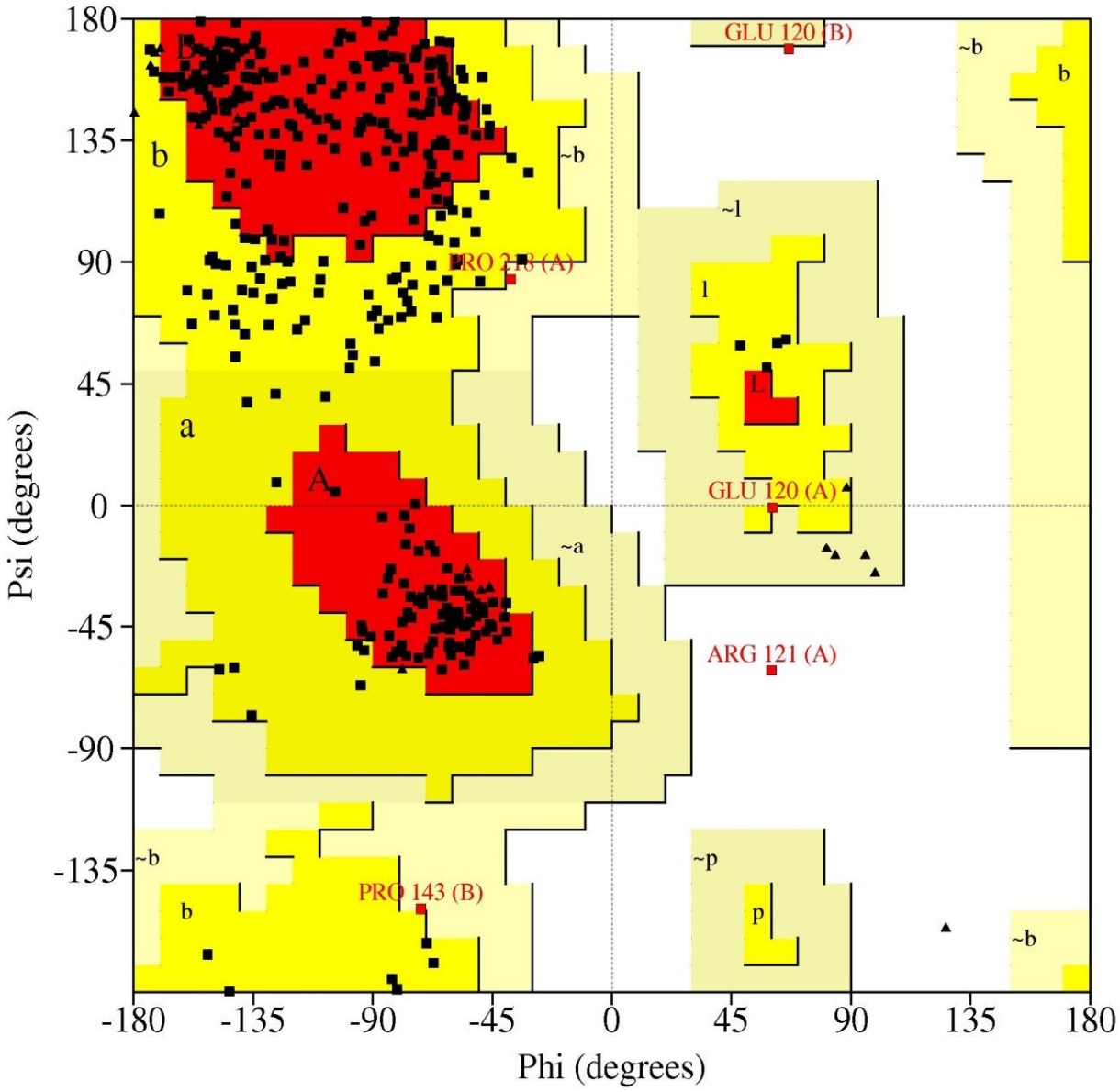

Figure 34. A Ramachandran plot of the candidate α7 ECD nAChR model for allosteric site 1. Phi and psi represent the backbone conformations of the amino acids.

Both **21** and **40** were docked in allosteric site 2 (characterized by Lys147) and they utilize three similar binding modes (Figures 35; orange, purple and white orientations). Two of these (orange and purple) exhibit guanidine moieties whose N2 and N3 atoms interact with Asp64 and Asp119, and the phenyl groups are oriented in opposite directions. One of the possible modes of

interaction (white orientation), located above the previous two, exhibit guanidinium interactions with Glu120 and Asp123 and the phenyl group is oriented toward Ile145. Furthermore, one of the rotamers of **21** has a distinctive binding mode (green orientation) wherein the guanidinium group also interacts with Glu120 and Asp123, but the phenyl group is oriented toward Glu120. The guanidine moiety in each of these binding modes shows an ionic hydrogen bond interaction with one or two carboxyl groups whereas the phenyl groups engage in hydrophobic interactions with a number of amino acid residues including the experimentally-implicated Lys147.

Although four clusters of docking solutions were observed in MD-354 (**21**) binding orientations, three docking solution clusters were observed for the N-methyl analog (**40**) (Figure 35). The introduction of an N1-methyl group to MD-354 (i.e., **40**) allows for the disfavoring of one of the docking clusters and appears to be the key difference in the allosteric site 2, assuming both **20** and **40** bind to the same site. If all of the compounds bind at allosteric site 2, different interacting residues could represent the key point that explains the functional data differences between **21** and **40** (Table 10).

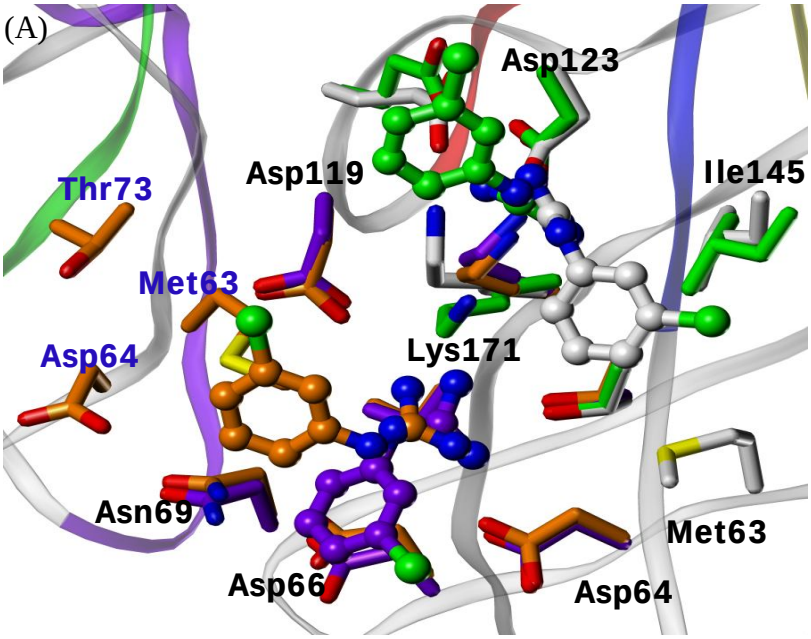

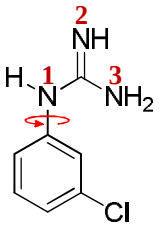

21

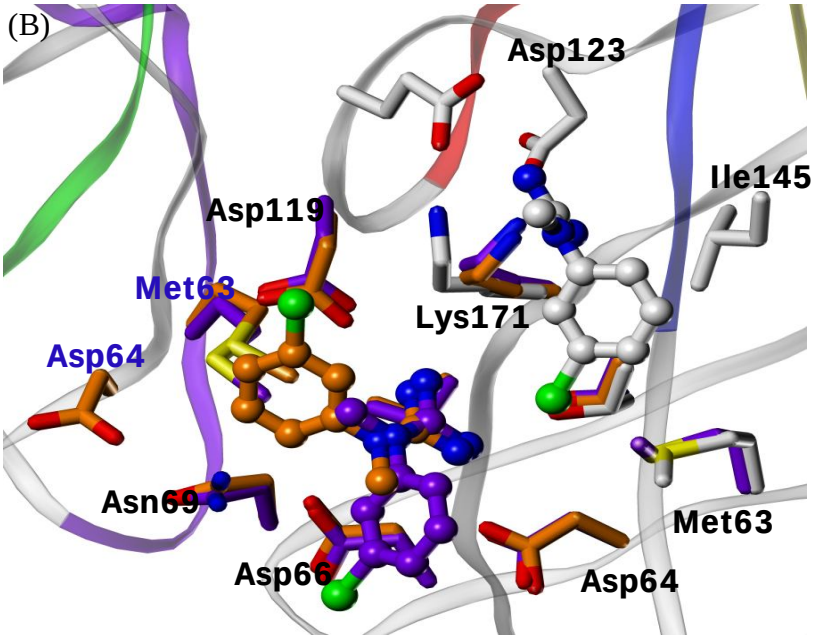

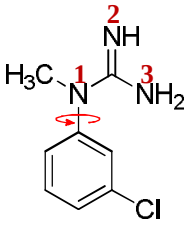

40

Figure 35. Binding modes of **21** (A) and **40** (B) at allosteric site 2. Residues labeled in black represent the principal face, whereas residues labeled in blue represent the complementary face.

Table 10. List of amino acid residues at allosteric site 2 interacting with **21** and **40**.

	MD-354 (21)	**40**
N1	–	–
N2	Asp64, Asp119 Glu120, Asp123	Asp64, Asp119 Glu120, Asp123
N3	Asp64, Asp119 Glu120, Asp123	Asp64, Asp119 Glu120, Asp123
Phenyl	Ile145, Glu120 Asp66, Met63 Lys147	Ile145, Asp66 Met63, Lys147
-Cl	Ile145	Asp66

The stereochemistry of the candidate α7 nAChR ECD model for allosteric site 2 was examined by PROCHECK analysis and the generated Ramachandran plot was analyzed. The plot showed that 72.5% of the residues were in the most favored regions, 26.7% of residues were in the additionally allowed regions, and, like with the previous model, 0.3% of residues were in the generously allowed regions, and 0.6% of residues were in the disallowed regions (Figure 36). Arg121 and Glu120, amino acids from the principal and the complementary subunit, respectively, were in the disallowed region; however, the two residues' relative location are in areas distant from the binding site.

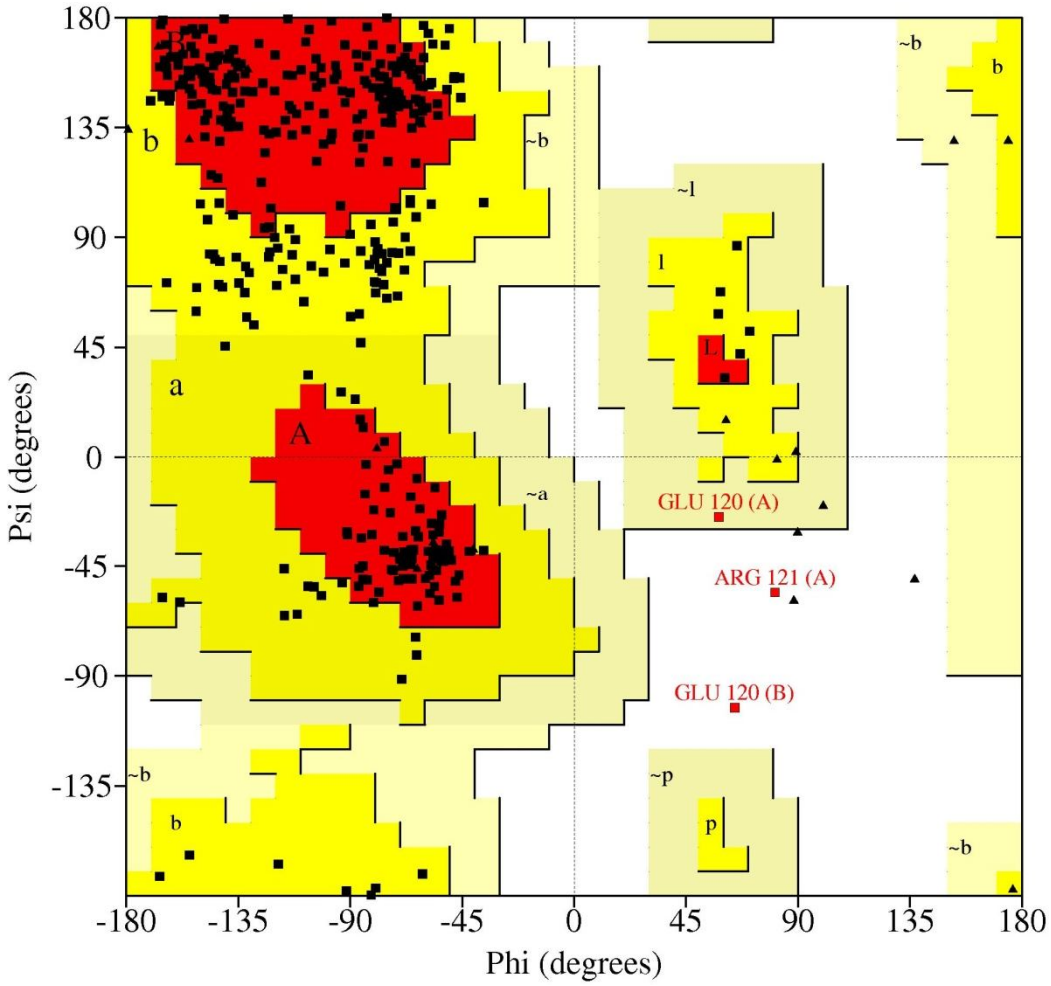

Figure 36. A Ramachandran plot of the candidate α7 ECD nAChR model for allosteric site 2. Phi and psi represent the backbone conformation of the amino acids.

Although the differences in the pose of interactions of **21** and **40** at the α7 nACh receptor's putative allosteric sites might explain the differences in their biological effect, it is also possible that each molecule interacts with distinct allosteric sites. The two models proposed here might answer the question about the possible ways by which better α7 nAChR negative allosterism is achieved by the introduction of a methyl group to MD-354 (i.e., **40**), if we assume the compounds act at the ECD.

V. Conclusions

A number of MD-354 analogs were synthesized and evaluated for their activity as allosteric modulators of α7 nACh receptors and their ability to bind at 5-HT_3 serotonin receptors. That is, MD-354 is the first example of a small-molecule allosteric modulator of α7 nAChRs. However, MD-354 binds with high affinity at 5-HT_3 serotonin receptors and, indeed, was initially developed as a 5-HT_3 receptor agonist. The focus of this investigation was on those structural features of arylguanidines already known to be detrimental to 5-HT_3 receptor binding. The incorporation of these substituents into novel arylguanidines led to compounds with enhanced selectivity as NAMs of α7 nACh receptors. We showed that the two actions can be divorced and that removing the structural feature required for 5-HT_3 binding also results in an enhancement of α7 nACh receptor NAM potency. Among the compounds tested, the N-methyl analog of MD-354 (i.e., **40)** shows more than 5,000-fold higher selectivity (i.e., 5-HT_3 receptor K_i = 6,200 nM) and higher potency at α7 nACh receptors (i.e., IC_{50} = 1.26 μM) compared to MD-354 (**21**) (i.e., 5-HT_3 receptor K_i = 35 nM; IC_{50} = 7.98 μM).

A new N-methyl series was synthesized and the purpose was to optimize their inhibitory effect at α7 nACh receptors. The modifications included the replacement of the 3-position

substituent of N-methyl MD-354 with several other substituents considering the electronic, lipophilic, and steric character of the substituent. Halogen atoms (i.e., -F, -Br, and –I in **52**, **51**, and **53**, respectively) were introduced at the 3-position mainly to test the effect of substituent size variation over a relatively fixed range of electron-withdrawing effects and/or possible change in pharmacological profile of the new molecules.

Another reason for synthesizing the new N-methyl series was to investigate whether or not both series bind in the same manner. The functional data on two compounds from each series (i.e., **21** and **31** of the MD-354 series, and **40** and **50** of the N-methyl series) revealed different relative potencies. The remaining compounds are still under investigation.

One hundred homology models of α7 nAChR ECD were generated based on the crystal structure of ECD of the mouse α1 nAChR subunit bound to α-bungarotoxin at 1.94 Å resolution (PDB ID 2QC1). At the validation step, two models were able to successfully predict the receptor interactions with agonists (i.e., ACh (**1**), nicotine (**2**), and EPI (**5**)) and the antagonist MLA (**11**) which might represent the open and the close states of the ECD of α7 nACh receptors, respectively. High fitness score of GOLD Suite 5.0 as well as the visualized residue orientations allowed for model validation by comparing the results with previously published biochemical and crystallographic data. The resultant automatic alignment showed good overlap within the conserved regions at the orthosteric site residues, except for the C loop of the agonists' model.

The exploration of possible allosteric sites at the ECD of α7 nACh receptors resulted in the identification of two potential binding sites. The first putative allosteric site is located beneath the orthosteric site and characterized by Thr221. The second putative allosteric site lines the channel and is characterized by Lys147. Both identified sites are in agreement with previously reported allosteric binding sites of α7 nACh receptor APLs. The α7 nACh receptor NAMs MD-354 (**21**) and **40** were computationally prepared and four low-energy rotamers of each were identified. Focusing on docking solutions of MD-354 (**21**) and **40** at these two identified allosteric sites was important to speculate the structural aspects that provide the major potency improvement at α7 nACh receptors. However, additional studies need to be done to explore the TM domain of the receptor.

The resultant docking poses were analyzed to detect the effect of the introduction of an N-methyl group on MD-354 binding. A high fitness score of GOLD Suite 5.0 and the visualized ligand-receptor interactions allowed for model validation. At allosteric site 1, the introduction of the N1-methyl group to MD-354 (i.e., **40**) prevents ionic hydrogen bonding with Asp219. At allosteric site 2, MD-354 (**21**) showed an additional binding orientation that is distinctive from the common three docking solution clusters that were observed for both compounds. Although, small-molecule NAMs **21** and **40** might utilize the same binding site(s) as APLs, the possibility of difference in the binding site or in the binding manner could not be excluded.

Overall, the study led to compound **40** which narrows the investigation window to a number of compounds that could guide us to a promising novel α7 nAChR small-molecule NAMs. Among the increasing reported evidence of the advantageous effect of α7 nACh receptor

inactivation on cognitive dysfunction, α7 nAChR-selective antagonists attenuated the undesired effects resulting from α7 nAChR–$A\beta_{1\text{-}42}$ interactions and tau protein hyperphosphorylation. So, if α7 nACh receptor antagonists are beneficial as symptomatic therapy for AD, small-molecule NAMs (guanidines) might represent a mechanistically unique approach.

VI. Experimental

A. Synthesis

Melting points were taken in a glass capillary on a Thomas Hoover melting point apparatus and are uncorrected. Proton nuclear magnetic resonance (^{1}H NMR) spectra were obtained using a Bruker ARX 400MHz spectrometer at which peak positions are given in parts per million (δ) downfield from the internal standard tetramethylsilane (TMS). Infrared spectra were obtained on a Thermo Nicolet iS10 FT-IR. Purity of compounds was determined by elemental analysis performed by Atlantic Microlab (Norcross, GA) for the indicated elements, and the obtained values are within 0.4% of theoretical values. Reactions were monitored by thin-layer chromatography (TLC) on silica gel GHLF plates (250 µm, 2.5 X 10 cm; Analtech Inc. Newark, DE), and Flash chromatography was performed on a CombiFlash Companion/TS (Teledyne Isco Inc. Lincoln, NE).

***N*-(3-Chlorophenyl)-*N*-methylguanidine Hydrochloride (40).** *N*-(3-Chlorophenyl)-*N*-methylguanidine hydrochloride (**40**) was prepared according to a literature procedure.[73] Cyanamide (0.59 g, 14.03 mmol) was added to a solution of 3-chloro-*N*-methylaniline

hydrochloride (**49**) (1.70 g, 9.55 mmol) in absolute EtOH (15 mL). The reaction mixture was allowed to stir at reflux for 24 h, and then the reaction mixture was concentrated under reduced pressure. The residue was recrystallized from a mixture of absolute EtOH/Et_2O to give 0.70 g (33%) of the desired product as white crystals: mp 259-261 °C (lit.[73] mp 261-262°C); IR (diamond, cm^{-1}): 3041, 3111 (NH), 3201 (NH_2); ^1H NMR (DMSO-d_6) δ: 3.27 (s, 3H, CH_3), 7.37 (d, *J* = 7.24 Hz, 1H, ArH), 7.52 (m, 2H, ArH), 7.56 (m, 1H, ArH).

3-Chloroformanilide (48). 3-Chloroformanilide (**48**) was prepared according to a literature procedure.[91] A solution of 3-chloroaniline (**47**) (3.0 g, 23.5 mmol) in an aqueous solution of formic acid (95-97%, 10 mL) was heated at reflux for 30 min. The solution was then concentrated under reduced pressure and Et_2O (20 mL) was added. The resulting solution was extracted by successive solvents: an aqueous solution of 5% citric acid (3×5 mL), H_2O (3×5 mL), and an aqueous solution of 5% $NaHCO_3$ (3×5 mL). The combined aqueous portion was extracted with Et_2O (3×10 mL). The Et_2O portion was then dried ($MgSO_4$) and the solvent was removed under reduced pressure. The obtained solid was recrystallized from H_2O to give 3.4 g (92%) of the desired product as tan-colored crystals: mp 45-47 °C (lit.[91] mp 45-50 °C); IR (diamond, cm^{-1}): 1595 (CO), 3073, 3194 (NH); ^1H NMR (DMSO-d_6) δ: 7.14 (td, *J* = 6.76, 1.10 Hz, 1H, ArH), 7.35 (t, *J* = 8.02 Hz, 1H, ArH), 7.44 (dd, *J* = 8.24, 0.68 Hz, 1H, ArH), 7.79 (t, *J* = 1.94 Hz, 1H, ArH), 8.29 (s, 1H, CH).

3-Chloro-*N*-methylaniline Hydrochloride (49). 3-Chloro-*N*-methylaniline hydrochloride (**49**) was prepared using a literature procedure for a similar compound.[92] A solution of 1 M BH_3•THF (62.1 mL, 62.10 mmol) was added in a dropwise manner to a stirred solution of 3-chloroformanilide (**48**) (3.00 g, 19.28 mmol) in anhydrous THF (10 mL). The solution was

heated at reflux under an N_2 atmosphere for 3 h. The reaction mixture was allowed to cool to room temperature and a saturated solution of HCl in Et_2O (30 mL) was added. The solution was then heated at reflux for 1 h. The THF was allowed to evaporate while stirring and heating and the reaction mixture was allowed to cool to room temperature. An aqueous solution of NaOH (15%, 30 mL) was added and the obtained mixture was extracted with Et_2O (3×15 mL). The organic portion was concentrated under reduced pressure and a saturated solution of HCl in Et_2O (50 mL) was added. The precipitate was collected by filtration and recrystallized from *i*-PrOH to yield 1.85 g (54%) of the product as yellow crystals: mp 160-162 °C (lit.[93] mp 164 °C); IR (diamond, cm^{-1}): 1597, 2634 (NH); ^1H NMR (DMSO-d_6) δ: 2.77 (s, 3H, CH_3), 6.97 (m, 2H, ArH), 7.05 (s, 1H, ArH), 7.29 (t, J = 8.06 Hz, 1H, ArH).

***N*-Methyl-*N*-phenylguanidine Hydrochloride (50).** *N*-Methyl-*N*-phenylguanidine hydrochloride (**50**) was prepared according to a literature procedure.[1] Cyanamide (1.23 g, 29.2 mmol) was added to a solution of *N*-methylaniline hydrochloride (**60**) (2.00 g, 13.9 mmol) in absolute EtOH (14 mL). The stirred reaction mixture was heated at reflux for 58 h. Next, the solvent was removed under reduced pressure and the resultant solid was cooled to 0 °C. The solid was dissolved in absolute EtOH (14 mL), and the solution was heated at reflux, and was allowed to stir with charcoal for decolorization. After that, the mixture was filtered and the filtrate was evaporated under reduced pressure. The solid was dissolved in hot absolute EtOH (14 mL), the solution was cooled to room temperature, and Et_2O was added until permanent turbidity was reached. The mixture was cooled to 0 °C to give a white precipitate that was collected by filtration and dried in an Abderhalden for 6 h to yield 0.87 g (34%) of the crude product. The solid was recrystallized from MeCN three times to give 0.53 g (21%) of the desired product as white crystals: mp (216.5-218 °C) (lit.[85] mp 217-218°C); IR (diamond, cm^{-1}): 1585,

1612, 3129 (NH), 3285 (NH_2); ^{1}H NMR (DMSO-d_6): δ 3.26 (s, 3H, CH_3), 7.35 (d, *J* = 7.32 Hz, 2H, ArH), 7.43 (t, *J* = 7.38 Hz, 1H, ArH), 7.51 (t, *J* = 7.5 Hz, 2H, ArH).

***N*-(3-Bromophenyl)-*N*-methylguanidine Hydrochloride (51).** *N*-(3-Bromophenyl)-*N*-methylguanidine hydrochloride (**51**) was prepared using a literature procedure for a similar compound.[85] Cyanamide (154 mg, 3.66 mmol) was added to a solution of 3-bromo-*N*-methylaniline (**61**) (407 mg, 1.83 mmol) in absolute EtOH (5 mL). The reaction mixture was allowed to stir at reflux for 24 h, and then the solvent was removed under reduced pressure. The resultant oily residue was crystallized from H_2O to give 178 mg (37%) of the desired product as white crystals: mp 278-280 °C; IR (diamond, cm^{-1}): 3118 (NH), 3276 (NH_2); ^{1}H NMR (DMSO-d_6) δ: 3.26 (s, 3H, CH_3), 7.4 (qd, *J* = 8.06, 1.00 Hz, 1H, ArH), 7.47 (t, *J* = 7.96 Hz, 1H, ArH), 7.64 (td, *J* = 7.92, 1.32 Hz, 1H, ArH), 7.68 (t, *J* = 1.86 Hz, 1H, ArH). Anal. Calcd ($C_8H_{10}BrN_3$·HCl) C, 36.32; H, 4.19; N, 15.88. Found: C, 36.23; H, 4.28; N, 15.77.

***N*-(3-Flourophenyl)-*N*-methylguanidine Hydrochloride (52).** *N*-(3-Flourophenyl)-*N*-methylguanidine hydrochloride (**52**) was prepared using a literature procedure for a similar compound.[85] Cyanamide (203 mg, 4.84 mmol) was added to a solution of 3-flouro-*N*-methylaniline (**62**) (392 mg, 2.42 mmol) in absolute EtOH (10 mL). The reaction mixture was allowed to stir at reflux for 24 h, and then the reaction mixture was concentrated under reduced pressure. The residue was recrystallized from *i*-PrOH to give 112 mg (22%) of the desired product as white crystals: mp 197-199 °C; IR (diamond, cm^{-1}): 3123 (NH), 3288 (NH_2); ^{1}H NMR (DMSO-d_6) δ: 3.27 (s, 3H, CH_3), 7.24 (dd, *J* = 7.36, 0.96 Hz, 1H, ArH), 7.29 (td, *J* = 8.60, 2.40 Hz, 1H, ArH), 7.35 (d, *J* = 9.88 Hz, 1H, ArH), 7.56 (q, *J* = 8.06 Hz, 1H, ArH). Anal. Calcd ($C_8H_{10}FN_3$·HCl) C, 47.18; H, 5.44; N, 20.63. Found: C, 47.08; H, 5.57; N, 20.84.

***N*-(3-Iodophenyl)-*N*-methylguanidine Hydrochloride (53).** *N*-(3-Iodophenyl)-*N*-methylguanidine hydrochloride (**53**) was prepared using a literature procedure for a similar compound.[85] Cyanamide (5.83 g, 13.88 mmol) was added to a solution of 3-iodo-*N*-methylaniline (**67**) (1.87 g, 6.94 mmol) in absolute EtOH (18 mL). The stirred reaction mixture was heated at reflux for 24 h, and then the reaction mixture was concentrated under reduced pressure. The residue was recrystallized from absolute EtOH to give 0.55 g (25%) of the desired product as brown crystals: mp 285-287 °C; IR (diamond, cm^{-1}): 3121 (NH), 3280 (NH_2); ^1H NMR (DMSO-d_6) δ: 3.25 (s, 3H, CH_3), 7.30 (t, *J* = 8.16 Hz, 1H, ArH), 7.41 (td, *J* = 8.00, 1.50 Hz, 1H, ArH), 7.79 (m, 1H, ArH), 7.80 (m, 1H, ArH). Anal. Calcd ($C_8H_{10}IN_3 \cdot HCl$) C, 30.84; H, 3.56; N, 13.49. Found: C, 31.07; H, 3.71; N, 13.28.

***N*-(3-Methylphenyl)-*N*-methylguanidine Nitrate (54).** *N*-(3-Methylphenyl)-*N*-methylguanidine nitrate (**54**) was prepared using a literature procedure for a similar compound.[94] An aqueous solution of cyanamide (50%; 1.5 mL) was added to a solution of 3-methyl-*N*-methylaniline hydrochloride (**63**) (300 mg, 1.90 mmol) in absolute EtOH (25 mL). The stirred reaction mixture was heated at reflux for 25 h, and then cooled to 0 °C (freezer) for 24 h. The solution was concentrated under reduced pressure and was dissolved in H_2O (3 mL). The solution was washed with Et_2O (3 x 20 mL), followed by evaporation of H_2O under reduced pressure. The resultant oily residue was dissolved in H_2O (3 mL), followed by addition of NH_4NO_3 (380 mg, 4.74 mmol). The solvent was removed under reduced pressure and the resultant semisolid was recrystallized from H_2O and, then, from a mixture of *i*-PrOH/Et_2O to give 18 mg (6%) of the desired product as white crystals: mp 139-141 °C; IR (diamond, cm^{-1}): 3172 (NH), 3345 (NH_2); ^1H NMR (DMSO-d_6) δ: 2.34 (s, 3H, CH_3), 3.25 (s, 3H, CH_3), 7.16 (d, *J*

= 7.88 Hz, 1H, ArH), 7.19 (s, 1H, ArH), 7.26 (d, *J* = 7.60 Hz, 1H, ArH), 7.40 (t, *J* = 7.72 Hz, 1H, ArH). Anal. Calcd ($C_9H_{13}N_3 \cdot HNO_3$) C, 47.78; H, 6.24; N, 24.77. Found: C, 47.69; H, 6.29; N, 24.86.

***N*-(3-Methoxyphenyl)-*N*-methylguanidine Hydrochloride (55).** *N*-(3-Methoxyphenyl)-*N*-methylguanidine hydrochloride (**55**) was prepared using a literature procedure for a similar compound.[85] Cyanamide (247 mg, 5.89 mmol) was added to a solution of 3-methoxy-*N*-methylaniline (**64**) (512 mg, 2.94 mmol) in absolute EtOH (15 mL). The reaction was allowed to stir and heated at reflux for 24 h, and then the reaction mixture was concentrated under reduced pressure. The resulting residue was recrystallized from a mixture of absolute EtOH/Et_2O to give 310 mg (47%) of the desired product as off-white crystals: mp 219-221 °C; IR (diamond, cm^{-1}): 3122 (NH), 3292 (NH_2); ^{1}H NMR (DMSO-d_6) δ: 3.27 (s, 3H, CH_3), 3.79 (s, 3H, CH_3), 6.93 (dq, *J* = 7.80, 0.72 Hz, 1H, ArH), 6.98 (t, *J* = 2.14 Hz, 1H, ArH), 7.01 (dt, *J* = 8.28, 1.84 Hz, 1H, ArH), 7.42 (t, *J* = 8.06 Hz, 1H, ArH). Anal. Calcd ($C_9H_{13}N_3O \cdot HCl$) C, 50.12; H, 6.54; N, 19.48. Found: C, 50.12; H, 6.60; N, 19.45.

3-Iodo-*N*-methylaniline Hydrochloride (67). 3-Iodo-N-methylaniline (**67**) was prepared according to a literature procedure.[95] Two drops of H_2SO_4 was added to a mixture of 3-iodoaniline (**65**) (2.00 g, 9.13 mmol) and trimethyl orthoformate (**66**) (1.49 mL, 13.69 mmol). The reaction mixture was heated at 120 °C in a distillation setup for 2 h and librated MeOH was collected. The solution was heated at 170 °C for 30 min and then was allowed to cool to room temperature. An aqueous solution of HCl (8 mL, 10%) was added and the mixture was heated at reflux for 3 h, then cooled to 0 °C (ice-bath) and neutralized with an aqueous solution of NaOH (20%, 15 mL). The reaction mixture was extracted with EtOAc (3×20 mL) and the organic

portion was concentrated under reduced pressure. The oily residue was purified by flash chromatography (silica gel; hexane/EtOAc; 9:1) and the resultant oil was dried under vacuum for 6 h to yield 1.77 g (83%) of the free base of **67** as a yellow oil. The free base was dissolved in Et_2O and a saturated solution of HCl in Et_2O (70 mL) was added. The precipitate was collected by filtration and recrystallized from a mixture of absolute EtOH/Et_2O to give 1.9 g (83%) of the product as brown crystals: mp 150-152 °C; IR (diamond, cm^{-1}): 2897, 3194 (NH); ^{1}H NMR (DMSO-d_6) δ: 2.73 (s, 3H, CH_3), 6.89 (d, *J* = 7.48 Hz, 1H, ArH), 7.02 (t, *J* = 7.92 Hz, 1H, ArH), 7.18 (d, *J* = 7.52 Hz, 1H, ArH), 7.23 (s, 1H, ArH).

B. Cell Transfection and Culture[a]

"Stably transfected HEK 293 cells expressing rat α3β4 or rat α7 and SH-EP1 cells expressing human α4β2 neuronal nAChRs, respectively, were prepared as described previously.[96-99] All three cell lines were maintained at 37 °C with 5% CO_2 in the incubator. Growth medium for HEK 293 cells was minimum essential medium supplemented with 10% fetal bovine serum, 100 U/ml penicillin, and 100 mg/ml streptomycin. The stably transfected cell line was raised in selective growth medium containing 0.7 mg/ml of geneticin (Invitrogen Corp, Carlsbad, CA). Growth medium for SH-EP1 cells was Dulbecco's Modified Eagle's medium with high glucose supplemented with 10% heat inactivated horse serum, 5% fetal bovine serum, 100 U/ml penicillin, 100 mg/ml streptomycin, 8 mM L-glutamine, 1 mM sodium pyruvate, and 0.25 mg/ml amphotericin (all from Invitrogen Corp, Carlsbad, CA). This stably transfected cell line was raised in selective medium containing 0.5 mg/ml zeocin (Invitrogen) and 0.4 mg/ml hygromycin B (Roche Diagnostics Corp, Indianapolis, IN)."[66]

C. Whole-cell Current Recordings[a]

"Functional expression of nAChRs was evaluated in the whole-cell configuration of the patch-clamp technique using an Axopatch 200B amplifier (Molecular Devices, Sunnyvale, CA, USA). The patch electrodes, pulled from borosilicate glass capillaries (Sutter Instrument Company, Novato, CA, USA), had a resistance of 2.5–3.5 MΩ when filled with an internal solution containing 110 mM Tris phosphate dibasic buffer, 28 mM Tris base, 11 mM EGTA, 2 mM $MgCl_2$, 0.1 mM $CaCl_2$, and 4 mM Mg-ATP (pH adjusted to 7.3 with Tris base).[99,100] In some cells, ~85% of electrode resistance was compensated electronically, so that the effective

[a] The studies were conducted in the laboratory of Dr. Abdrakhmanova.

series resistance in the whole-cell configuration was accepted when less than 20 MΩ. Stably transfected HEK cells were studied for 2–3 days after plating the cells on 15-mm round plastic cover slips (Thermanox, Nalge Nunc, Napierville, IL, USA). Generation of voltage-clamp protocols and acquisition of the data were carried out using pCLAMP 9.0 software (Molecular Devices). Sampling frequency was 5 kHz and current signals were filtered at 5 or 10 kHz before digitization and storage. All experiments were performed at room temperature (22–25 °C).

Cells plated on cover slips were transferred to an experimental chamber mounted on the stage of an inverted microscope (Olympus IX50, Olympus Corporation, Tokyo, Japan) and were bathed in a solution containing 140 mM NaCl, 3 mM KCl, 2 mM $MgCl_2$, 25 mM D-glucose, 10 mM HEPES, and 2 mM $CaCl_2$ (pH adjusted to 7.4 with Tris base). The experimental chamber was constantly perfused with control bathing solution (1–2 ml/min). The high-speed solution exchange system, HSSE-2 (ALA Scientific Instruments, Westbury, NY, USA), was used to deliver control and test solutions. Under optimal conditions, the delay in switching between solutions was ~10 ms. Data presented herein were obtained through subtraction from the leak current."[9]

D. Molecular Modeling

The homology modeling studies were performed using SYBYL 8.1 (Tripos Inc. St. Louis, MO), Modeller (Version 9.7; University of California San Francisco, San Francisco, CA), GOLD (Version 5.0; Cambridge Crystallographic Data Centre, Cambridge, UK), and AutoDock (Version 4.1; Scripps Research Institute, La Jolla, CA). The sequence alignment of the three nAChRs was performed in Clustal X 2.0 using the following Protein Knowledgebase (UniProtKB) accession codes: P36544 (human α7 nAChR; *Homo sapiens*), Q05941 (rat α7 nAChR; *Rattus norvegicus*), P04756 (mouse α1 nAChR; *Mus musculus*). The construction of the homology models was based on the crystal structure of the ECD of the mouse α1 nAChR subunit bound to α-bungarotoxin at 1.94 Å resolution (PDB ID 2QC1). The initial models were energetically optimized using the Tripos Force Field (Gasteiger–Hückel charges, distance-dependent dielectric constant = 4.0). Ligands were built in SYBYL and systematic search algorithm was applied (semi-empirical molecular orbital AM1 calculations) to prepare the four

low-energy rotamers. PROCHECK program was used for geometry quality assessment of the models.

Bibliography

Bibliography

1. Baeyer, A. I. Ueber das neurin. *Justus Liebigs Ann. Chem.* **1867**, *142*, 322-326.

2. As reported in: Zimmermann, H. ATP and acetylcholine, equal brethren. *Neurochem. Int.* **2008**, *52*, 634–648.

3. Tansey, E. M. Henry Dale and the discovery of acetylcholine. *C. R. Biol*. **2006**, *329*, 419–425.

4. Tuesta, L. M.; Fowler, C. D.; Kenny, P. J. Recent advances in understanding nicotinic receptor signaling mechanisms that regulate drug self-administration behavior. *Biochem. Pharmacol*. **2011**, *82*, 984–995.

5. Albuquerque, E. X.; Pereira, E. F.; Alkondon, M.; Rogers, S. W. Mammalian nicotinic acetylcholine receptors: From structure to function. *Physiol. Rev.* **2009**, *89*, 73-120.

6. Arias, H. R. Positive and negative modulation of nicotinic receptors. *Adv. Protein Chem. Struct. Biol.* **2010**, *80*, 153-203.

7. Haydar, S. N.; Dunlop, J. Neuronal nicotinic acetylcholine receptors - targets for the development of drugs to treat cognitive impairment associated with schizophrenia and Alzheimer's disease. *Curr. Top. Med. Chem.* **2010**, *10*, 144-152.

8. Hu, M.; Waring, J. F.; Gopalakrishnan, M.; Li, J. Role of GSK-3β activation and α7 nAChRs in $A\beta_{1\text{-}42}$-induced tau phosphorylation in PC12 cells. *J. Neurochem.* **2008**, *106*, 1371-1377.

9. Dukat, M.; Wesołowska, A.; Alley, G.; Young, S.; Abdrakhmanova, G. R.; Navarro, H. A.; Young, R.; Glennon, R. A. MD-354 selectively antagonizes the antinociceptive effects of (-)nicotine in the mouse tail-flick assay. *Psychopharmacology* **2010**, *210*, 547-557.

10. Ewins, A. J. V. Acetylcholine, a new active principle of ergot. *Biochem. J.* **1914**, *8*, 44–49.

11. Holmstedt, B.; Jenden, D. J.; Hammear, C. G.; Hanin, I.; Kitz, R. J.; Karlen, B. Identification of acetylcholine in fresh rat brain by combined gas chromatography-mass spectrometry. *Nature* **1968**, *220*, 915–917.

12. Brown, D. A. Acetylcholine. *Br. J. Pharmacol*. **2006**, *147*, S120–S126.

13. Duncan, G.; Collison, D. J. Role of the non-neuronal cholinergic system in the eye: A review. *Life Sci.* **2003**, *72*, 2013-2019.

14. Dencker, D.; Thomsen, M.; Wörtwein, G.; Weikop, P.; Cui, Y.; Jeon, J.; Wess, J.; Fink-Jensen, A. Muscarinic acetylcholine receptor subtypes as potential drug targets for the treatment of schizophrenia, drug abuse, and Parkinson's disease. *ACS Chem. Neurosci.* **2012**, *3*, 80-89.

15. Felder, C. C. Muscarinic acetylcholine receptors: signal transduction through multiple effectors. *FASEB J.* **1995**, *9*, 619-625.

16. Jensen, A. A.; Frølund, B.; Liljefors, T.; Krogsgaard-Larsen, P. Neuronal nicotinic acetylcholine receptors: structural revelations, target identifications, and therapeutic inspirations. *J. Med. Chem.* **2005**, *48*, 4705–4745.

17. Millar, N. S. A review of experimental techniques used for the heterologous expression of nicotinic acetylcholine receptors. *Biochem. Pharmacol*. **2009**, *78*, 766–776.

18. Changeux, J. –P.; Devillers-Thiery, A.; Chemouilli, P. Acetylcholine receptor: An allosteric protein. *Science* **1984**, *225*, 1335–1345.

19. Sumikawa, K.; Houghton, M.; Emtage, J. S.; Richards, B. M.; Barnard, E. A. Active multi-subunit ACh receptor assembled by translation of heterologous mRNA in Xenopus oocytes. *Nature* **1981**, *292*, 862–864.

20. Gopalakrishnan, M.; Buisson, B.; Touma, E.; Giordano, T.; Campbell, J. E.; Hu, I. C.; Donnelly-Roberts, D.; Arneric, S. P.; Bertrand, D.; Sullivan, J. P. Stable expression and pharmacological properties of human α_7 nicotinic acetylcholine receptor. *Eur. J. Pharmacol*. **1995**, *290*, 237–246.

21. Millar, N. S.; Gotti, C. Diversity of vertebrate nicotinic acetylcholine receptors. *Neuropharmacology* **2009**, *56*, 237–246.

22. Wu, J.; Lukas, R. J. Naturally-expressed nicotinic acetylcholine receptor subtypes. *Biochem. Pharmacol*. **2011**, *82*, 800–807.

23. Flores, C. M.; Rogers, S. W.; Pabreza, L. A.; Wolfe, B. B.; Kellar, K. J. A subtype of nicotinic cholinergic receptor in rat brain is composed of α4 and β2 subunits and is up-regulated by chronic nicotine treatment. *Mol. Pharmacol.* **1991**, *41*, 31–37.

24. Lukas, R. J.; Changeux, J. –P.; Le Novere, N.; Albuquerque, E. X.; Balfour, D. J. K.; Berg, D. K.; Bertrand, D.; Chiappinelli, V. A.; Clarke, P. B. S.; Collins, A. C.; Dani, J. A.; Grady, S. R.; Kellar, K. J.; Lindstrom, L. M.; Marks, M. J.; Quik, M.; Taylor, P. W.; Wannacott, S.

International Union of Pharmacology. XX. Current status of the nomenclature for nicotinic acetylcholine receptors and their subunits. *J. Pharmacol. Exp. Ther.* **1999**, *51,* 397–401.

25. Shen, J. –X.; Yakel, J. L. Nicotinic acetylcholine receptor-mediated calcium signaling in the nervous system. *Acta Pharmacol. Sin.* **2009**, *30,* 673–680.

26. Hucho, F.; Weise, C. Ligand-gated ion channels. *Angew. Chem., Int. Ed.* **2001**, *40,* 3100-3116.

27. Ortells, M. O.; Lunt, G. G. Evolutionary history of the ligand-gated ion-channel superfamily of receptors. *Trends Neurosci.* **1995**, *18,* 121-127.

28. Unwin, N. Neurotransmitter action: Opening of ligand-gated ion channels. *Cell* **1993**, *72,* 31-41.

29. Hucho, F. The nicotinic acetylcholine receptor and its ion channel. *Eur. J. Biochem.* **1986**, *158,* 211-226.

30. Brejc, K.; van Dijk, W. J.; Klaassen, R. V.; Schuurmans, M.; van Der Oost, J.; Smit, A. B.; Sixma, T. K. Crystal structure of an ACh-binding protein reveals the ligand-binding domain of nicotinic receptors. *Nature* **2001**, *411,* 269-276.

31. Bertaccini, E.; Trudell, J. R. Predecting the transmembrane secondary structure of ligand-gated ion channels. *Protein Eng.* **2002**, *15,* 443-453.

32. Dellisanti, C. D.; Yao, Y.; Stroud, J. C.; Wang, Z. Z.; Chen, L. Crystal structure of the extracellular domain of nAChR α1 bound to α-bungarotoxin at 1.94 Å resolution. *Nat. Neurosci.* **2007**, *10,* 953-962.

33. Miyazawa, A.; Fujiyoshi, Y.; Stowell, M.; Unwin, N. Nicotinic acetylcholine receptor at 4.6 Å resolution: Transverse tunnels in the channel wall. *J. Mol. Biol.* **1999**, *288,* 765-786.

34. Unwin, N. Nicotinic acetylcholine receptor at 9 Å resolution. *J. Mol. Biol.* **1993**, *229,* 1101-1124.

35. Valenzuela, C. F.; Weign, P.; Yguerabide, J.; Johnson, D. A. Transverse distance between the membrane and the agonist binding sites on the *Torpedo* acetylcholine receptor: A fluorescence study. *Biophys. J.* **1994**, *66,* 674-682.

36. Monod, J.; Wyman, J.; Changeux, J. –P. On the nature of allosteric transitions: A plausible model. *J. Mol. Biol.* **1965**, *12,* 88-118.

37. Changeux, J. –P.; Edelstein, S. J. Allosteric receptors after 30 years. *Neuron* **1998**, *21,* 959-980.

38. Hansen, S. B.; Sulzenbacher, G.; Huxford, T.; Marchot, P.; Taylor, P.; Bourne, Y. Structures of *Aplysia* AChBP complexes with nicotinic agonists and antagonists reveal distinctive binding interfaces and conformations. *EMBO J.* **2005**, *24*, 3635-3646.

39. Cheng, X.; Wang, H.; Grant, B.; Sine, S. M.; McCammon, J. A. Targeted molecular dynamics study of C-loop closure and channel gating in nicotinic receptors. *PLoS Comput. Biol.* **2006**, *2*, 1173-1184.

40. Unwin, N. Refined structure of the nicotinic acetylcholine receptor at 4Å resolution. *J. Mol. Biol*. **2005**, *346*, 967–989.

41. Gotti, C.; Moretti, M.; Gaimarri, A.; Zanardi, A.; Clementi, F.; Zoli, M. Heterogeneity and complexity of native brain nicotinic receptors. *Biochem. Pharmacol.* **2007**, *74*, 1102-1111.

42. Gotti. C.; Clementi, F.; Fornari, A.; Gaimarri, A.; Guiducci, S.; Manfredi, I.; Moretti, M.; Pedrazzi, P.; Pucci, L.; Zoli, M. Structural and functional diversity of native brain neuronal nicotinic receptors. *Biochem. Pharmacol.* **2009**, *78*, 703-711.

43. Whiting, P.; Schoepfer, R.; Lindstrom, J.; Priestley, T. Structural and pharmacological characterization of the major brain nicotinic acetylcholine receptor subtype stably expressed in mouse fibroblasts. *Mol. Pharmacol.* **1991**, *40*, 463–472.

44. Sine, S. M.; Claudio, T. Stable expression of the mouse nicotinic acetylcholine receptor in mouse fibroblasts. Comparison of receptors in native and transfected cells. *J. Biol. Chem.* **1991**, *266*, 13679-13689.

45. Parri, H. R.; Hernandez, C. M.; Dineley, K. T. Research update: Alpha7 nicotinic acetylcholine receptor mechanisms in Alzheimer's disease. *Biochem. Pharmacol*. **2011**, *82*, 931–942.

46. Bencherif, M.; Lippiello. P. M. Alpha7 neuronal nicotinic receptors: The missing link to understanding Alzheimer's etiopathology? *Med. Hypotheses* **2010**, *47*, 281-285.

47. Wallace, T. L.; Porter, R. H. P. Targeting the nicotinic alpha7 acetylcholine receptor to enhance cognition in disease. *Biochem. Pharmacol*. **2011**, *82*, 891–903.

48. Martin, S. E.; de Fiebre, N. E.; de Fiebre, C. M. The alpha7 nicotinic acetylcholine receptor-selective antagonist, methyllycaconitine, partially protects against β-amyloid$_{1-42}$ toxicity in primary neuron-enriched cultures. *Brain Res.* **2004**, *1022*, 254-256.

49. Flammia, D.; Dukat, M.; Damaj, M. I.; Martin, B.; Glennon, R. A. Lobeline: Structure-affinity investigation of nicotinic acetylcholinergic receptor binding. *J. Med. Chem.* **1999**, *42*, 3726-3731.

50. Gu, R. -X.; Zhong, Y. -Q.; Wei, D. -Q. Structural basis of agonist selectivity for different nAChR subtypes: Insights from crystal structures, mutation experiments and molecular simulations. *Curr. Pharm. Des.* **2011**, *17*, 1652-1662.

51. Huang, X.; Zheng, F.; Chen, X.; Crooks, P. A.; Dwoskin, L. P.; Zhan, C. G. Modeling subtype-selective agonists binding with α4β2 and α7 nicotinic acetylcholine receptors: Effects of local binding and long-range electrostatic interactions. *J. Med. Chem.* **2006**, *49*, 7661-7674.

52. Pohanka, M. Alpha7 nicotinic acetylcholine receptor is a target in pharmacology and toxicology. *Int. J. Mol. Sci.* **2012**, *13*, 2219-2238.

53. Banerjee, P.; Samoriski, G.; Gupta, S. Comments on "memantine blocks α7* nicotinic acetylcholine receptors more potently than *N*-methyl-D-aspartate receptors in rat hippocampal neurons. *J. Pharmacol. Exp. Ther.* **2005**, *313*, 928-929.

54. Aracava, Y.; Pereira, E. F.; Maelicke, A.; Albuquerque, E. X. Memantine blocks α7* nicotinic acetylcholine receptors more potently than *N*-methyl-D-aspartate receptors in rat hippocampal neurons. *J. Pharmacol. Exp. Ther.* **2005**, *312*, 1195-1205.

55. Yoshimura, R. F.; Hogenkamp, D. J.; Li, W. Y.; Tran, M. B.; Belluzzi, J. D.; Whittemore, E. R.; Leslie, F. M.; Gee, K. W. Negative allosteric modulation of nicotinic acetylcholine receptors blocks nicotine self-administration in rats. *J. Pharmacol. Exp. Ther.* **2007**, *323*, 907-915.

56. Schrattenholz, A.; Godovac-Zimmermann, J.; Schäfer, H. J.; Albuquerque, E. X.; Maelicke, A. Photoaffinity labeling of *Torpedo* acetylcholine receptor by physostigmine. *Eur. J. Biochem.* **1993**, *216*, 671-677.

57. Schröder, B.; Reinhardt-Maelicke, S.; Schrattenholz, A.; McLane, K. E.; Kretschmer, A.; Conti-Tronconi, B. M.; Maelicke, A. Monoclonal antibodies FK1 and WF6 define two neighboring ligand binding sites on *Torpedo* acetylcholine receptor α-polypeptide. *J. Biol. Chem.* **1994**, *269*, 10407-10416.

58. Hansen, S. B.; Taylor, P. Galanthamine and non-competitive inhibitor binding to ACh-binding protein: Evidence for a binding site on non-α-subunit interfaces of heteromeric neuronal nicotinic receptors. *J. Mol. Biol.* **2007**, *369*, 895-901.

59. Ludwig, J.; Höffle-Maas, A.; Samochocki, M.; Luttmann, E.; Albuquerque, E.; Fels, G.; Maelicke, A. Localization by site-directed mutagenesis of a galantamine binding site on α7 nicotinic acetylcholine receptor extracellular domain. *J. Recept. Signal Transduct. Res.* **2010**, *30*, 469–483.

60. Christopoulos, A. Allosteric binding sites on cell-surface receptors: Novel targets for drug discovery. *Nat. Rev. Drug Discov.* **2002**, *1*, 198-210.

61. Conn, P. J.; Christopoulos, A.; Lindsley, C. W. Allosteric modulators of GPCRs: A novel approach for the treatment of CNS disorders. *Nat. Rev. Drug Discov.* **2009**, *8*, 41-54.

62. Kim, J. S.; Padnya, A.; Weltzin, M.; Edmonds, B. W.; Schulte, M. K.; Glennon, R. A. Synthesis of desformylflustrabromine and its evaluation as an α4β2 and α7 nACh receptor modulator. *Bioorg. Med. Chem. Lett.* **2007**, 17, 4855-4860.

63. Bertrand, D.; Gopalakrishnan, M. Allosteric modulation of nicotinic acetylcholine receptors. *Biochem. Pharmacol.* **2007**, *74*, 1155-1163.

64. Williams, D. K.; Wang, J.; Papke, R. L. Positive allosteric modulators as an approach to nicotinic acetylcholine receptor-targeted therapeutics: Advantages and limitations. *Biochem. Pharmacol.* **2011 ,** *82*, 915-930.

65. Dukat, M.; Abdel-Rahman, A. A.; Ismaiel, A. M.; Ingher, S.; Teitler, M.; Gyermek, L.; Glennon, R. A. Structure-activity relationships for the binding of arylpiperazines and arylbiguanides at 5-HT_3 serotonin receptors. *J. Med. Chem.* **1996**, *39*, 4017-4026.

66. Abdrakhmanova, G. R.; Blough, B. E.; Nesloney, C.; Navarro, H. A.; Damaj, M. I.; Carroll, F. I. *In vitro* and *in vivo* characterization of a novel negative allosteric modulator of neuronal nAChRs. *Neuropharmacology* **2010**, *59*, 511-517.

67. Dukat, M.; Young, R.; Darmani, N. N.; Ahmed, B.; Glennon, R. A. The 5-HT_3 agent *N*-(3-chlorophenyl)guanidine (MD-354) serves as a discriminative stimulus in rats and displays partial agonist character in a shrew emesis assay. *Psychopharmacology* **2000**, *150*, 200-207.

68. Dukat, M.; Glennon, R. A.; Young, S. MD-354: What is it good for? *CNS Drug Rev.* **2007**, *13*, 1-20.

69. Wesolowska, A.; Young, S.; Dukat, M. MD-354 potentiates the antinociceptive effect of clonidine in the mouse tail-flick but not hot-plate assay. *Eur. J. Pharmacol.* **2004**, *495*, 129-136.

70. Dziewczapolski, G.; Glogowski, C. M.; Masliah, E.; Heinemann, S. F. Deletion of the α7 nicotinic acetylcholine receptor gene improves cognitive deficits and synaptic pathology in a mouse model of Alzheimer's disease. *J. Neurosci.* **2009**, *29*, 8805-8815.

71. Zheng, W. H.; Bastianetto, S.; Mennicken, F.; Ma, W.; Kar, S. Amyloid β peptide induces tau phosphorylation and loss of cholinergic neurons in rat primary septal cultures. *Neuroscience* **2002**, *115*, 201-211.

72. Glennon, R. A.; Dukat, M. Serotonin receptors and drugs affecting serotonergic neurotransmission. In *Foye's Medicinal Chemistry*, 6 ed.; Lemke, T. L.; Williams, D. A., Eds. Lippincott Williams & Wilkins: Baltimore, 2008; pp 417-443.

73. Dukat, M.; Choi, Y. N.; Teitler, M.; Du Pre, A.; Herrick-Davis, K.; Smith, C.; Glennon, R. A. The binding of arylguanidines at 5-HT_3 serotonin receptors: A structure-affinity investigation. *Bioorg. Med. Chem. Lett.* **2001**, *11*, 1599-1603.

74. Glennon, R. A.; Daoud, M. K.; Dukat, M.; Teitler, M.; Herrick-Davis, K.; Purohit, A.; Syed, H. Arylguanidine and arylbiguanide binding at 5-HT_3 serotonin receptors: A QSAR study. *Bioorg. Med. Chem.* **2003**, *11*, 4449-4454.

75. Portoghese, P. S. A new concept on the mode of interaction of narcotic analgesics with receptors. *J. Med. Chem.* **1965**, *8*, 609-616.

76. Dukat, M. 5-HT_3 serotonin receptor agonists: A pharmacophoric journey. *Curr. Med. Chem.* **2004**, *4*, 1-18.

77. Broad, L. M.; Felthouse, C.; Zwart, R.; McPhie, G. I.; Pearson, K. H.; Craig, P. J.; Wallace, L.; Broadmore, R. J.; Boot, J. R.; Keenan, M.; Baker, S. R.; Sher, E. PSAB-OFP, a selective α7 nicotinic receptor agonist, is also a potent agonist of the 5-HT_3 receptor. *Eur. J. Pharmacol.* **2002**, *452*, 137-144.

78. Larkin, M. A.; Blackshields, G.; Brown, N. P.; Chenna, R.; McGettigan, P. A.; McWilliam, H.; Valentin, F.; Wallace, I. M.; Wilm, A.; Lopez, R.; Thompson, J. D.; Gibson, T. J.; Higgins, D. G. Clustal W and Clustal X version 2.0. *Bioinformatics* **2007**, *23*, 2947-2948.

79. Brams, M.; Gay, E. A.; Saez, J. C.; Guskov, A.; van Elk, R.; van der Schors, R. C.; Peigneur, S.; Tytgat, J.; Strelkov, S. V.; Smit, A. B.; Yakel, J. L.; Ulens, C. Crystal structures of a cysteine-modified mutant in loop D of acetylcholine-binding protein. *J. Biol. Chem.* **2011**, *286*, 4420-4428.

80. Celie, P. H.; van Rossum-Fikkert, S. E.; van Dijk, W. J.; Brejc, K.; Smit, A. B.; Sixma, T. K. Nicotine and carbamylcholine binding to nicotinic acetylcholine receptors as studied in AChBP crystal structures. *Neuron* **2004**, *41*, 907-914.

81. Zhu, C. Z.; Chin, C. L.; Rustay, N. R.; Zhong, C.; Mikusa, J.; Chandran, P.; Salyers, A.; Gomez, E.; Simler, G.; Lewis, L. G.; Gauvin, D.; Baker, S.; Pai, M.; Tovcimak, A.; Brown, J.; Komater, V.; Fox, G. B.; Decker, M. W.; Jacobson, P. B.; Gopalakrishnan, M.; Lee, C. H.; Honore, P. Potentiation of analgesic efficacy but not side effects: Co-administration of an α4β2 neuronal nicotinic acetylcholine receptor agonist and its positive allosteric modulator in experimental models of pain in rats. *Biochem. Pharmacol.* **2011**, *82*, 967-976.

82. Stokes, C.; Papke, R. L. Use of an α3β4 nicotinic acetylcholine receptor subunit concatamer to characterize ganglionic receptor subtypes with specific subunit composition reveals species-specific pharmacologic properties. *Neuropharmacology* **2012**, .

83. Gill, J. K.; Dhankher, P.; Sheppard, T. D.; Sher, E.; Millar, N. S. A series of α7 nicotinic acetylcholine receptor allosteric modulators with close chemical similarity but diverse pharmacological properties. *Mol. Pharmacol.* **2012**, *81*, 710-718.

84. Hansch, C.; Leo, A.; Unger, S. H.; Kim, K. H.; Nikaitani, D.; Lien, E. J. "Aromatic" substituent constants for structure-activity correlations. *J. Med. Chem.* **1973**, *16*, 1207-1216.

85. Braun, C. The preparation of some structurally related monoguanidines. *J. Am. Chem. Soc.* **1933**, *55*, 1280–1284.

86. Padmanabhan, S.; Reddy, N. L.; Durant, G. J. A convenient one pot procedure for N-methylation of aromatic amines using trimethyl orthoformate. *Synth. Commun.* **1997**, *27*, 691-699.

87. Konstantakaki, M.; Tzartos, S. J.; Poulas, K.; Eliopoulos, E. Model of the extracellular domain of the human α7 nAChR based on the crystal structure of the mouse α1 nAChR extracellular domain. *J. Mol. Graph. Model.* **2008**, *26*, 1333-1337.

88. Li, S. X.; Huang, S.; Bren, N.; Noridomi, K.; Dellisanti, C. D.; Sine, S. M.; Chen, L. Ligand-binding domain of an α_7-nicotinic receptor chimera and its complex with agonist. *Nat. Neurosci.* **2011**, *14*, 1253-1259.

89. Luttmann, E.; Ludwig, J.; Hoffle-Maas, A.; Samochocki, M.; Maelicke, A.; Fels, G. Structural model for the binding sites of allosterically potentiating ligands on nicotinic acetylcholine receptors. *ChemMedChem* **2009**, *4*, 1874-1882.

90. Alley, G. S.; Mosier P. D.; Dukat, M. Arylguanidines as analgesic adjuvants: Graphics modeling studies. Presented at the 240th National ACS Meeting and Exposition [Online], Boston, MA, August 22-26, 2010. Web site. http://www.acsmedchem.org/ (accessed Jun 19, 2012).

91. Rosowsky, A.; Forsch, R. A.; Queener, S. F. 2,4-Diaminopyrido[3,2-d]pyrimidine inhibitors of dihydrofolate reductase from *Pneumocystis carinii* and *Toxoplasma gondii*. *J. Med. Chem.* **1995**, *38*, 2615-2620.

92. Northrop, R. C.; Russ, P. L. Selective reduction of some *N*-formyl dipeptide esters with borane-tetrahydrofuran. *J. Org. Chem.* **1977**, *42*, 4148-4150.

93. La Coste, W.; Bodewig, J. Uber methylformyl-*o*-amidochlorbenzoesaure und methylpseudochlorisatin aus *m*-chlorchinolinmethylchlorid. *Chem. Ber.* **1885**, *18*, 428-432.

94. Hughes, John L.; Liu, R. C.; Enkoji, T. Cardiovascular activity of aromatic guanidine compounds. *J. Med. Chem.* **1975**, *18*, 1077–1088.

95. Padmanabhan, S.; Reddy, N. L.; Durant, G. J. A convenient one pot procedure for N-methylation of aromatic amines using trimethyl orthoformate. *Synth. Commun.* **1997**, *27*, 691-699.

96. Eaton, J. B.; Peng, J. H.; Schroeder, K. M.; George, A. A.; Fryer, J. D.; Krishnan, C.; Buhlman, L.; Kuo, Y. P.; Steinlein, O.; Lukas, R. J. Characterization of human α4β2-nicotinic acetylcholine receptors stably and heterologously expressed in native nicotinic receptor-null SH-EP1 human epithelial cells. *Mol. Pharmacol.* **2003**, *64,* 1283-1294.

97. Moaddel, R.; Oliveira, R. V.; Kimura, T.; Hyppolite, P.; Juhaszova, M.; Xiao, Y.; Kellar, K. J.; Bernier, M.; Wainer, I. W. Initial synthesis and characterization of an α7 nicotinic receptor cellular membrane affinity chromatography column: Effect of receptor subtype and cell type. *Anal. Chem.* **2008**, *80,* 48-54.

98. Xiao, Y.; Meyer, E. L.; Thompson, J. M.; Surin, A.; Wroblewski, J.; Kellar, K. J. Rat α3/β4 subtype of neuronal nicotinic acetylcholine receptor stably expressed in a transfected cell line: Pharmacology of ligand binding and function. *Mol. Pharmacol.* **1998**, *54,* 322-333.

99. Xiao, Y.; Abdrakhmanova, G. R.; Baydyuk, M.; Hernandez, S.; Kellar, K. J. Rat neuronal nicotinic acetylcholine receptors containing α7 subunit: Pharmacological properties of ligand binding and function. *Acta Pharmacol. Sin.* **2009**, *30,* 842-850.

100. Abdrakhmanova, G. R.; Carroll, F. I.; Damaj, M. I.; Martin, B. R. 3'-Fluoro substitution in the pyridine ring of epibatidine improves selectivity and efficacy for α4β2 versus α3β4 nAChRs. *Neuropharmacology* **2008**, *55,* 1287-1292.

Appendix A

Primary binding assay for the N-methyl series compounds **40** and **50**-**55** at 10 μM concentration

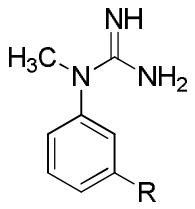

Compound	R	K_i (nM)[a]							
		5-HT_3	α2β2	α2β4	α3β2	α3β4	α4β2	α4β2**	α4β4
40	Cl	> 10,000	> 10,000	> 10,000	> 10,000	> 10,000	> 10,000	> 10,000	> 10,000
50	H	> 10,000	> 10,000	> 10,000	> 10,000	> 10,000	> 10,000	> 10,000	> 10,000
51	Br	> 10,000	> 10,000	> 10,000	> 10,000	> 10,000	> 10,000	> 10,000	> 10,000
52	F	> 10,000	> 10,000	> 10,000	> 10,000	> 10,000	> 10,000	> 10,000	> 10,000
53	I	> 10,000	> 10,000	> 10,000	ND[b]	> 10,000	> 10,000	> 10,000	> 10,000
54	CH_3	ND[b]	> 10,000	> 10,000	> 10,000	> 10,000	> 10,000	> 10,000	> 10,000
55	OCH_3	> 10,000	> 10,000	> 10,000	> 10,000	> 10,000	> 10,000	> 10,000	> 10,000

[a] N = 4 determinations; radioligand for 5-HT_3=[^{3}H] LY278584; and for all nAChRs = [^{3}H]epibatidine.

[b] ND not determined.

** = all are cloned except where marked, (endogenous rat forebrain).

Vita

Osama Ibrahim Alwassil was born on December 22, 1981, in Riyadh, Saudi Arabia. Osama received his Bachelors of Science in Pharmaceutical Sciences from College of Pharmacy, King Saud University in Riyadh, Saudi Arabia in 2005. He worked as a teaching assistant in the College of Clinical Pharmacy, King Faisal University in Ahsaa, Saudi Arabia from 2005 to 2008. In 2008, he was awarded a scholarship from King Faisal University towards a Master of Science degree at Virginia Commonwealth University.